DISS. ETH NO. 27373

Numerical modelling of suspended sediment transport in pre-alpine river basins

A thesis submitted to attain the degree of

DOCTOR OF SCIENCES of ETH ZURICH

(Dr. sc. ETH Zurich)

presented by

GIULIA BATTISTA

MSc in Environmental and Land Engineering, University of Trento, Italy

born on 31.05.1991

citizen of Italy

accepted on the recommendation of

Prof. Dr. Paolo Burlando

Prof. Dr. Peter Molnar

Prof. Dr. Christine Alewell

Prof. Dr. Stuart Lane

2021

Abstract

Rivers can transport large amounts of suspended sediment, which is the cause of problems such as reservoir siltation, increased risk of flooding and reduced water quality. Therefore, it is of paramount importance to be able to identify the sources and to make predictions of suspended sediment load in river basins. However, this understanding is hindered by the very strong spatial and temporal variability of the mechanisms of sediment production and transport. In this thesis, I developed a new hydrology-sediment model for soil erosion and sediment transport in pre-Alpine basins and carried out a numerical investigation of the sources of such variability.

In the first part of the thesis, I investigated the impact of spatially variable climatic and landscape controls for diffuse hillslope erosion and suspended sediment transport. To this aim, I compared simulations on a pre-Alpine basin with uniform and spatially variable precipitation and erodibility. I found that spatial variability of such drivers affects the suspended sediment dynamics, because it determines the location, productivity, and connectivity to the basin outlet of the sediment sources. In particular, our results highlighted the key role of clusters of high soil moisture produced by spatially variable precipitation, and the effect of specific landscape elements acting as obstacles to the sediment flux by a variable surface erodibility.

In the second part of the thesis, the role of localized sources of sediment on the dynamics and provenance of sediment is investigated. In this step, the modelling of hillslope erosion, landslides and incised areas was combined with geomorphic mapping, terrain analysis and sediment tracing with ^{10}Be. The results highlighted that hotspots of soil erosion may dominate the sediment budget of pre-Alpine basins, and the control exerted by their morphological properties on the hillslope-channel connectivity and the sourcing of sediment.

In the third part of the thesis, I explored how the presence of sediment available for transport on the hillslopes and in the channels of a river basin affects the variability and temporal dynamics of suspended sediment. To do so, I simulated conditions of transport and supply limitation, and compared them with observations in several Alpine and pre-Alpine basins. Both simulations and observations indicated that supply limitation reduces the variability of the suspended sediment concentration at the outlet, while the alternation between low and high sediment availability favours it. The observed seasonality of sediment load in the case study is also compatible with the seasonality of the sediment reservoir predicted by the model.

To conclude, in this thesis we present a new model for diffuse and localized soil erosion on the hillslopes and in the channels, and for the routing of such eroded sediment to the basin outlet. The model is used to gain insights into the suspended sediment dynamics of pre-Alpine basins.

Sommario

I fiumi sono in grado di trasportare una grande quantità di sedimenti, che può causare problemi come l'interramento dei bacini idrici, l'aumento del rischio di alluvione e una ridotta qualità acqua. È quindi fondamentale essere in grado di identificare e prevedere le sorgenti e i carichi dei sedimenti in sospensione nei bacini fluviali. Tuttavia la comprensione di questi fenomeni è ostacolata dalla grande variabilità temporale e spaziale dei meccanismi di produzione e trasporto dei sedimenti. In questa tesi, ho sviluppato un nuovo modello idro-sedimentologico per l'erosione del suolo e il trasporto dei sedimenti in bacini pre-alpini e ho condotto esperimenti numerici per capire le sorgenti di tale variabilità.

Nella prima parte della tesi, ho studiato l'impatto dei fattori climatici e geomorfologici variabili nello spazio sull'erosione diffusa dei versanti e il trasporto dei sedimenti. A tal fine ho confrontato diverse simulazioni su un bacino alpino, caratterizzate da precipitazione e erodibilità del suolo variabili ed uniformi nello spazio. Ho trovato che la variabilità nello spazio di questi fattori influenza la dinamica dei sedimenti in sospensione nel fiume attraverso il controllo della posizione, produttività e connettività alla sezione di uscita del bacino delle sorgenti dei sedimenti. In particolare, i nostri risultati hanno messo in evidenza il ruolo chiave della concentrazione spaziale di un'alta umidità del suolo, creata da una precipitazione variabile nello spazio, e l'effetto di elementi del paesaggio che bloccano il flusso di sedimenti, descritti da un'erodibilità del suolo variabile nello spazio.

Nella seconda parte della tesi, è stato studiato il ruolo delle sorgenti localizzate di sedimenti sulla dinamica e l'origine dei solidi sospesi. In questa parte, la modellazione dell'erosione dei versanti, delle frane e delle zone incise del bacino è stata combinata con una mappatura geomorfologica, un'analisi della topografia del bacino e il tracciamento dei sedimenti tramite l'uso di ^{10}Be. I risultati hanno messo in evidenza il ruolo chiave delle sorgenti localizzate di sedimenti nel bilancio sedimentologico dei bacini pre-alpini, e l'influenza dalle loro caratteristiche morfologiche sulla connettività tra versanti e canali, e sull'origine dei sedimenti.

Nella terza parte della tesi, ho studiato come la presenza di sedimenti disponibili per il trasporto sui versanti e nei canali di un bacino fluviale influenzi la variabilità spaziale e temporale dei sedimenti in sospensione. Per fare questo, ho simulato condizioni in cui il trasporto di sedimenti era limitato dalla capacità di trasporto del fiume, e altre in cui era limitato dalla disponibilità di sedimenti alla sorgente. Queste simulazioni sono state successivamente comparate con osservazioni

su diversi bacini alpini e pre-alpini. Sia i risultati delle simulazioni che le osservazioni hanno mostrato che una mancanza di sedimenti disponibili per il trasporto riduce la variabilità delle concentrazioni di sedimenti in sospensione all'uscita del bacino. Invece, l'alternanza di periodi con alta e bassa disponibilità di sedimenti la favorisce. La stagionalità dei carichi sospesi osservata nel caso studio è inoltre compatibile con la stagionalità della disponibilità di sedimenti predetta dal modello.

In conclusione, in questa tesi è stato presentato un nuovo modello per l'erosione del suolo sia diffusa che localizzata sui versanti e nei canali, e per il trasporto dei sedimenti così erosi. Il modello è stato utilizzato per approfondire la conoscenza della dinamica dei sedimenti in sospensione nei bacini pre-alpini.

Acknowledgements

I would like to thank my co-authors and the people who supported me in the work presented in this thesis.

I want to thank my supervisor Paolo Burlando for the opportunity to join the DAFNE European project, with the challenges it posed, which were and still are a motivation to pursue this research, but also for the enriching experiences it brought. I also thank him for taking the time to listen to me anytime I needed, and for following my research also in the parts that most departed from hydrology.

I thank my daily supervisor Peter Molnar for supporting me with countless discussions and inputs in these years, for the patience of repeating the same concept when we were not on the same page, and sometimes even convincing me of the value of my own work. He gave me the freedom to develop the topic of my PhD in the direction that I found most interesting, and in this way allowed me to become independent.

A sincere thank goes to Fritz Schlunegger, who brought a fresh look at the modelling work and gave me the tools to venture from the numerical world a few steps towards geology. His availability and helpfulness motivated me in crucial moments of my PhD.

I also thank Scott Sinclair and Enrico Weber for the very valuable technical support in the development of the numerical model, for the collaboration on the DAFNE case studies and for the nice time sharing the office.

A big thank goes to Han Winterwerp and Bas van Maren who made my time at Deltares before the PhD extremely fruitful, providing me with the most important tools to do my first steps in research. What I learned at Deltares gave me the confidence to dive into the experience of a PhD and has been helpful until today.

I thank my colleagues Martina, Elena, Sebastian, Jacob, Scott, Chunming, Anna, Theo, Mosisa, Jess, Gianluca, Marius and Chuanyun for the daily life in the office, the runs in the forest, barbecues and evenings together, and the real and virtual drinks.

I also want to take this occasion to thank all my dearest friends, who give priceless value to the everyday life. Elena, Gloria and Martina for continuing walking together no matter the physical distance between us, and for the magic of talking after a long time and share what we discovered about life. Camilla, with whom no time can break the syntony, together with Giovanni,

Luca F., Luca Z., Niccolò, Andrea and Martin for sharing together the funniest moments and the greatest achievements in the last ten years of our lives, and for remaining close to each other in the times we would have never wanted to live. Giovanna for her contagious energy and authentic affection. Alessandro e Gianira for the countless Friday and Saturday night dinners in our beloved Salerstrasse, and for choosing us as “congiunti” in social distancing times. Marco for letting me into his project group at the university, and for remaining a reference point since then. Davide and Elisa for welcoming me in Zurich, and for each moment and experience we shared until now. Evi for her spontaneity and for the nice time in Gubelstrasse where I felt at home.

I thank my family, who mostly contributed to this achievement. My sister Anna for having always been my guide in the discovery of the next step in education, but most importantly in life. With her, Stefano and my favorite kid in the world Zaccaria. My brother Tommaso for his affection, for making fun of me and for being an example in building his own path. My parents for listening to my complaints since the very first day of school, and for teaching me to step out of my comfort zone and explore the world around me.

Francesco Caponi gave an invaluable contribution to this work, with his strength he pushed me over the obstacles where I would have given up.

Contents

Abstract **i**

Sommario **iii**

Acknowledgements **v**

Contents **vii**

1 Introduction **1**
1.1 Motivation 1
1.2 State of the art 2
1.3 Research gaps 6
1.4 Research questions 6

2 The TOPKAPI-ETH hydrology and sediment model **9**
2.1 The hydrological module 9
2.2 The sediment module 12

3 Modelling impacts of spatially variable erosion drivers on suspended sediment dynamics **17**
3.1 Introduction 18
3.2 Methods 20
3.3 Erosion driver numerical experiments 25
3.4 Results 25
3.5 Discussion 31
3.6 Conclusions 34

4 Modelling localized sources of sediment in mountain catchments for provenance studies **37**
4.1 Introduction 38
4.2 Data and Methods 39
4.3 Results 45
4.4 Discussion 50
4.5 Conclusions 54

5 Sediment supply effects in hydrology-sediment modelling of a pre-Alpine basin **57**
5.1 Introduction 58
5.2 Study basins 59

5.3 Methods 61
5.4 Results 65
5.5 Discussion 71
5.6 Conclusions 74

6 Conclusion **77**
6.1 Summary 77
6.2 Discussion and implications 80
6.3 Outlook 83

A Supporting information for chapter 3 **1**
A.1 Model inputs and calibration 1
A.2 Suspended sediment concentration variability at the outlet 4

B Supporting information for chapter 4 **7**

C List of symbols for the sediment module **9**

Bibliography **11**

CHAPTER 1

Introduction

1.1 Motivation

Humans have actively modified the landscape since the beginning of civilization. Extensive areas of natural land cover have been replaced by practices such as agriculture for the production of food, mining for the extraction of raw materials, and deforestation to gain land for settlements. Despite the growing awareness of the consequences of such land use transformation, recent research shows that this trend continues still today (Hansen *et al.*, 2013; Robinson *et al.*, 2017). The landscape is also indirectly modified by humans through climate change, which is responsible for land cover change, the retreat of glaciers, permafrost thawing and extreme meteorological events.

A major consequence of such anthropization is an increase in soil erosion rates. The traditional practices increase erosion to much higher rates than soil production by rock weathering, therefore inducing soil thinning (Montgomery, 2007; Borrelli *et al.*, 2017, 2020). Thinner soils are less productive and lead to lower crop yields, defining a limited lifespan of soils, which some authors even associated with the decline of ancient societies (Montgomery, 2012). A transition from traditional practice to conservation agriculture has been observed in several regions, however it still remains of limited extension in other areas (Garcia-Torres *et al.*, 2003; Hobbs *et al.*, 2008; Govaerts *et al.*, 2009; Valbuena *et al.*, 2012).

The removal of natural land cover on hillslopes also favours soil erosion by reducing their stability. This results in more frequent natural hazard events such as debris flows and landslides, especially in mountainous steep terrain (Milliman and Syvitski, 1992). Furthermore, the retreat of glaciers exposes unstable sediment deposits previously covered by ice, and determines a temporary increase in sediment yield in the period following deglaciation (Church and Ryder, 1972; Ballantyne, 2002). Proglacial areas are hotspots of hazardous instabilities and geomorphic activity, and paraglaciation is expected to become the controlling process of sediment supply and landscape change in the next decades (Knight and Harrison, 2009).

Excessive rates of soil erosion not only affect the locations of sediment production, but also the downstream riverine and coastal environment. In fact, these locations often see an increase in the sediment load transported by water. High amounts of fine sediment produced in the upland areas may deteriorate the water quality of the lowland rivers by generating high suspended sediment concentrations, which not only increase the water turbidity, but may also transport pollutants such as heavy metals and nutrients bound to the sediment particles (Sellier *et al.*, 2020; Horowitz *et al.*, 2001; Botter *et al.*, 2019). In this way, they represent a threat both for the ecosystems, by reducing the hospitality of the riverine environment as a habitat for fish, invertebrates and plants (Marks and Rutt, 1997; Owens *et al.*, 2005; Wenger *et al.*, 2011), and for humans, whose access to the fresh water resource becomes more problematic and leads to extra costs to purify it. Excessive volumes of sediment in the river also increase the risk of flooding in the lowlands, where the river stream power decreases and the deposition of the coarser sediment reduces the depth available for water (e.g. van Maren *et al.*, 2009). The delivery of excessive sediment inputs into shallow-water coastal environments also induces problems of sedimentation in estuaries and harbours (e.g. de Nijs *et al.*, 2009).

Humans intervened in the landscape also by deviating and stabilizing the course of rivers, and by building impoundments for the storage of water and electricity production. It is estimated that about 50 000 large dams are in operation across the globe (Syvitski and Kettner, 2011; Lehner *et al.*, 2011) and that only 23 percent of the major world's river flow uninterrupted to the ocean (Grill *et al.*, 2019). These infrastructures affect the pathways of sediment from sources downstream in different ways.

Dams and water impoundments retain the sediment produced in the upland areas, unless flushing of the infrastructure is regularly carried out. Therefore they may introduce sediment sinks, which disconnect the sources of sediment from the basin outlet and reduce the sediment flux downstream, and at the outlet of the river basins (Syvitski and Milliman, 2007; Vörösmarty *et al.*, 2003). Excessively low concentrations of fine sediment can also be hazardous for the ecosystems, because they imply reduced nutrient fluxes and morphological modifications of the habitat (Quinton *et al.*, 2010). Starvation of coarse sediment induces channel incision, bank erosion and damages to infrastructures built within the river, such as bridge pillars (Kondolf, 1997). Finally, the reduction of sediment delivery by rivers to the coasts contributes to coastal erosion driven by sea level rise (Syvitski and Kettner, 2011; Winterwerp *et al.*, 2005).

Other interventions such as the artificial cutting of meanders, bed stabilization or river width confinement may have instead the opposite effect. By increasing the river flow velocity they favour the transfer of sediment, thus reducing the attenuation of the sediment wave which may become more hazardous for the downstream location where deposition is possible (Parker and Andres, 1976).

The combination of such effects modify the natural dynamics of sediment fluxes at the scale of entire river basins, and continents (Walling, 2006; Syvitski *et al.*, 2005) and brings up a number of issues that are of paramount importance for sustainable development. These issues include questions such as: What is the net effect of human induced alterations on sediment load? Does accelerated soil erosion dominate dam sediment retention, or vice versa? How will fluxes and sources of sediment change under scenarios of future climate? And ultimately, what is a sustainable management of sediment?

Addressing such questions requires in the first place a thorough understanding of the processes of sediment production and transport (i.e. sediment dynamics), and the availability of models that allow predictions under different types of forcing and physical configurations. The aim of this thesis is the development of such a tool, to advance our understanding of sediment dynamics.

1.2 State of the art

The issues mentioned above highlight the importance for modern societies of understanding the sediment dynamics in river basins, and how it is affected by anthropic modifications of the landscape. However, a quantitative and complete description of it is hindered by the very strong spatial and temporal variability of the processes of sediment production and transport. Such intrinsic natural variability causes a high uncertainty in the estimates and predictions of sediment load and a typically highly scattered sediment concentration-discharge relation (Asselman, 2000; Horowitz, 2003). Additionally, it also makes the generalization of observations from a case study to other basins and time frames practically impossible.

The sources of natural variability in the sediment flux can be summarized into three main classes:

a) The temporal and spatial variability of the erosion drivers

   These include the physical properties of the basin and the hydro-meteorological conditions, such as rainfall intensity and duration, and the wetness of the basin prior to a rainfall even,

which are crucial in determining the basin hydrological and sediment response. Their variability in time and space generates a strong non-uniqueness of the sediment to discharge relation and determines the ability of the catchment to transfer sediment from the sources to the outlet, i.e. the sediment transport connectivity.

b) The activation and non-linearity of localized sediment sources

Localized stocks of sediment may be present in a basin, but contribute to the sediment flux only under specific runoff conditions. This is the case of the sediment mobilized by debris flows, landslides or bank collapses, which are triggered by high soil moisture or bed shear stresses exceeding a critical threshold. The contribution of such sources are characterized by a strongly non-linear behavior, enhancing the variability of the basin sediment response.

c) The basin sediment availability

The presence or absence of sediment available for mobilization on the hillslopes and in the channels is key in determining the sediment response of a river basin to a rainfall event. Sediment availability depends on the temporally variable sediment supply by e.g. rock weathering, bank collapses, and mass wasting, and on sediment export by flood events. Exceptional floods can exhaust the major sources of sediment, while sudden inputs of material from the hillslopes temporally increase the sediment flux.

In the following I summarize the past research efforts that investigated the role of these three main sources of sediment flux variability. I will focus on suspended sediment transport, because it represents the main contribution to the total yield in most environments (Schlunegger and Hinderer, 2003; Turowski *et al.*, 2010).

1.2.1 Temporal and spatial variability of the erosion drivers

The antecedent soil moisture, timing and spatial distribution of rainfall are known to determine the timing of the hydro-sedimentological response (Paschalis *et al.*, 2014; Peleg *et al.*, 2020). The direction of hysteresis loops of suspended sediment concentration (SSC) against discharge (Q) is considered indicative of the location of the sediment sources and the antecedent state of soil wetness (Seeger *et al.*, 2004; Zabaleta *et al.*, 2007; Misset *et al.*, 2019). Clockwise hysteresis loops are associated with sediment sources located near the channel, with a limited storage rapidly flushed way, or to early sediment supply from tributaries (Asselman, 1999). Counterclockwise loops indicate distant sources from the channel, widespread and long lasting contributions generated by diffuse near-saturation conditions all over the catchment before the event, or delays to erosion when a catchment has to wet up before there is sufficient overland flow for erosion to start. The combined effect of spatial and temporal characteristics of the rainfall is evident in the different geomorphic response produced by summer and winter storms (Kampf *et al.*, 2016). The spatial patterns of rainfall and antecedent soil moisture has also been proposed as the reason for different tributary contributions (Smith *et al.*, 2003).

Topographical, physical and climatic properties of the basin also influence the sediment response by affecting the local hydrology, soil erodibility and sediment transport connectivity. In the Rhône basin, Costa *et al.* (2018b) associated a sudden increase in the sediment flux in the mid-1980s with the simultaneous increase in air temperature, probably causing the activation of new glacial sediment sources. Vaughan *et al.* (2017) demonstrated the critical role of the near channel morphology in the steepness of the SSC-Q relation. The correlation between land use changes and sediment export has been tackled by several authors, and indicates agricultural land use and deforestation as responsible for increased sediment fluxes, and reforestation as a way to reduce erosion and sediment loads (Siakeu *et al.*, 2004; Liébault *et al.*, 2005; Boix-Fayos *et al.*, 2008). Bakker *et al.*

(2008) also highlighted that land use change affects sediment flux not only by modifying the on-site sediment production, but also by changing the source connectivity to the outlet. A conceptual framework for the connectivity of sediment transport is provided by the ideas of structural and functional connectivity, to distinguish between the physical connection among landscape units, and the linkages generated by process interactions such as streamflow and sediment fluxes (Wainwright *et al.*, 2011; Fryirs, 2013; Bracken *et al.*, 2015).

These elements of spatial and temporal variability are especially important in mesoscale catchments and mountain environments, where the climatic gradients are superimposed on strong physical and morphological variability. However, research on mesoscale catchments has so far mostly focused on the integrated response of the basin observed at the outlet (e.g. López-Tarazón *et al.*, 2010). Only a few studies looked specifically into the spatial variability of the sediment response and its dependence on the erosion drivers (e.g. Uber *et al.*, 2020).

A valuable tool to study the sediment dynamics in mesoscale mountain basins are spatially distributed physically based numerical models of hydrology and sediment transport. They allow representation of the interactions between the main hydrological processes and the topography and morphology of the basin, and account both for their temporal dynamics and spatial variability. In this way, they represent structural connectivity and provide a dynamic evaluation of the functional connectivity.

Several models of this type are present in the literature. Some were especially developed for event and/or small basin scale applications, such as Answers (Beasley *et al.*, 1980), KINEROS (Woolhiser *et al.*, 1990) and WEPP (Nearing *et al.*, 1989). Other models allow long term simulations at larger basin scales, however for computational reasons they rely on a simplified representation of the hydrology and runoff processes. This is the case of landscape evolution models, e.g. CAESAR-Lisflood (Coulthard *et al.*, 2013) and SIBERIA (Hancock *et al.*, 2000), the WATEM/SEDEM model (Van Rompaey *et al.*, 2001) and the model by Tsuruta *et al.* (2018). The model tRIBS (Francipane *et al.*, 2012) includes a rigorous physically based hydrology and erosion component and is meant for long term simulations in small basins. Similarly, DSHVM (Doten *et al.*, 2006) features a detailed hydrology–vegetation component and sediment module. However, tRIBS and DSHVM are also computationally demanding, because of the great number of processes represented. In fact, their applications have so far been limited to small basins and/or short timescales.

In this framework, there is a need for a model that combines a complete physically based representation of the hydrology with a soil erosion and sediment transport component, and at the same time is computationally suitable for long-term applications in mesoscale basins.

1.2.2 The role of localized sources and provenance of sediment

Point sources of sediment may have a dominant role in the sediment budget of river basins. This is the case especially in mountain environments, where the sediment budget is often dominated by mass movements, such as landslides and debris flows (Slaymaker, 1993; Hovius *et al.*, 2002; Korup *et al.*, 2004; Cruz Nunes *et al.*, 2015; Clapuyt *et al.*, 2019), or by processes that are strongly limited in space but contribute much more than the rest of the basin, as in the case of glacial outwash (Stutenbecker *et al.*, 2019; Delunel *et al.*, 2014). In such basins, numerical models based on diffuse hillslope erosion only, such as the widely used RUSLE approach, have been shown to fail in estimating the sediment load (Van Rompaey *et al.*, 2005; Borrelli *et al.*, 2014, 2018).

The role of localized sediment sources is not only crucial in defining the sediment budget of a river basin, but also for studies of denudation rates of river basins. In the past decade, a method to estimate long-term denudation rates based on cosmogenic radionuclide (CRN) dating has shown great potential (von Blanckenburg, 2005; Bierman and Steig, 1996). Its application is based on the assumption that a sample of river bed sand is representative of the long-term erosion rates of

the upstream area, and of each part of the basin proportionally to its erosion rates. Due to the episodic and localized character of the sediment transport in mountain regions, these assumptions are very often not satisfied. This limits the application of the CRN approach in these environments (Niemi *et al.*, 2005; Yanites *et al.*, 2009). Therefore, it is crucial to improve our understanding of the provenance of sediment in streams and its temporal dynamics.

Sediment provenance can be traced by fingerprinting methods by means of measurable and conservative sediment properties (Walling, 2005; Haddadchi *et al.*, 2013). To do so, sediment properties such as the concentration of radionuclides (e.g. ^{10}Be, ^{7}Be, ^{137}Cs, excess ^{210}Pb), and geochemical elements (e.g. Al, Ca, Mg, Ti, Fe, K, Na) are measured both in the sources of sediment and in the suspended sediment samples at the outlet of the river basin. Statistical mixing models are then used to estimate the relative contribution of each sediment source in the sample (e.g. Collins *et al.*, 2010; Pulley *et al.*, 2017; Pulley and Collins, 2018). These methods allow reconstruction of the spatial origin of sediment, and its dependence on meteorological forcing (e.g. Belmont *et al.*, 2007; Navratil *et al.*, 2012; Evrard *et al.*, 2011). However, they only reconstruct the sediment provenance at the moment of the sampling, and also do not provide information about its temporal dynamics.

Such temporal dynamics can be reproduced by including the episodic activation of localized sediment sources in physically based distributed modelling of hydrology and sediment transport, and by keeping track of the origin of sediment. Although localized mass wasting processes have been included in some spatially distributed models, such as SHETRAN (Bathurst and Burton, 1998), DHSVM (Doten *et al.*, 2006) and CAESAR-Lisflood (Coulthard *et al.*, 2013), yet they do not keep track of the origin of sediment in its path to the outlet. Time-dependent modelling of sediment provenance at the event time scale has recently been performed with the hydraulic, soil erosion and sediment transport model by Cea *et al.* (2016) (Uber *et al.*, 2020), however a tool that keeps track of sediment origin in long term simulations is still missing.

1.2.3 Basin sediment availability

The sediment response of a river basin to the meteorological forcing is strongly dependent on the availability of sediment on the hillslopes and in the channel. This is supported by field observations, which show that the magnitude and frequency of debris flows depend on the recharge rate of the sediment reservoir, and sediment-generating events such as landslides or rock avalanches (Jakob *et al.*, 2005; Bennett *et al.*, 2014; Frank *et al.*, 2019). The increasing frequency of debris flows observed in some cases at the margins of retreating glaciers is also attributed to a greater sediment availability, due to the exposure of loose sediment by the melting ice (Chiarle *et al.*, 2007). Interannual sediment flux fluctuations have also been attributed to shifts between supply- and transport-limited conditions of the basin (Fuller *et al.*, 2003; Hovius *et al.*, 2002).

The quantification of sediment availability in a basin and its temporal evolution requires the estimation both of processes of sediment supply, and of sediment evacuation from the reservoir by runoff. In mountain river basins, sediment supply may be dominated by mass wasting, e.g. rock avalanches, landslides, debris flows, and therefore can be characterized by high stochasticity (Korup *et al.*, 2004; Hovius *et al.*, 2002). Although previous research demonstrated a dependence of landslide movement on high soil moisture (Iverson and Major, 1987; Coe *et al.*, 2003; Schwab *et al.*, 2007; Coe, 2012; Handwerger *et al.*, 2019a), and some field studies attempted a quantification of inputs and outputs of the basin sediment reservoir (Schuerch *et al.*, 2006; Berger *et al.*, 2011; Fuller and Marden, 2010), our knowledge on the temporal dynamics of sediment availability remains limited.

A comprehensive description of such dynamics is difficult to achieve by means of field observations, because they are limited in the spatial and temporal quantification of the sediment fluxes.

On the other hand, most spatially distributed numerical models of sediment transport available today assume transport-limited sediment fluxes, and do not allow for simulation of time dependent sediment availability (e.g. SHETRAN, DHSVM). Therefore, there is a need to keep track of the volume of basin sediment reservoir in numerical modelling of sediment transport, to allow exploration of the effects of supply-limitation on sediment dynamics.

1.3 Research gaps

From the current state of the research on the sources of variability of the suspended sediment dynamics in river basins three research gaps emerge:

1) In mesoscale ($\approx$ 500 km^2) mountain basins, there is a lack of studies on the spatial variability of the sediment response and its dependence on the erosion drivers. To perform such studies, there is a need for a model that combines a physically based representation of the hydrology with a soil erosion and sediment transport component that allows long-term simulations in medium to large catchments ($\approx$ 500 - 1000 km^2).

2) The contribution of localized sources of suspended sediment in mountain basins is of fundamental importance. However, the tools currently available only provide us with a limited understanding of the sediment provenance. In particular, a model is missing that includes sediment production both from diffuse hillslope erosion and localized sources, and also allows for time dependent quantification of the sediment source contributions.

3) Sediment availability plays a crucial role in the sediment dynamics of a river basin. However, the dependence of sediment availability in the hillslopes and in the channel on the drivers of sediment supply and export is still poorly understood. There is a need to account for the variability of the sediment reservoir in the modelling of sediment transport in river basins, to allow analysis of its influence on the sediment dynamics.

1.4 Research questions

Based on the research gaps identified above, I formulated the following three research questions in my thesis (see Fig. 1.1):

(RQ 1) **How does spatial variability in the erosion drivers impact suspended sediment dynamics?**

To address this question, I developed a new numerical model for diffuse hillslope erosion and suspended sediment transport in medium and large mountain river basins. The model is physically based and spatially distributed, and is an extension of the hydrological model TOPKAPI-ETH (Fatichi *et al.*, 2015). It combines the temporal and spatial variability of the climatic forcing with the distributed physical characteristics of the basin, such as slope, aspect, land use and soil properties. In this way, it allows to simulate sediment mobilization by overland flow across the basin, its deposition and remobilization along the flowpaths, and advection in the channel. The model is computationally efficient, and therefore allows long term simulations in medium and large catchments with high spatial and temporal resolutions. I applied it to a mesoscale pre-Alpine catchment to investigate: (i) its potential to capture the variability in suspended sediment concentrations, (ii) the effects of spatially distributed surface erodibility and precipitation on the location, productivity and connectivity to the

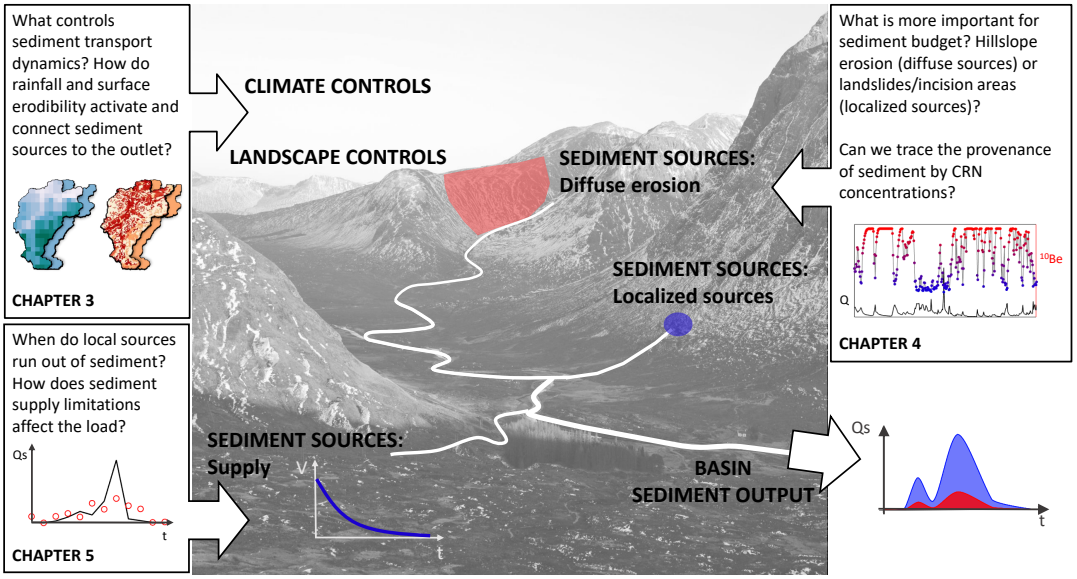

FIGURE 1.1: Research questions addressed in this thesis. In Chapter 3 the role of spatially distributed climatic and landscape controls on the suspended sediment dynamics is investigated. In Chapter 4 localized sources of sediment are implemented in the TOPKAPI-ETH numerical model to trace the sediment provenance. The temporal variability of sediment supply and its effect on sediment load are studied in Chapter 5.

river network of the sediment sources, and (iii) how such effects modify the sediment load at the basin outlet. To address such points, in the model I combined spatially variable and uniformly distributed inputs of precipitation and properties of surface erodibility. I quantified their effects on the patterns of erosion and deposition, and on sediment mobilization. The sediment delivery ratio was used to quantify the dynamics function connectivity between sources and river network. These effects of the spatial variability of the erosion drivers were used to explain the sediment loads simulated at the basin outlet.

This research question is addressed in Chapter 3.

(RQ 2) **What is the effect of localized sediment sources on the sediment provenance?**

This question has been addressed by introducing three additional sediment mobilization processes in the model developed in Chapter 3: by overland flow erosion on the body of landslides, by river incision at the toe of landslides and in inner gorges. These processes are threshold based and strongly non-linear in order to represent the properties of localized sediment sources in mountain basins. With this new feature, the model allows simulation of the sediment mobilization from three sediment sources (hillslopes, landslides and incised areas), and routes them in parallel along the hillslopes and in the channel. In this way, the sediment flux can be uniquely traced back to the sources and therefore provides a time series of the sediment provenance. To apply the model to the case study, I combined it with detailed geomorphic mapping of the potential sediment production areas based on remote observations (DEM) and geological mapping. I explored the dependence of the simulated sediment provenance on the basin parametrization, and estimated a likely composition of the load in the study basin by independent validation of the model results with topographic analysis and observed CRN concentrations.

This research question is addressed in Chapter 4.

(RQ 3) **How does suspended sediment dynamics depend on basin sediment availability?**

To investigate this question, I used the TOPKAPI-ETH hydrology and sediment transport model including the features developed in Chapters 3 and 4. Additionally, I introduced a temporally variable sediment supply by landslides, which are the sediment sources mostly affecting the seasonality of the sediment availability in pre-Alpine basins, and the possibility to monitor the sediment reservoir of the basin. The sediment supply rate was assumed to be a function of the landslide soil moisture and topography, and of the intensity of hillslope activity. In this way, the input and export sediment fluxes to the sediment reservoir and its temporal evolution are modelled. By varying the intensity of hillslope activity the model allows to create supply- and transport-limited sediment conditions, and to explore their effects on the sediment flux at the outlet. I applied the model to a pre-Alpine river basin and compared the result with observations of suspended sediment concentrations in several Alpine and pre-Alpine basins, to investigate: (i) the dependence of suspended sediment concentration variability on basin sediment availability, (ii) the effect of hydrology on the seasonality of sediment storage and suspended sediment load, and (iii) the presence of signatures of sediment supply limitation in sediment measurements. I compared the observed variability in suspended sediment concentration with simulations of scenarios of supply limitation, and used the simulated temporal variability of the sediment reservoir to explain the seasonality of sediment loads at the outlet. The effect of supply limitation on the location of sediment sources was also explored.

This research question is addressed in Chapter 5.

The relevant components of the TOPKAPI-ETH numerical model that have been used in this thesis are presented in Chapter 2. These include the new components of the sediment module developed in the context of this thesis, which are also presented separately in Chapters 3, 4 and 5.

CHAPTER 2

The TOPKAPI-ETH hydrology and sediment model

In this chapter are presented the components of the hydrology-sediment model TOPKAPI-ETH that have been used in this thesis. The hydrological module has been previously developed by Liu and Todini (2002, 2005), Fatichi *et al.* (2015) and Carenzo *et al.* (2009), while the sediment module has been developed in the context of this thesis. In the following, a summary of the main components of the hydrological and the sediment modules is provided. The components of the sediment module are also presented separately in Chapters 3, 4 and 5.

The model is fully distributed in space, meaning that the study basin is represented as a square grid in the horizontal dimension (see Fig. 2.1). In the vertical dimension, each cell of the domain is discretized into three layers: upper soil layer, lower soil layer and groundwater layer. The connectivity between cells and layers is provided by water fluxes both in the horizontal and in the vertical direction, on the surface and in the subsurface layers. On the surface, the connectivity is also provided by the fluxes of sediment on the hillslopes and in the channels. The model is suitable for application in mountainous regions, because it includes the processes of snow precipitation and snow and ice melt, and for continuous simulations over multi-decadal time periods with relatively high spatial and temporal resolution ($\Delta x \approx 100$ m, $\Delta t \approx 1$ h), thanks to its computationally inexpensive numerical approach.

2.1 The hydrological module

2.1.1 Climatic inputs

The TOPKAPI-ETH hydrological model is based on the following climatic inputs: precipitation, temperature and cloud cover transmissivity.

In this thesis, precipitation was given as a spatial map derived from the combination of a gridded precipitation dataset and rain gauge data. The spatial distribution provided by the gridded dataset was used to interpolate the rain gauge data, based on Thiessen polygons. A threshold temperature was used to define the transition between the liquid and solid state of precipitation. Time series of air temperature at three meteorological stations were given as input, and internally interpolated by the model depending on the elevation and a temperature lapse rate. Time series of cloud cover transmissivity were derived from the hourly sunshine duration measured at the same meteorological stations, following the empirical relation proposed by Kasten and Czeplak (1980). Cloud cover transmissivity affects the evaporation of the surface water content and therefore the generation of overland flow.

2.1.2 Hydrological processes

The hydrological processes used in the simulations of this thesis are: evapotranspiration, interception, snow precipitation and melt, infiltration, routing of water on the surface, subsurface and channel network and in the groundwater layer.

Evapotranspiration

Potential evapotranspiration (ET) is computed using the Priestley-Taylor equation, in which net radiation is a function of incoming shortwave radiaton, albedo and air temperature (Priestley and Taylor, 1972; Brutsaert, 2005). This is corrected for each month and land use type by means of a crop factor to distinguish between land uses and to account for the seasonality of leaf area index. The actual ET is the part of potential ET that is available from the liquid precipitation, interception and the soil moisture of the upper soil layer.

Interception

Interception of liquid precipitation is simulated as a simple bucket model, where the maximum storage capacity a linear function of the maximum height of water on the leaf surface, and the leaf area index. Interception of snow is not accounted for.

Snow cover

Snow cover is simulated as an additional layer on the cell surface, replenished by new snow fall and emptied by melt. Snowmelt is computed based on the enhanced temperature index model by Pellicciotti *et al.* (2005), which predicts melt above a given air temperature threshold and proportionally to the air temperature, the incoming shortwave radiation and the albedo (see also Carenzo *et al.*, 2009). The model does not account for snow avalanches, and the erosion produced by them.

Infiltration

The infiltration rate is computed with an explicit solution of the Green-Ampt equation by Salvucci and Entekhabi (1994). Overland flow on the surface is produced either when the soil is saturated, or when the precipitation rate exceeds the infiltration capacity of the soil.

Groundwater

The groundwater component is simulated as a linear reservoir, where the flow is proportional to the horizontal saturated hydraulic conductivity, the local slope and the volume of water stored in the groundwater layer of the cell. Groundwater may exfiltrate to the lower soil layer, and from here to the upper soil layer and the surface to feed overland flow (Liu *et al.*, 2005).

Water routing

Horizontal fluxes of water on the surface, in the subsurface and in the channels are based on the kinematic wave approximation. The solution of the kinematic wave in the model is based on the integration of the point equations over the dimensions of the pixel, to transform them into ordinary differential equations, i.e. non-linear reservoir equations (Liu and Todini, 2005).

The kinematic wave formulations for subsurface flow, overland and channel flow are reported below following Liu and Todini (2005).

Subsurface flow. The kinematic wave approximation for subsurface flow q_{SS} [m^2 s^{-1}] is given by:

$$\begin{cases} (\theta_s - \theta_r) L \frac{\partial \Theta}{\partial t} + \frac{\partial q_{SS}}{\partial x} = p \\ q_{SS} = S k_s L \phi^{\delta_{SS}} \end{cases} \tag{2.1}$$

where x is the main direction of flow along a cell, S is the cell slope, k_s [m s^{-1}] the saturated hydraulic conductivity, L [m] the thickness of the subsurface soil layer, δ_{SS} a parameter that depends on soil characteristics, i.e. a function of the pore size distribution index in the Brooks-Corey relations (Brooks and Corey, 1964; Todini, 1995), p [m s^{-1}] the intensity of precipitation, and Θ the mean saturation percentage along the vertical:

$$\Theta = \frac{1}{L} \int_0^L \frac{\theta - \theta_r}{\theta_s - \theta_r} dz \tag{2.2}$$

with θ the soil water content, θ_s the and θ_r the saturated and residual soil moisture content, respectively.

By combining the two equation in Eq. 2.1, and introducing the actual total water content:

$$\eta = (\theta_s - \theta_r) L \Theta \tag{2.3}$$

and the following substitution:

$$C_{SS} = \frac{L k_s S}{(\theta_s - \theta_r)^{\delta_{SS}} L^{\delta_{SS}}} \tag{2.4}$$

the following kinematic equation is obtained:

$$\frac{\partial \eta}{\partial t} = p - \frac{\partial (C_{SS} \eta^{\delta_{SS}})}{\partial x} \tag{2.5}$$

By assuming that the variation within a cell of the water content η is negligible, Eq. 2.5 can be integrated in the longitudinal and lateral directions of the cell i to obtain a non-linear reservoir equation:

$$\frac{\partial V_{SSi}}{\partial t} = p_i X^2 + Q^u_{iOF} + Q^u_{iSS} - \frac{C_{SSi} X}{X^{2\delta_{SS}}} V_{SSi}^{\delta_{SS}} \tag{2.6}$$

where V_{SSi} [m^3] is the volume of water stored in the cell i ($V_{SSi} = X^2 \eta_i$), X the cell dimension both in the flow and cross sectional direction, Q^u_{iOF} [m^3 s^{-1}] is the discharge entering the cell i as overland flow from the upstream contributing area, Q^u_{iSS} [m^3 s^{-1}] the discharge entering the cell i as subsurface flow.

Overland flow. The kinematic wave approximation for overland flow is given by:

$$\begin{cases} \frac{\partial h}{\partial t} = r - \frac{\partial q_{OF}}{\partial x} \\ q_{OF} = C_{OF} h^{\delta_{OF}} \end{cases} \tag{2.7}$$

where h [m] is the water depth over the surface, r [m s^{-1}] the water flux generated by precipitation excess and soil exfiltration on the given cell, $\delta_{OF} = 5/3$ and $C_{OF} = \sqrt{S}/n$ according to the Manning equation, where n [m$^{-1/3}$] is the Manning coefficient and S the cell slope.

By assuming that h is constant over the cell, the kinematic equation can be integrated both in the flow and cross sectional directions of the cell i, resulting in a non-linear reservoir equation:

$$\frac{\partial V_{OFi}}{\partial t} = r_i X^2 + Q^u_{iOF} - \frac{C_{OFi} X}{X^{2\delta_{OF}}} V_{OFi}^{\delta_{OF}} \tag{2.8}$$

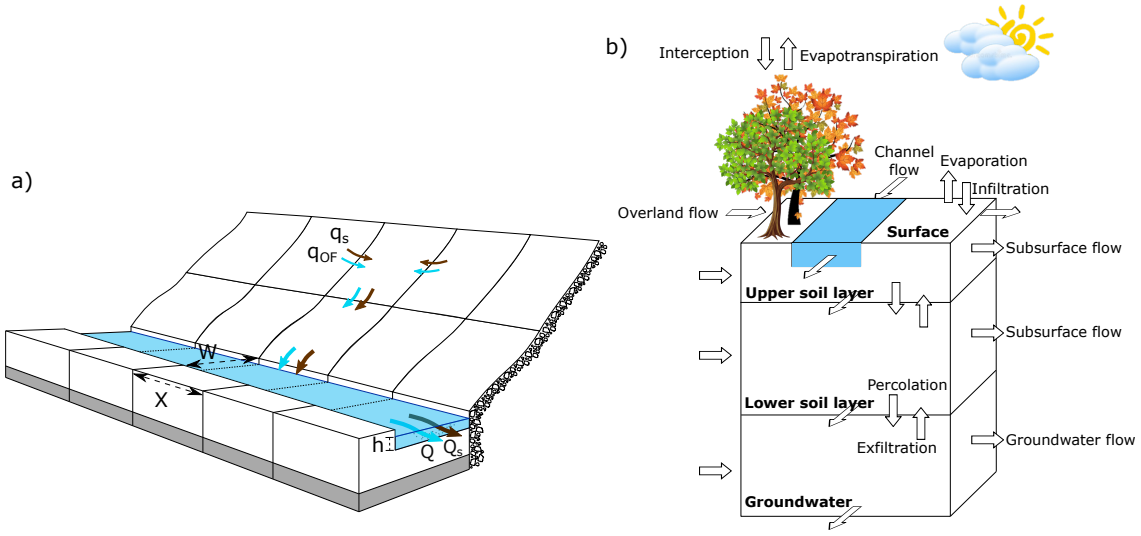

FIGURE 2.1: Schematic description of the TOPKAPI-ETH hydrological model. (a) The model domain is represented as a regular square grid of size X, where some cells belong to the hillslopes and others are partially occupied by the river network depending on its width W. The hillslope cells are connected by overland flow (q_{OF}) and sediment fluxes (q_s) according to a D4 routing scheme based on the steepest gradient. Each river cell receives water (Q) and sediment fluxes (Q_s) from the upstream river cells and from the hillslope cells. (b) Representation of the hydrological fluxes in a cell. Each cell is discretized into three vertical layers, connected between each other by percolation and exfiltration, and with the surface by evaporation and infiltration. The channel, surface and each subsurface layers are connected to the neighboring cells via horizontal fluxes. Vegetation affects the hydrological cycle by intercepting the precipitation, and by transpiration.

where V_{OFi} [m^3] the volume of water on the cell surface ($V_{OFi} = h_i X^2$), and Q^u_{iOF} the overland flow discharge entering the cell from the upstream area.

Channel flow. Analogously the equation in the channel network is:

$$\frac{\partial V_{Ci}}{\partial t} = r_{Ci} X W + Q^u_i - \frac{C_{Ci} W_i}{(X W_i)^{\delta_C}} V_{Ci}^{\delta_C} \tag{2.9}$$

where V_{Ci} is the volume of water in the river part of the cell only, the width of the cell X has been replaced by the width W_i of the river in the cell i, and Q^u_i is the discharge entering the cell from the upstream cells, r_{Ci} is the lateral drainage input.

In this way, four cascades of non-linear reservoirs describe the horizontal water fluxes in the two soil layers, on the surface and in the channel. These equations, or a suitable approximation of them, are solved analytically as explained in Liu and Todini (2002). Thanks to this analytical approach the use of numerical solutions is avoided. This significantly reduces the time requirements of the hydrological model, and guarantees a high numerical performance. The flow directions are determined based on the maximum difference in elevation between the active cell and the four surrounding cells connected along the edges, following a D4 approach. The active cell drains to a single downstream cell, but can receive contributions from up to three cells.

2.2 The sediment module

The sediment module of the TOPKAPI-ETH model was developed in the context of this thesis, and focuses on the simulation of erosion and transport of fine material in pre-Alpine basins. Fine

material in this case indicates the finer particles eroded across the catchment that are transported in suspension in the river channels (i.e. mainly clay, silt and fine sand). This material represents the most relevant contribution to the total sediment yield in most environments, including pre-Alpine basins, and therefore has been selected as the focus of the modelling framework (Schlunegger and Hinderer, 2003; Turowski *et al.*, 2010).

2.2.1 The conceptual model

In pre-Alpine basins, besides the contribution of diffuse soil erosion by overland flow, a key role in the sediment production is played by hillslope instabilities, e.g. landslides, and by fluvial incision in inner gorges that dissect the landscape (e.g. Van Den Berg *et al.*, 2012; Dürst Stucki *et al.*, 2012). In landslides, soil creep produces loose sediment at high rates, thus making them hotspots of the basin sediment availability. When the connectivity between the landslides and the river network is switched on, they contribute to the sediment flux (Schwab *et al.*, 2008; Clapuyt *et al.*, 2019). Inner gorges are areas along the river, where the river has incised deeply into the floodplain glacial deposits. They are frequent in previously glaciated environments, where the landscape is still adapting to the post-glacial base level via erosional waves that create knickpoints in the channel network (Schlunegger and Schneider, 2005). Here the river has oversteepened banks that provide high availability of sediment by frequent debris flows and collapses. In the following I will refer to them as incised areas.

For this reason, on top of the diffused overland flow erosion, sediment production from landslides and incised areas has been accounted for in the sediment module. The model is aimed at decadal time scale simulations, during which it is unlikely to observe the formation of new landslides in moderately active pre-Alpine environments. In the same way, over the typical model time scales it is not possible to observe the development of new incised areas, typically taking place over centuries or thousands of years. Therefore, landslides and incised areas have been considered in the model as fixed features of the landscape, which have to be defined by the user based on high-resolution DEMs and field surveys. Because of the considered time scales, a feedback between the geomorphology and the hydrology, as well as a dynamic update of the basin elevations has not been included. This is expected to be significantly relevant only on centennial time scales, which are addresses by landscape evolution models. In pre-Alpine basins glaciers are usually absent, or have a very small extent, therefore also the process of glacial erosion has been neglected. To guarantee a balance between model accuracy and model complexity, and to avoid overparameterization of it, also the processes of sediment storage in the floodplain, deposition and resuspension of the sediment in the channel, and subsurface erosion have not been included.

The drivers of soil erosion that have been considered are overland flow and channel flow. Erosion by overland flow can take place on the hillslopes, as long as the overland flow is greater than zero. Such erosion is enhanced on top of landslide bodies, where an additional sediment flux can be generated when the bed shear stress exceeds a given threshold. Channel flow can erode the landslides from their toes, and it can mobilizes the sediments in incised areas.

To summarize, sediment mobilization in the sediment module of TOPKAPI-ETH is possible through four processes (see Fig. 4.2 and Sect. 2.2.2):

- OF: overland flow erosion on the hillslopes
- LS_{HS}: overland flow erosion on landslide surfaces
- LS_R: river erosion at the toe of landslides
- I: river erosion in incised areas

The *OF* process is a diffuse process, because it happens on any hillslope cell of the basin provided that overland flow q_{OF} is greater than zero. LS_{HS}, LS_R and I simulate instead localized sources of sediment because they can only take place in the locations of landslides and incised areas.

It is assumed that in landslides and incised areas geomorphological activity continuously fractures sediment and makes it available for transport. In landslides, such sediment availability was assumed to depend on the sliding velocity of the landslide mass, therefore it is temporally variable and can be controlled by the user (see Sect. 2.2.3). The sediment availability in the incised areas is assumed to be unlimited. The sediment mobilized by these processes is assumed to consist mostly of fine sediment, and therefore it is transported in the river network as suspended sediment (see Sect. 2.2.4).

2.2.2 Processes of sediment mobilization

In this section, a complete description of the implementation of the sediment mobilization processes is provided. For the list of parameters used in this module the reader is referred to Appendix C.

Overland flow erosion (*OF*)

Erosion by overland flow on the hillslopes is assumed to follow a transport capacity approach. Therefore, the sediment flux on each hillslope cell always equals the transport capacity of overland flow. The overland flow transport capacity is modelled following Prosser and Rustomji (2000) as a function of the specific overland flow discharge q_{OF} [m^2 s^{-1}] and the surface slope S [m/m]:

$$qs_{OF} = \alpha q_{OF}^{\beta} S^{\gamma}, \tag{2.10}$$

where β and γ are transport exponents, which can be derived experimentally or from literature values (Prosser and Rustomji, 2000), and α [kg s$^{0.4}$ m$^{-4.8}$] is a calibration parameter that captures the effect of land surface and soil properties on erosion and sediment transport.

The sediment flux qs_{OF} is directed to the downstream cell with the steepest gradient. Erosion and deposition in each cell take place based on the imbalance between the incoming sediment flux and the transport capacity at the cell. If the incoming sediment flux exceeds the transport capacity of the active cell, there will be deposition. In the opposite case, overland flow in the active cell will erode the surface to fulfill the transport capacity. For example, sediment mobilized on steep mountain flanks, where overland flow is highly erosive, will partially deposit as soon as it reaches less steep floodplain cells, where the transport capacity is lower.

Sediment mobilization from incised areas (*I*)

Incised areas are located along the river network, therefore sediment can be mobilized from them only by river flow and is directly input into the channels. Sediment mobilization from incised areas takes place when the applied shear stresses on the river bed exceeds a threshold:

$$qs_I = k\,(\theta - \theta_c)^{\mu} \tag{2.11}$$

where qs_I [m^2 s^{-1}] is the specific sediment flux, θ and θ_c the dimensionless bed shear stress and critical bed shear stress, respectively. The dimensionless bed shear stress on the river bed is derived from the specific river discharge q [m^2 s^{-1}] and flow velocity u [m s^{-1}] computed by the hydrological module:

$$\theta = \frac{1}{G-1}\frac{qS}{u\,d_s}, \tag{2.12}$$

where G [-] is the specific gravity of sediment and d_s [m] the grain size. The parameters k and μ are calibration parameters that regulate the sediment flux. They depend on the grain size, sediment mass density and the magnitude and non-linearity of the morphological response to the hydrological forcing.

Sediment mobilization from landslides (LS_{HS}, LS_R)

Landslides are located on the hillslopes, and their toes may be adjacent to the river network. Therefore, sediment mobilization from landslides is possible both by overland flow erosion on their surfaces (LS_{HS}), and by river incision at their toes (LS_R). Sediment input from landslides is assumed to follow the same behaviour of the incised areas, with a threshold activation and non-linear response to the river and overland flow. Sediment mobilization from landslide toes adjacent to the river network is described by Eq. 2.11. To model the LS_{HS} process, the erosivity of overland flow on the landslide surface is described by a parameter λ for the competence of the gullies incised on the surface of landslides:

$$\lambda = \frac{X}{w_{LS}}. \tag{2.13}$$

λ describes the degree of development of gullies by means the width of an equivalent gully w_{LS}, which gives the confinement of overland flow on the landslide cells, and therefore the applied bed shear stress θ_{HS} generated by the overland flow q_{OF} [m^2 s^{-1}] on the surface of landslides:

$$\theta_{HS} = \frac{1}{G-1}\frac{q_{OF}\,\lambda\,S}{u\,d_s}. \tag{2.14}$$

To summarize, sediment can be mobilized from landslides by

- river erosion at their toes LS_R: $qs_R = k \cdot (\theta - \theta_c)^{\mu}$
- overland flow on their surfaces LS_{HS}: $qs_{HS} = k \cdot \left(\frac{1}{G-1}\frac{q_{OF}\,\lambda\,S}{u\,d_s} - \theta_c\right)^{\mu}$

Sediment that is mobilized from the landslide toes is a direct input into the river network, while material from the surfaces is routed on the hillslopes until the river network. Here it is assumed that overland flow can only transport a sediment load up to the transport capacity defined by qs_{HS}, which therefore defines the connectivity between the hillslope sediment sources and the river network.

2.2.3 Sediment availability in landslides

Material is exported from the landslides by the river flow at their toes and by overland flow from their surfaces, and is assumed to be made available by the sliding of the landslide mass. Therefore, the model simulates the temporal variability of the sediment volume available for mobilization at landslides. The slip rates of landslides u_{LS} define the recharge rate of the such sediment reservoir and were assumed proportional to the soil moisture v, thickness H and slope $\hat{\alpha}$ of each landslide, according to the Bingham plastic model proposed by Schwab *et al.* (2007):

$$u_{LS} = c_{LS}\,v\,H^2\,\sin\hat{\alpha}. \tag{2.15}$$

The parameter c_{LS} represents the level of hillslope activity and shifts the distribution of landslides velocities by Eq. 2.15 towards lower or higher values.

By combining the recharge rate Eq. 2.15 with the export sediment fluxes given by Eq. 2.11 and 2.14, the volume of sediment available for transport at each landslide V is:

$$\frac{dV}{dt} = u_{LS} A_{LS} - \sum_{i=1}^{n_R} qs_{Ri} w_{Ri} - \sum_{i=1}^{n_{HS}} qs_{HSi} w \,, \tag{2.16}$$

where A_{LS} is the area of contact between the landslide and the river network, n_R and n_{HS} the number of river and hillslope cells where runoff mobilizes sediment from the landslide, qs_R and qs_{HS} the sediment flux from the toe and the landslide surface respectively, w_{Ri} the river width in the cell i and w_{LS} the gully width on landslide. Please see Fig. 5.2 in Chapter 5 for a graphical summary of these processes.

2.2.4 Suspended sediment transport

Sediment mobilized by OF, LS_{HS} LS_R and I is routed independently from each other both on the hillslopes (for OF and LS_{HS}) and in the channel. In this way, the sediment flux at each river network cell is given by the sum of four sediment waves, which provide a temporally variable information of the sediment provenance.

In the channel, the transport of sediment of each sediment wave is assumed to take place in suspension and is approximated as an advection process, neglecting the diffusion process. The advection equation is solved by following the same numerical approach used for water flow. The equation of suspended sediment flux in the channel along the flow direction is:

$$\frac{\partial h SSC}{\partial t} = \frac{E}{W} - \frac{\partial q SSC}{\partial x}, \tag{2.17}$$

where q [m^2 s^{-1}] is the river discharge, SSC [g m^{-3}] is the suspended sediment concentration, W is the river width and E [g m^{-1} s^{-1}] is sum of the sediment flux between the water column and the river bed, and the input from local sediment sources. By following the approach used in Eq. 2.7 and 2.8, the variables were assumed to be constant within each grid cell to allow integration of Eq. 2.17 along the width W and length X of the river cell, and then solved analytically as a first-order ordinary differential equation:

$$\frac{\partial V_i SSC_i}{\partial t} = E_i X + Q_{in} SSC_{in} - \frac{U_i}{X} SSC_i V_i, \tag{2.18}$$

where U_i [m s^{-1}] the mean flow velocity, SSC_i and E_i are the mean values of SSC and E inside the grid-cell. Q_{in} and SSC_{in} are the discharge and sediment concentration entering the cell i from the upstream grid cells. It is worth noticing that the sediment flux between the river bed and the water column E has been taken equal to zero in this thesis.

While the assumption of neglecting the diffusion of the sediment wave is necessary to allow analytical resolution of the suspended sediment transport equation, it introduces an approximation in the representation of the sediment wave velocity, by assuming it equal to the flow velocity. To account for the delay in the sediment wave observed in nature with respect to the flow, an additional parameter that reduces the flow velocity U_i in Eq. 2.18 could be introduced in the future.

CHAPTER 3

Modelling impacts of spatially variable erosion drivers on suspended sediment dynamics

---

Published in *Earth Surface Dynamics*, authored by Giulia Battista, Peter Molnar and Paolo Burlando.

Abstract

Suspended sediment load in rivers is highly uncertain because sediment production and transport at catchment scale are strongly variable in space and time, and affected by catchment hydrology, topography, and land cover. Among the main sources of this variability are the spatially distributed nature of overland flow as an erosion driver, and of surface erodibility given by soil type and vegetation cover distribution. Temporal variability mainly results from the time sequence of rainfall intensity during storms and snowmelt leading to soil saturation and overland flow.

We present a new spatially distributed soil erosion and suspended sediment transport module integrated into the computationally efficient physically based hydrological model TOPKAPI-ETH, with which we investigate the effects of the two erosion drivers - precipitation and surface erodibility - on catchment sediment fluxes in a typical pre-alpine mesoscale catchment. By conducting a series of numerical experiments, we quantify the impact of spatial variability of the two key erosion drivers on erosion-deposition patters, sediment delivery ratio, and catchment sediment yields.

Main findings are that the spatial variability of erosion drivers affects sediment yield by (i) increasing sediment production due to a spatially variable precipitation, while decreasing it due to a spatially variable surface erodibility, (ii) favoring the clustering of sediment source areas in space by surface runoff generation, and (iii) decreasing their connectivity to the river network by magnifying sediment buffers. The results highlight the importance of resolving spatial gradients controlling hydrology and sediment processes when modelling sediment dynamics at the mesoscale, in order to capture the key effects of sediment sources, buffers, and hillslope hydrological pathways in determining the sediment signal.

Battista G, Molnar P, Burlando P. 2020. Modelling impacts of spatially variable erosion drivers on suspended sediment dynamics. *Earth Surface Dynamics* 8(3): 619–635.
https://esurf.copernicus.org/articles/8/619/2020/

3.1 Introduction

Fine sediment produced in catchments by upland erosion and transported by rivers as suspended load is an important part of the global sediment budget (e.g. Peucker-Ehrenbrink, 2009) and an important driver of water quality and aquatic biota in rivers (e.g. Bilotta and Brazier, 2008). Human activity strongly interacts with the natural processes of suspended sediment production and transport, on the one hand by practices that enhance soil erosion, like agriculture, mining and deforestation, and on the other hand with the construction of sediment retention structures such as dams (e.g., Syvitski *et al.*, 2005; Montgomery, 2007; Syvitski and Kettner, 2011; Borrelli *et al.*, 2017). In the context of enhanced soil erosion, phenomena like the loss of soil productivity, the reduction of water quality due to higher turbidity and concentration of pollutants, and accelerated reservoir siltation are expected (e.g. Pimentel *et al.*, 1987; Davies-Colley and Smith, 2001). The combined effect of enhanced soil erosion and sediment retention by dams modifies the river sediment equilibrium and can result in river incision in the case of sediment starvation, contributing to undermine the stability of bridges and other infrastructures, and leading to coastal erosion (Kondolf, 1997; Chen and Zong, 1998; Schmidt and Wilcock, 2008). The opposite case of excessive sediment load in rivers may also lead to an increase in flood risk in alluvial floodplains due to sediment deposition (Yu, 2002; Walling, 2006; Rickenmann *et al.*, 2016). The intensity of these effects is expected to grow in the future, as the magnitude and number of highly erosive extreme precipitation events are foreseen to increase in some parts of the world due to climate change and/or anthropic influence on land cover (e.g. Yang *et al.*, 2003; Nearing *et al.*, 2004; Peleg *et al.*, 2020). Therefore, the monitoring and understanding of suspended sediment dynamics is essential to explain how disturbances produced by such human interventions may affect the sediment balance.

Fine sediment yield in rivers is usually estimated from intermittent measurements of sediment concentration by means of sediment-discharge rating curves (see Gao (2008) for a review). However, the development and use of these curves is often highly problematic because of the strong non-uniqueness of suspended sediment concentrations (SSCs), especially in small to medium sized catchment (up to 1000 km^2). Here, the same value of discharge (Q) often leads to a wide range of SSCs, producing highly scattered SSC-Q rating curves (e.g., Walling, 1977; Walling and Webb, 1982; Ferguson, 1986; Asselman, 2000; Horowitz, 2003). The strong variability in SSC is attributed to the high non-linearity of the sediment production and transport processes in time and space, and the presence of threshold and feedback mechanisms in sediment mobilization and transfer (e.g., Asselman, 1999; Collins and Walling, 2004; Seeger *et al.*, 2004; Fryirs *et al.*, 2007; Bracken *et al.*, 2015).

Temporal and spatial variability in suspended sediment transport can originate from several sources (see Vercruysse *et al.* (2017) for a review). Among the sources of temporal variability, the role of hydrometeorological conditions (e.g. rainfall, antecedent wetness conditions, runoff) has been widely investigated, with a particular focus on the shape and direction of the hysteresis loops of the SSC-Q relation (Smith *et al.*, 2003; Seeger *et al.*, 2004; Zabaleta *et al.*, 2007; Duvert *et al.*, 2010; Dominic *et al.*, 2015; Misset *et al.*, 2019). Other sources of variability are the exhaustion of preferential sediment sources, the activation of new ones, and changes in the connectivity of such sources to the river network. These aspects have been studied for example as consequences of land use change and flow regulation (Olarieta *et al.*, 1999; Siakeu *et al.*, 2004; Costa *et al.*, 2018a). Variability of sediment transport in space depends on the distribution of sediment sources within the catchment, the catchment sediment connectivity, and the efficiency of sediment transport within the stream network. Wass and Leeks (1999) related differences in sediment loads across the basin to geomorphic and climatic gradients, while Fryirs and Brierley (1999) and Lang *et al.* (2003) reconstructed the change of sediment sources in time and their coupling with the channels. The problem of catchment sediment connectivity has been addressed from a conceptual point of

view, by introducing the ideas of structural and functional connectivity, to distinguish between the physical connection among landscape units and the connectivity generated by the system process interactions (Wainwright *et al.*, 2011; Fryirs, 2013; Bracken *et al.*, 2015). Based on these concepts, several indices have been introduced to assess sediment connectivity in a river basin (see Heckmann *et al.* (2018) for a review).

The above studies highlight the need to account for both types of variability (temporal and spatial) in order to investigate basin sediment dynamics. Including this variability is especially important at the medium and large catchment scale and in mountainous environments, where the gradients of climatic and physiographic variables are most relevant. Few studies have focused specifically on the impacts of spatially variable erosion drivers on suspended sediment dynamics in such environments. A systematic investigation of this research gap can be performed by means of numerical models that include the main hydrological processes, their temporal dynamics and distribution in space, as well as their interaction with the topography and morphology of the basin. Several existing models are partially suitable for this task. The main limitations are that many are only suitable for event-applications (Answers (Beasley *et al.*, 1980), KINEROS (Woolhiser *et al.*, 1990), WEPP (Nearing *et al.*, 1989)) or present simplified hillslope hydrology and runoff formation solutions, as in the case of WATEM/SEDEM (Van Rompaey *et al.*, 2001), landscape evolution models, e.g. Caesar-Lisflood (Coulthard *et al.*, 2013), SIBERIA (Hancock *et al.*, 2000), or some large-scale sediment flux models, e.g. WBMsed (Cohen *et al.*, 2013) and Pelletier (2012). More suitable approaches are tRIBS (Francipane *et al.*, 2012), which includes a physically based hydrological component suitable for long-term process simulations, and DSHVM (Doten *et al.*, 2006), which features a detailed hydrology-vegetation component and sediment module. However, the number of processes represented in these two models requires a high computational power and their applications have so far been limited to small basins and/or short time scales. Finally, Tsuruta *et al.* (2018) present a spatially distributed model especially for large basins, which, being based on a land-surface model, features an approximated coarse-scale representation of hydrological and sediment connectivity on the hillslopes.

In this work, we present a modelling approach especially suitable for alpine catchments with highly variable climate and complex topography, that integrates a new spatially distributed soil erosion and suspended sediment transport module within the computationally efficient, physically based hydrological model TOPKAPI-ETH (Fatichi *et al.*, 2015). The model combines unsteady simulation of surface and subsurface water fluxes with a simple hillslope erosion and sediment transport component. The sediment component is simple by design, to avoid over-parameterization and to maintain computational efficiency enabling applications to medium and large catchments. The model allows continuous high spatial resolution (Δx=100 m) simulations to track overland flow and hillslope sediment transport by local changes in soil moisture dynamics produced by rainfall, snowmelt and lateral drainage over long periods of time. The model also allows high temporal resolution (Δt=1 hr) simulations to capture fast runoff response to the hydrological drivers, which, together with the topographically driven flow routing, reproduces the connectivity of water and sediment pathways in the catchment over time. The combined hydrology-sediment model is unique in its process completeness and applicability to mesoscale catchment simulation at high resolutions, compared to most other approaches.

The overall aim of this research is to provide a state-of-the-art catchment hydrology-sediment modelling framework to better understand the sources of variability in suspended sediment concentrations and their effects on predictions of sediment yield. Accordingly, we conducted numerical experiments on a mesoscale pre-alpine river basin, where we turned on and off the spatial variability in two key erosion drivers - rainfall and surface erodibility - to quantify their individual and combined effect on suspended sediment mobilization and transfer. We address the following specific research questions: (RQ1) Does fully distributed physically-based hydrology-sediment

modelling predict variability in SSC-Q relations that is in agreement with observations? We argue which key hydrological processes are needed in such a model and why. (RQ2) Can we identify the location of sediment sources and quantify their productivity and connectivity with such a modelling approach? We assess the effect of the spatial distribution of rainfall and surface erodibility on hillslope erosion-deposition patterns and sediment mobilization, and we quantify the sediment source connectivity to the river network by analysing the sediment delivery ratio along the main stream and in tributary basins. (RQ3) Is the effect of spatially distributed erosion drivers visible in sediment yield at the catchment outlet? We show how integration of the spatially variable inputs in space impacts sediment yield under different scenarios.

3.2 Methods

3.2.1 Hydrology-sediment model description

The model we present in this work is an extension of the hydrological model TOPKAPI-ETH (Fatichi *et al.*, 2015), which we integrated with a new hillslope erosion and channel suspended sediment flow module. The TOPKAPI-ETH hydrological model was chosen because of its spatially distributed nature and physically based representation of the major hydrological processes, combined with a reasonable computational demand. The model is based on a regular square grid discretization in space and a 3-layer vertical discretization of the subsurface. The river network is identified in the domain by means of a flow accumulation algorithm based on the topography. The transition between hillslope and channel process description, i.e. the beginning of the model river network, is set by a user-defined critical upstream area, or river initiation threshold RT, above which water flow is modelled as channel flow. Each river network cell can be fully or partially covered by the stream, depending on the actual stream width and grid cell resolution.

In TOPKAPI-ETH surface and subsurface flow is simulated by the kinematic wave approximation, with resistance to flow given by surface roughness and soil transmissivity as a function of soil properties. Water may saturate the soil locally and lead to overland flow generation by saturation excess or by infiltration excess in case of high rainfall intensities. Soil is dried by evapotransporation, lateral drainage and percolation to groundwater storage. The model includes snow cover accumulation and melt, which are important in the water balance of alpine basins. For further details about the model see Fatichi *et al.* (2015). TOPKAPI-ETH allows long-term, high resolution simulations (time step Δt=1hr, grid size Δx=100 m) in medium and large catchments (>1000 km^2), even when integrated with a sediment mobilization and transfer component, since the kinematic wave approximation of the surface and subsurface flow routing are solved analytically (Liu and Todini, 2002).

In the new sediment module of TOPKAPI-ETH, the mobilization and routing of fine sediment on the hillslopes takes place by action of overland flow, which is assumed to transport sediment at its maximum capacity. As a consequence, deposition and erosion can occur on the hillslopes at a rate D [kg m^{-3} s^{-1}] depending on the hydraulic and topographic properties of the cells along the flow path:

$$D = \nabla \cdot q_s, \tag{3.1}$$

where q_s [kg m^{-2} s^{-1}] is the overland flow transport capacity, modelled following Prosser and Rustomji (2000) as a function of the specific overland flow discharge q [m^2 s^{-1}] and the surface slope S [m/m]:

$$q_s = \alpha q^{\beta} S^{\gamma}, \tag{3.2}$$

where β and γ are transport exponents, and α [kg s$^{0.4}$ m$^{-4.8}$] is a calibration parameter that captures the effect of land surface and soil properties on erosion and sediment transport. The sediment flux

q_s is directed to the downstream cell with the steepest gradient. Sediment inflow into a cell can be from one or more upstream cells. Once the sediment mobilized and routed on the hillslopes reaches the channel, it is assumed to move as suspended sediment load.

The suspended sediment flux in the river network is treated as an advection process and solved with the same numerical methods used for water flow. The 1D equation of suspended sediment flux in the channel, integrated over the river cross-section, is:

$$\frac{\partial AC}{\partial t} = E - \frac{\partial QC}{\partial x}, \tag{3.3}$$

where Q [m^3 s^{-1}] is the river discharge, C [g m^{-3}] is the SSC, A [m^2] is the cross-section area of flow and E [g m^{-1} s^{-1}] represents the exchange of sediment with the bed and local sediment sources. By following the reasoning of Liu and Todini (2002), Eq. 3.3 can be integrated along the length of the grid cell (i.e. in the flow direction), within which the values of the variables are assumed to be constant, and then solved analytically as a first-order ordinary differential equation:

$$\frac{\partial V_i C_i}{\partial t} = E_i X + Q_{in} C_{in} - \frac{U_i}{X} C_i V_i, \tag{3.4}$$

where X [m] is the length of the grid cell size, V_i [m^3] the volume of water inside a cell ($V_i = A_i X_i$), U_i [m s^{-1}] the mean flow velocity, C_i and E_i are the mean values of C and E inside the grid-cell. Q_{in} and C_{in} are the discharge and sediment concentration entering the cell i from the upstream grid cell $(i-1)$.

3.2.2 Study site

We chose to investigate the research questions outlined above on the Kleine Emme river basin, a pre-alpine catchment located in central Switzerland. Here the natural regime of water and sediment flow is almost unaltered, and the basin is sufficiently large for spatial variability in erosion drivers to have an impact. The basin has an area of 477 km^2, an elevation range of 430-2300 m. a.s.l. and a mean annual precipitation of 1650 mm (Fig. 3.1a). The mean annual discharge at the outlet is 12.6 m^3/s. The catchment is mostly natural, with more than 50% of the surface covered by forest and grassland (Fig. 3.1c). No use of water for irrigation or hydropower is known and significant sediment-retaining infrastructures are absent. Moreover, the absence of glaciers means that fine sediment production in the basin is mostly driven by overland flow and rainfall processes. Finally, the diverse geomorphology of the basin has been the subject of several studies and long-term estimates of denudation rates are available (e.g., Schlunegger and Schneider, 2005; Schwab *et al.*, 2008; Dürst Stucki *et al.*, 2012; Van Den Berg *et al.*, 2012; Clapuyt *et al.*, 2019).

Measurements of precipitation, air temperature and sunshine duration are available from automatic weather stations located inside or in the vicinity of the basin operated by MeteoSwiss. The information about the spatial distribution of precipitation inside the basin is available from the 1x1 km daily gridded product of MeteoSwiss RhiresD (Frei and Schär, 1998; Schwarb, 2000). Streamflow is monitored at Werthenstein and at the basin outlet by the Federal Office of the Environment (FOEN) and at Sörenberg by the Canton Luzern (Fig. 3.1a). FOEN also provided the cross section measurements for the main channel of the river and measurements of suspended sediment concentration. SSCs have been manually sampled at the outlet since 1974, but with a regular frequency of two samples a week only since 2004. Because of the low temporal resolution of these measurements, which is typical of many river sediment monitoring networks, we expect this dataset to miss extreme SSCs generated by flood events or very localized sediment sources. Finally, the information about soil type and depth for the basin is available from the soil map of

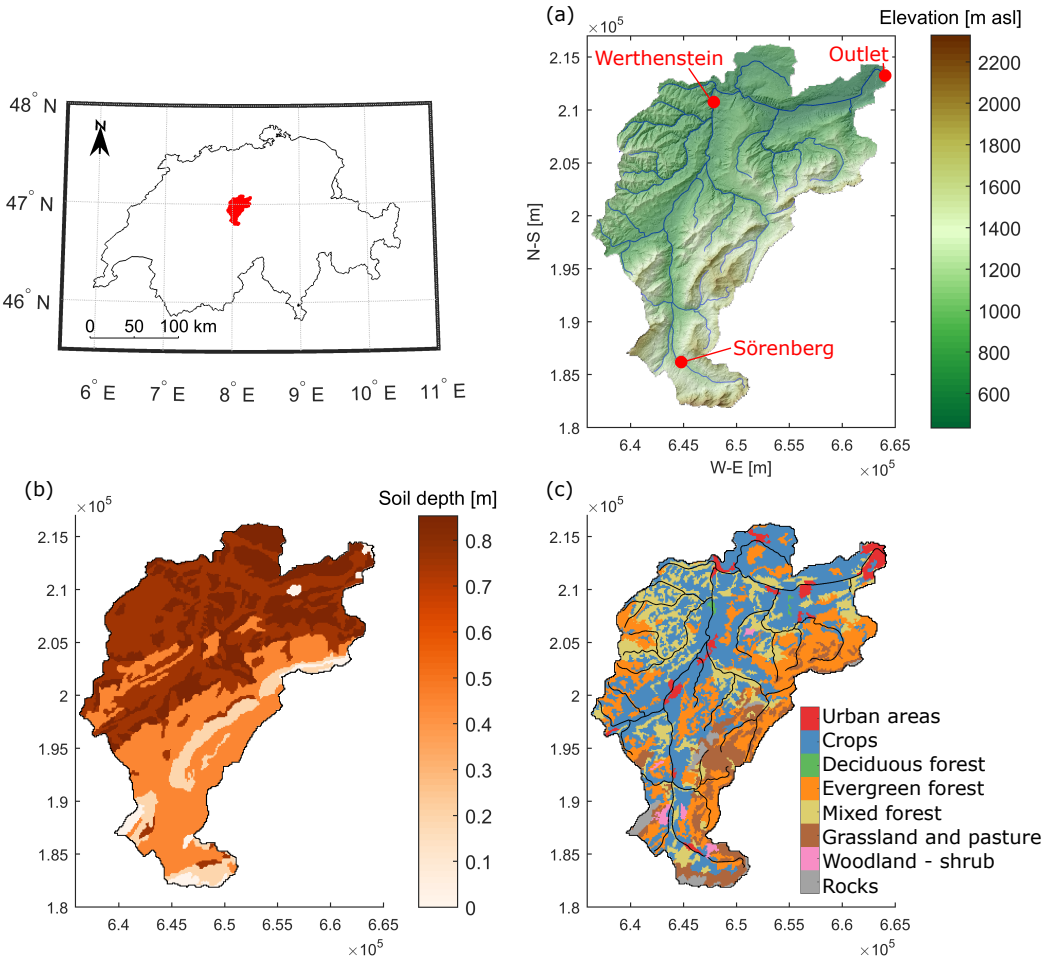

FIGURE 3.1: (a) Digital Elevation Model (DEM) of the Kleine Emme basin and location of discharge gauges (source SwissAlti3D, 2017), (b) Soil depth, derived from the Swiss soil map (Bodeneignungskarte, 2012) and (c) Land cover derived from Corine Land Cover map (CLC, 2014). The coordinate system is CH1903.

Switzerland (Bodeneignungskarte, 2012) (Fig. 3.1b) and land cover is provided by the Corine Land Cover dataset (Fig. 3.1c).

3.2.3 Model setup and calibration

3.2.3.1 Hydrology

Given the period of availability of suspended sediment measurements in the Kleine Emme, the simulation was set up for the years 2003 to 2016, where the first year is considered a warm-up period. The meteorological input data required by the hydrological component of TOPKAPI-ETH are hourly precipitation, air temperature and cloud cover. The precipitation input file was created by combining station and gridded precipitation datasets following the approach of Paschalis *et al.* (2014). In this approach hourly precipitation measured at the rain gauges was spatially interpolated to match the spatial distribution of the daily precipitation in the gridded RhiresD dataset. The hourly time series of measured air temperature were extrapolated across the model domain to different elevations with a temperature lapse rate of -5.5 °C/km. Cloud cover transmissivity was derived from

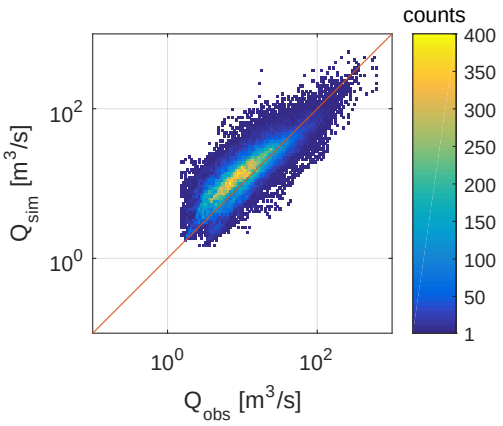

FIGURE 3.2: Performance of the hydrological model: density plot of observed vs simulated hourly discharges at the outlet of the river basin for the period 2004-2016.

TABLE 3.1: Hydrological performance for the simulation period 2004-2016 at the three flow monitoring stations in terms of correlation coefficient (r), Nash-Sutcliffe efficiency (NSE) and root mean square error (RMSE) for data simulated at the hourly resolution and aggregated to daily, monthly and annual values.

	Outlet			Werthenstein			Sörenberg (2005-16)		
	r [-]	NSE [-]	RMSE $[m^3/s]$	r [-]	NSE [-]	RMSE $[m^3/s]$	r [-]	NSE [-]	RMSE $[m^3/s]$
Hour	0.84	0.69	0.75	0.84	0.65	0.74	0.63	0.72	1.43
Day	0.91	0.80	0.53	0.90	0.78	0.52	0.80	0.56	0.83
Month	0.93	0.76	0.28	0.92	0.77	0.26	0.88	0.77	0.38
Year	0.93	-	0.18	0.92	-	0.13	0.79	-	0.10

the hourly sunshine duration measurements following the empirical relation proposed by Kasten and Czeplak (1980).

The model was run at a Δx=100 m spatial resolution and a constant time step Δt=1 hour. To initiate the model calibration, realistic values of the hydrological parameters were assigned based on the soil characteristics and previous investigations (Paschalis *et al.*, 2014; Pappas *et al.*, 2015). The soil hydraulic conductivity and the residual and saturation soil water content parameters were then adjusted in order to maximize the performance of the hydrological model in terms of correlation coefficient (r), Nash-Sutcliffe efficiency (NSE) and root mean square error (RMSE) for discharge measured at three streamflow gauging stations.

The final configuration of the hydrological model performed very well in reproducing the observed discharge at the outlet and at Werthenstein (see Table 3.1 and Fig. 3.2). Discharge data are available at a sub-daily resolution at Sörenberg only from the year 2005; therefore, the evaluation of the performance at this station does not consider the first year of simulation. The model performance at this station is slightly worse, probably also due to the lower accuracy of the measurements, but still satisfactory.

3.2.3.2 Setup of the sediment module

The inputs needed to run the hillslope erosion and suspended sediment transport modules are the parameters α, β and γ in Eq. 3.2. The β and γ parameters are assumed spatially uniform and equal

to 1.4, following Prosser and Rustomji (2000). The parameter α contains information about the soil and land surface properties that influence the rate of soil erosion. We derived the spatial distribution of α by the product of the soil erodibility parameter K of the Universal Soil Loss equation (USLE), computed for Switzerland by Schmidt *et al.* (2018), and the land use USLE parameter C, which we derived from Yang *et al.* (2003) (see Fig. A.1). In this way we implicitly account for the influence of particle size distribution, organic matter content, soil structure, permeability, surface roughness and vegetation cover in determining the spatial distribution of surface erodibility. A comparable approach is proposed by Hancock *et al.* (2017).

The ratio between the product of C and K of the different classes was then kept constant in the calibration process and α was calibrated by multiplying the CK values by a spatially constant parameter α_1:

$$\alpha(x,y) = \alpha_1 C(x,y) K(x,y), \tag{3.5}$$

where x and y are coordinates in space. With respect to channel processes, the water column-bed exchange and local sediment source term E in Eq. 3.3 is unknown. In the Kleine Emme significant deposits of fine sediment in the river bed are not present and bedrock is often exposed, indicating an efficient fine sediment transport downstream (Schwab *et al.*, 2008). Furthermore, the infrequent SSC measurements do not allow to quantify the term explicitly. This leads us to assume that E=0 for this river. However, by setting E=0 we neglect also local sediment sources along the channels, which is probably an approximation of the sediment production processes in this case study. Also on the hillslopes, localized sediment sources are not explicitly modelled and are present only insofar they are represented by high C and K values. The lack of explicit inclusion of point sediment sources and their modelling is a limitation of the current approach, which we will address in future work.

3.2.3.3 Calibration of the sediment module

We found that the parameters that have the highest influence on matching the observed and simulated SSC at the outlet are the river initiation threshold RT, i.e. the extension of the modelled river network, and the α_1 constant, defining the soil erodibility. RT has a small influence on discharge, as shown by Table A.2, while it is a relevant parameter for the modelling of hillslope erosion and sediment transport. Since fine sediment mobilization can only take place on the hillslopes, the extension of the channels onto the hillslopes influences the magnitude of the sediment input into first-order channels and subsequently downstream through the river network.

In the calibration of the model we focused on measurements below the 85th percentile, because flood events in the SSC data are likely under-sampled, due to the monitoring strategy, and the model is expected to underestimate the SSC extremes due to the simplified representation of the sediment mobilization processes. The calibration was performed by matching the trend and the dispersion of the measured and modelled SSC-Q cloud of points. This was done by visual matching and by comparing the mean and variance of the observed SSCs. The final calibrated parameters are α_1=0.0138 kg m$^{-1.8}$ s$^{-2.6}$ and RT=0.4 km^2. The histogram of α and its spatial distribution are shown in Fig. 3.3a and 3.7d, respectively; the spatial mean of α is 0.3412 kg s$^{0.4}$ m$^{-4.8}$. We note that the calibrated river initiation threshold is very close to the drainage area that Schlunegger and Schneider (2005) propose as the threshold area at which channelized processes start dominating over hillslope processes in the development of the landscape in this study basin (0.1-0.2 km^2).

Using this parameterization, the measured SSC-Q cloud of points is captured very well for moderate discharges (Fig. 3.3b), whereas the concentrations at highest discharges are underestimated, as expected. Overall, 90.4% of the simulated SSCs fall within the 5th and 95th percentile of the observations and, if the simulated SSCs are sampled at the hours of observations and compared

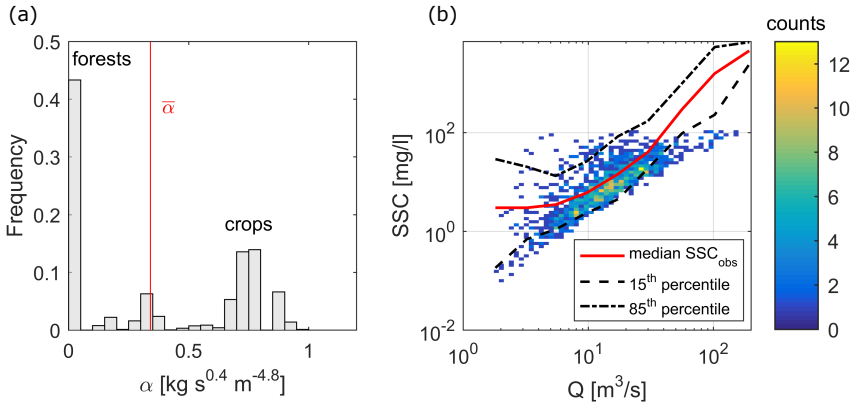

FIGURE 3.3: (a) Frequency distribution of the calibrated surface erodibility parameter α, with mean α indicated with the red line; (b) density plot of the simulated SSC at outlet compared with measurements, the lines show the median (red) and 15th and 85th percentile (black dashed) of the observations.

to the observations limited to their 85th percentile, the observed SSC mean and variance are reproduced with very small errors ($\overline{SSC}_{sim} = 12.40\ mg/l$, $\overline{SSC}_{obs} = 12.20\ mg/l$; $\sigma^2_{sim} = 210.47\ mg/l$, $\sigma^2_{obs} = 233.15\ mg/l$) (Fig. A.2). We attribute the underestimation of high sediment concentrations (above 85th percentile) to missing localized sediment sources, i.e. mass wasting processes in the model, which are responsible for point sediment sources, like landslides, debris flows and bank erosion. Further evaluation of the suspended sediment module performance can be found in Table A.1 and Fig. A.3.

3.3 Erosion driver numerical experiments

In order to investigate the processes leading to the scatter in the SSC-Q relation and how they affect the spatial organization of sediment transport, we performed simulation experiments that quantify the role of spatial variability in two key erosion drivers - precipitation and surface erodibility. Precipitation is the main hydrological driver of hillslope erosion through the overland flow term q^β in Eq. 3.2, while surface erodibility is represented by the parameter α in Eq. 3.2.

We designed four numerical experiments by combining spatially variable and/or uniform distributions of the two erosion drivers (Fig. 3.4). The reference experiment (SIM 1) accounts for the highest level of complexity by considering both precipitation and erodibility variable in space. This is the experiment with which the model was calibrated (see section 3.2.3.3). The second experiment (SIM 2) aims to quantify the role of the spatial variability in precipitation, by reducing it to be uniformly distributed in space. The temporal variability was preserved by setting the hourly precipitation in each cell equal to the mean hourly precipitation over the catchment. The third experiment (SIM 3) is designed to investigate the role of the spatial variability in surface erodibility by reducing it to uniform surface erodibility throughout the basin, equal to the mean value of the calibrated spatial distribution of α. A fourth experiment (SIM 4), where the spatial variability in both drivers was reduced to uniform, was run to quantify the combined effect of the two erosion drivers.

3.4 Results

In section 3.4.1 we evaluate the spatio-temporal variability in sediment mobilization and transport and the scatter of the SSC-Q relation it produces by the fully distributed erosion drivers in SIM 1

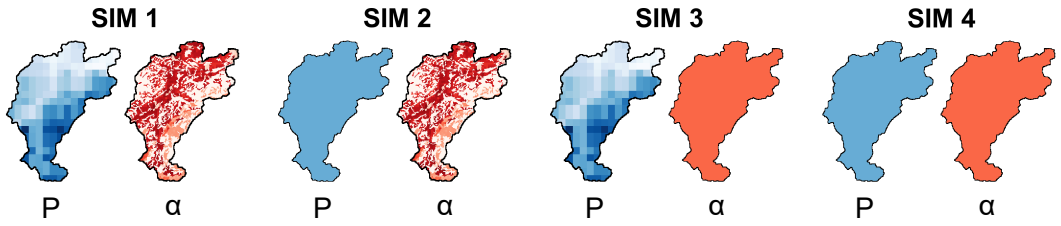

FIGURE 3.4: Summary of model runs: in SIM 1 sediment mobilization and transfer are driven by a spatially distributed precipitation (P) and surface erodibility (α), in SIM 2 and SIM 3 the spatial variability in precipitation and surface erodibility have been removed, respectively, and in SIM 4 both spatial variabilities have been removed.

(RQ 1). The spatial distribution of suspended sediment transport is then evaluated in subsequent sections and related to the hydrological response of the basin (RQ 2). We compare the activation of sediment sources and the sediment mobilization in the four simulations (section 3.4.2) and we quantify the connectivity of sediment transfer by means of the sediment delivery ratio (section 3.4.3). Finally, in section 3.4.4, we analyze the sediment load at the outlet as a function of the sediment spatial properties observed in the different scenarios (RQ3).

3.4.1 Spatio-temporal variability in erosion and sediment transport

The modelled scatter in the SSC-Q relation in SIM 1 explains about 30% of the measured concentration range for discharges up to the 85th percentile, while it shows a much more significant underestimation for the highest flows (Fig. 3.3b). For a comparison between the SSC-Q scatter generated by the different scenarios of erosion drivers, the reader is referred to Fig. A.5 and A.6. In the following we analyse the sources of this variability, by showing the time series of discharge and the sediment load and concentration for one representative year (Fig. 3.5a) and by analysing the pattern of erosion and deposition across the basin from the entire simulation period (Fig. 3.5b).

High sediment fluxes in April and May, which are evident both in observations and in the model (Fig. 3.5), indicate the contribution of snowmelt to discharge and the erosion of the surface by widespread overland flow. Summer events (storms) provide a small contribution to the yearly sediment yield. However, they generate some of the highest sediment concentrations in the model even though the runoff remains low. As expected, high SSCs are not observed in the measurements during summer, because sediment is rarely sampled during summer floods (see section 3.2.2). In winter months, snow covers the majority of the catchment and maintains the sediment flux very close to zero in both observations and simulations (Fig. 3.5a).

Most of the erosion is simulated in the south-eastern part of the basin, where slopes are steeper, soil is thinner and the highest precipitation, snow accumulation and melt occur (Fig. 3.5b). In these regions, it is easier to saturate the soil and generate runoff over larger areas that merge and generate connected areas of overland flow, thus producing wide erosional surfaces on steep mountain flanks. Deposition is simulated at the valley bottoms or at locations of slope reduction. In the north-western part of the basin, overland flow remains constrained to the channel headwaters due to the deeper soil and to the higher drainage density of the area. This distribution of erosion is coherent with the different geomorphological characteristics of the two areas of the basin, as further discussed in section 3.5.2. We observe that, because of the transport capacity approach in the hillslope transport module, areas of strong erosion are often associated with significant deposition downstream. In the following, we will refer to these areas of strong erosion as sediment source areas.

The mean annual suspended sediment load generated by SIM 1 is 1.42 10^4 t/y, which is significantly lower than the 2.83 10^5 t/y computed from the measurements at Littau by Hinderer

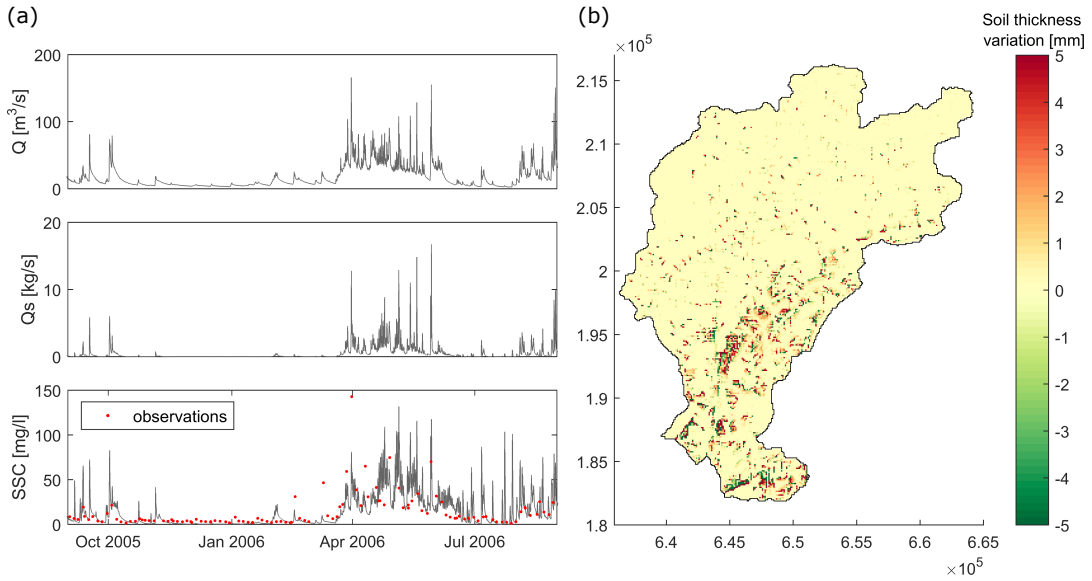

FIGURE 3.5: (a) Time series of hourly modelled discharge Q, suspended sediment load Qs and concentrations SSC for one year at the outlet. The red dots in the SSC time plot show the observed values. (b) Change in soil thickness at the end of the 13-year simulation. Positive values indicate erosion, negative values indicate deposition.

et al. (2013). Consistently, the mean annual erosion rate of 0.07 mm/y underestimates the denudation rates derived from ^{10}Be samples in the Entlen and Fontanne sub-basins by Wittmann *et al.* (2007), Norton *et al.* (2008) and Van Den Berg *et al.* (2012) (between 0.38 and 0.52 mm/y), which are from active erosion areas and integrate over a much longer time span of about 10^4 years. The lower estimates of sediment load and erosion rates by our model compared to such data is expected, given the underestimation of SSC at high flows by the model. This limitation will be further discussed in section 3.5.1.

3.4.2 Sediment sources and sediment production

To interpret the effect of the spatial variability of precipitation and surface erodibility on sediment transport, in Fig. 3.6 we compare the hydrological response of the basin in the four simulations in terms of the mean annual discharge Q_{mean}, annual flood Q_{max}, coefficient of variation CV of the hourly discharge at the basin outlet, and mean annual overland flow runoff over the basin Q_{OFmean}. Fig. 3.6 indicates that uniform precipitation (SIM 2 and 4) is less efficient in producing runoff (Q_{mean}, Q_{max} and Q_{OFmean}) and therefore has a lower erosive power. Spatially variable precipitation (SIM 1 and 3) produces a greater flow variability, because it allows to distinguish between convective rainfall patterns, which affect smaller regions of the basin, and stratiform rainfall patterns which affect the entire basin with lower precipitation intensities.

The sediment response of the basin in the four simulations is compared in the following by looking at the distribution of sediment source areas and their productivity. Fig. 3.7 compares soil thickness variation in SIM 2 and 3 respectively to SIM 1. Fig. 3.7b and 3.7c show the difference between the variable and uniform precipitation maps for erosion and deposition, respectively. Similarly, Fig. 3.7e and 3.7f show the difference between the variable and uniform surface erodibility maps for erosion and deposition separately. A positive value indicates more erosion/less

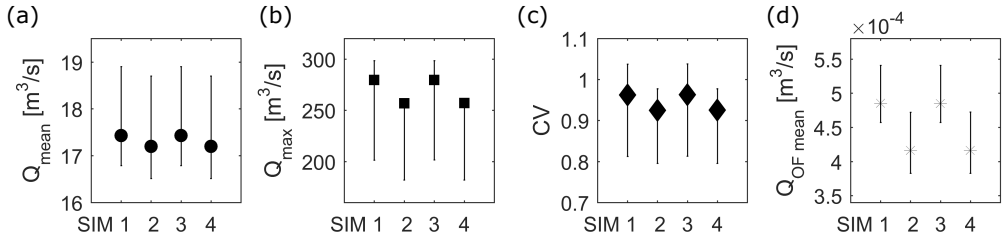

FIGURE 3.6: Comparison of the hydrological response of the basin in the four simulations: (a) mean annual discharge Q_{mean}, (b) annual flood Q_{max} and (c) the coefficient of variation CV of the hourly discharge at the basin outlet, and (d) the mean annual overland flow runoff over the basin $Q_{OF\,mean}$. The markers indicate the mean values and the lines the interval between the 25th and 75th percentile of the distribution from hourly data over the entire simulation period.

deposition by variable precipitation or surface erodibility, and a negative value indicates less erosion/more deposition.

The results show that with uniform precipitation, erosion and deposition are reduced in the south-eastern part of the basin and increased in the north-western (Fig. 3.7b and 3.7c). The overall patterns reflect the average spatial distribution of precipitation in the Kleine Emme catchment for the years 2004-2016, with the highest mean rain intensities associated with more erosion (Fig. 3.7a). Uniform surface erodibility increases sediment erosion and deposition in the forested areas and reduces them in crop areas (Fig. 3.7e and 3.7f). In both cases, the overall effect of removing the spatial variability in erosion drivers is a more uniform distribution of the sediment source areas across the basin.

To quantify the erosional power of the four combinations of erosion drivers, we computed the total sediment mass detached yearly across the whole basin (referred to as sediment production) in the four simulations. The distribution of the yearly sediment production with interannual variability is reported in Fig. 3.8. We observe that the removal of spatial variability generates two opposite effects for precipitation and surface erodibility. Sediment production increases when removing the spatial variability in surface erodibility and decreases when removing the spatial variability in precipitation, coherently with the reduced erosive power observed in Fig. 3.6. In SIM 4 the balance between the two opposing effects determines a slight overall reduction in sediment production. The differences between the scenarios are within natural interannual variability in sediment production, but they are all statistically significant for change in median.

3.4.3 Connectivity of sediment transfer

The connectivity of sediment transfer, i.e sediment source areas linked to the river network, within the catchment for the different simulation configurations has been quantified by means of the sediment delivery ratio (SDR). The SDR is defined according to Walling (1983) as the ratio of the sediment delivered at the outlet of a selected area to the gross erosion in that area. The mean annual SDRs, which were computed at the outlet point of the main tributaries and at several cross-sections along the main channel, are reported in Fig. 3.9 as a function of the drainage area.

Sediment connectivity along the main channel shows an increasing trend as a function of the upstream area for all simulations (Fig. 3.9c). This trend is explained by the higher SDR of the tributaries compared to that of the main channel (Fig. 3.9b) and by the absence of significant sediment sinks in the main channel. For the subbasins with outlets along the main channel, removing the spatial variability in surface erodibility (SIM 3) has the overall effect to increase sediment connectivity. In some tributaries, however, the opposite effect is observed (T5 and T6). Finally, Fig.

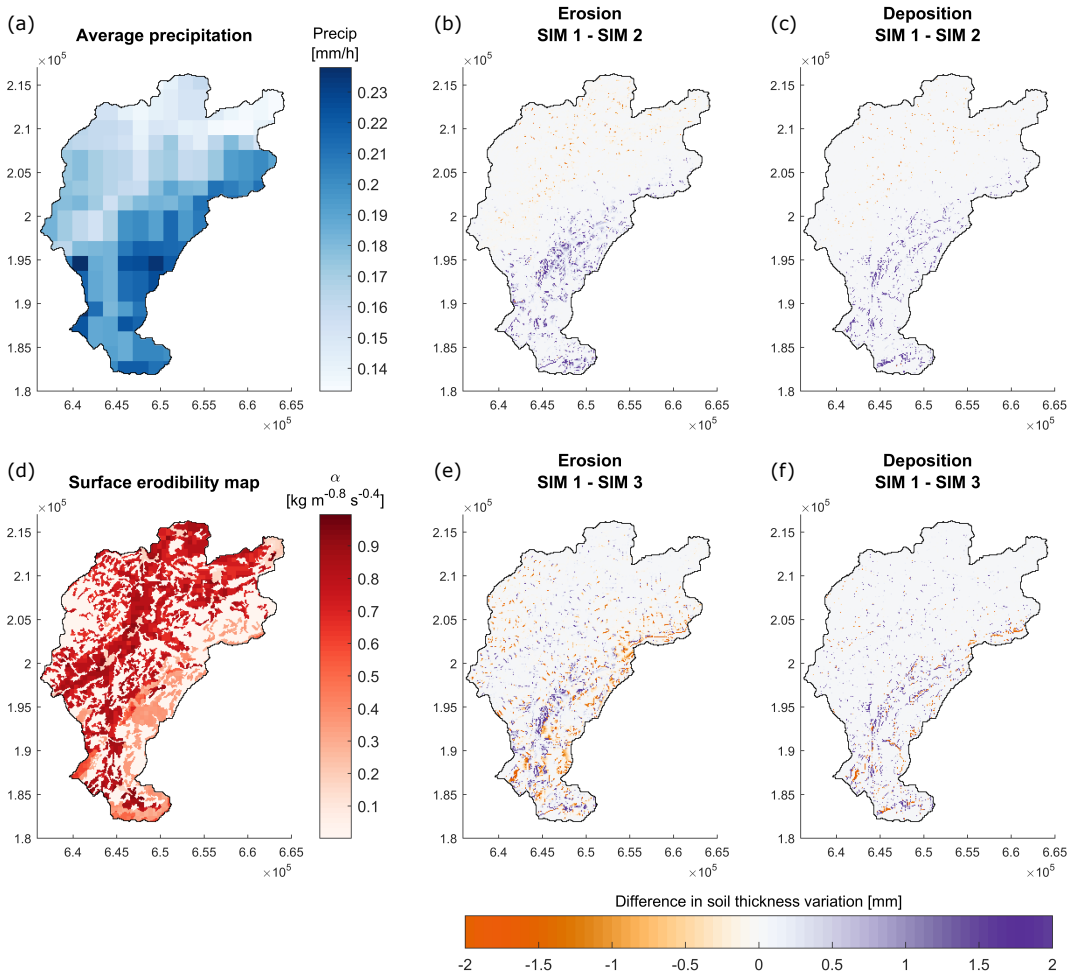

FIGURE 3.7: (a) Average spatial distribution of precipitation intensity for the period 2004-2016, (b, c) difference between erosion/deposition generated by variable and uniform rainfall in 13 years, (d) spatial distribution of calibrated surface erodibility α, (e, f) difference between erosion/deposition generated by variable and uniform surface erodibility in 13 years. A positive value indicates more erosion/less deposition by variable precipitation or surface erodibility and a negative value indicates less erosion/more deposition.

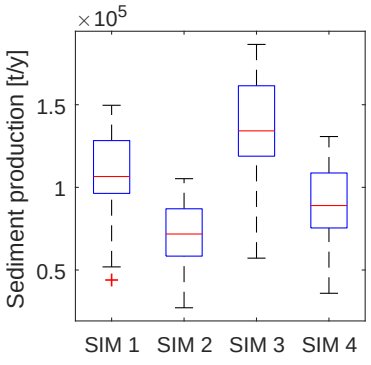

FIGURE 3.8: Sediment production in the basin as total sediment detached annually for the four simulations. Boxplots (median, interquartile range and outliers) show the interannual variability in the period 2004-2016.

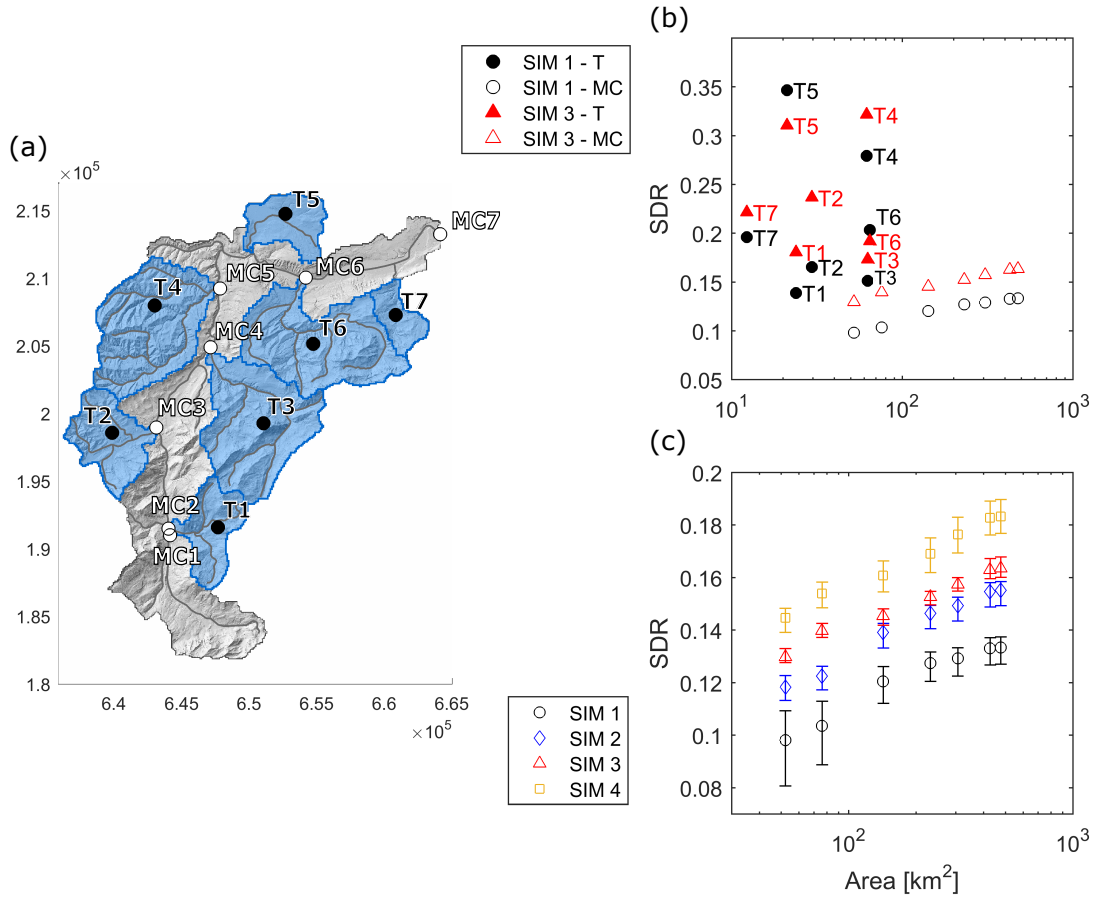

FIGURE 3.9: (a) Locations where the sediment delivery ratio has been computed: at the outlet of the main tributaries (T) and along the main channel (MC), (b) mean annual SDR vs drainage area for tributaries and points along the main channel for distributed rainfall simulations, (c) comparison of mean annual SDRs at the main channel points for the four simulations. The error bars show the interquartile range of the annual SDR variability.

3.9c shows that removing the spatial variability in precipitation (SIM 2 and 4) also increases the SDR, therefore sediment connectivity (compared to SIM 1 and 3, respectively).

3.4.4 Sediment loads and initial soil moisture

The distribution of annual sediment yields at the outlet generated by the four simulation experiments showed that distributed precipitation simulations (SIM 1 and 3) generated higher sediment loads than their uniform precipitation equivalents (SIM 2 and 4) (Fig. 3.10a). Distributed erodibility (SIM 1 and 2) produced smaller sediment loads than uniform erodibility (SIM 3 and 4).

To further investigate the differences among the sediment yield distributions, in Fig. 3.10b we show the influence of spatial variability in rainfall and surface erodibility on event-based sediment yields for high and low initial soil moisture (SM_0) conditions. After separating the outlet hydrograph into single events, we computed the total sediment yields for each event and compared the distributions of the events with high and low initial soil moisture. Low SM_0 events are defined as those with catchment-averaged SM_0 smaller than the 20^{th} percentile of the SM_0 distribution; high SM_0 events have a SM_0 greater than the 80^{th} percentile. The hydrological model performance for these events is good and comparable to the entire simulation performance, however it indicates a tendency to overestimate especially for low SM_0 events (see Table A.3 and Fig. A.4).

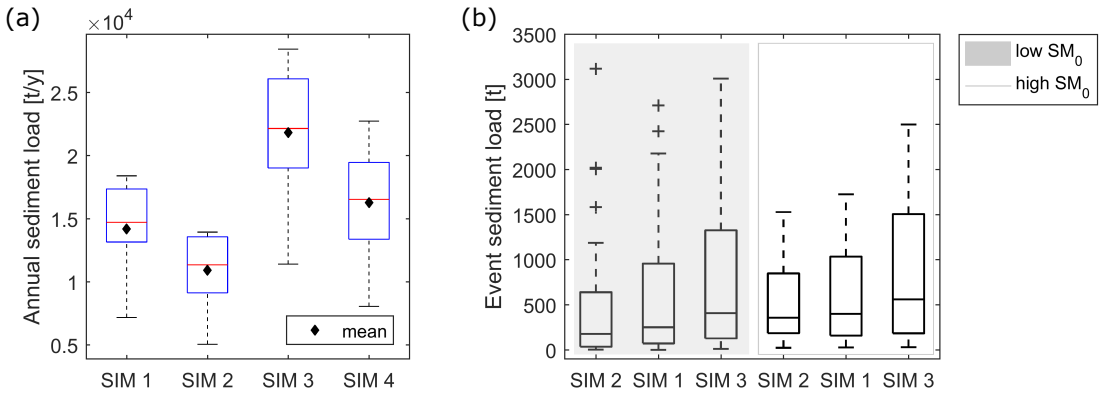

FIGURE 3.10: (a) Boxplots of annual sediment load and their mean values at the outlet of the catchment in the four simulation experiments, (b) boxplots of event sediment loads divided into low and high initial soil moisture conditions. The boxplots compare the effect of the spatial variability in precipitation and surface erodibility on events with different initial soil moisture.

The distributions of event sediment yields largely overlap, however it is possible to observe that sediment yield is more affected by the precipitation spatial variability when SM_0 is low. The differences between the median, 25^{th} and 75^{th} percentile of the SIM 1 and 2 are bigger for low SM_0 than for high SM_0. On the contrary, removing variability in surface erodibility seems to equally affect low and high initial SM_0 events (Fig. 3.10b).

3.5 Discussion

3.5.1 Sources of concentration variability

The modelling approach presented here can reproduce part of the observed SSC-Q scatter, implying that it contains some of the relevant sources of sediment concentration variability in the hydrological and sediment production processes at the catchment scale (Fig. 3.3b). However, it also highlights that to fully capture the scatter, other sources should be included. The comparison of simulated and observed hourly SSC is satisfactory (Fig. A.3).

The sources of variability accounted for by the deterministic modelling of the hydrology and sediment transfer are the time-varying meteorological inputs and the spatially distributed nature of the model. The precipitation input combines both temporal and spatial components of variability. The temporal component is visible in Fig. 3.5a, showing that the same sediment concentration can correspond to a large range of discharge values, depending on the type of event and the initial soil wetness conditions that precede it. Spatial variability in precipitation contributes to the SSC-Q scatter, by increasing the flow variability itself (Fig. 3.6c) and by allowing the same discharge at the outlet to be generated by many combinations of overland flow situations over the hillslopes. Each of these combinations activates different sediment sources that have a characteristic hydrological and sediment signal and connectivity to the river network. In particular, we identify localized high-intensity summer storms as a main source of scatter, while snowmelt and winter storms produce a more homogeneous response throughout the basin. The spatially variable surface erodibility can additionally contribute to the uniqueness of the sediment signals of the activated source areas, when its spatial distribution is such to enhance the topographic heterogeneity within the basin.

Other sources of variability in sediment transport are implicit in the spatially distributed nature of the model, which allows to account for the heterogeneity of topography, soil depth and soil

properties at very high resolution. These heterogeneities are responsible for the residual scatter of SIM 4, where the variability of both erosion drivers have been removed.

It is worth noting that, because the sediment storage on hillslope cells is not exhausted during our simulation experiments, sediment availability does not influence sediment production in our study. Therefore, sediment availability in the simulation experiments does not drive changes in the dominant sediment sources and does not add spatial variability to the sediment response.

The main limitation of our approach in reproducing SSC variability is, however, the lack of processes representing very localized sediment sources, which are usually characterized by a threshold behavior and therefore diversify the local sediment response. In this respect, Schwab *et al.* (2008) showed that in the Kleine Emme basin short timescale threshold processes are responsible for the export of regolith produced by soil creep in landslides. The absence of these processes in our model is likely one of the main reasons for the smaller-than-observed modelled SSC-Q scatter, but also for the underestimation of the highest SSCs, the soil erosion rate and annual sediment load, presented in section 3.4.1. Finally, we acknowledge that also inherent stochasticity in the sediment mobilization and transfer are responsible for part of the observed SSC-Q rating curve scatter (e.g. Fuller *et al.*, 2003; Malmon *et al.*, 2003). This inherent stochasticity cannot be reproduced by our modelling approach with deterministic simulation, but it can be included with stochastic simulation experiments and a probabilistic framework (e.g. Bennett *et al.*, 2014). We are working on overcoming these limitations in future research.

3.5.2 Spatial organization of suspended sediment transport

The explicit combination of hydrological processes and topographic and land use effects in the model can help to investigate the spatial organization of sediment transport, and in particular, how this is affected by the spatial variability in erosion drivers. Spatial variability enhances the heterogeneity of erosion and deposition across the catchment, thus favoring the clustering of sediment source areas (Fig. 3.7). Sediment production is increased by the spatially variable precipitation (SIM 1 and SIM 3), due to increased erosive power (Fig. 3.8). The effect of a spatially variable surface erodibility depends on the distribution of overland flow relative to that of surface erodibility and, in this case, the lower sediment productions of SIM 1 and 2 (Fig. 3.8) indicate that the two distributions combine more intense overland flow with lower erodibility areas, thus reducing the overall sediment production.

In Fig. 3.9 we use the modelled SDR as a measure of sediment transfer connectivity, as it quantifies the proportion of mobilized sediment that is routed to the outlet of a selected subbasin by action of overland and channel flow. As such, the modelled SDR can be seen as a dynamic indicator of functional connectivity, where the discharge is represented explicitly in time and space as a function of the hydrological forcings and topographic characteristics, as opposed to the widely used approximation as a function of the upstream area. In this way, our approach integrates the variability of functional connectivity both in time and space. A comparable approach to dynamically quantify functional connectivity has been proposed by Mahoney *et al.* (2018), which is also based on hydrological modelling.

The sediment delivery ratio shows that the connectivity of sediment sources is reduced by the spatial variability of precipitation and this effect can be explained by the geomorphic connectivity of the catchment. Higher precipitation, shallower soils, and steeper slopes in the southeastern region of the basin, i.e. tributaries T1, T3, T6 and the upper stretch of the main channel (see Fig. 3.9a), favor overland flow generation, and thus hydrological connectivity. However, the lower topographic connectivity of these subbasins overall causes a reduction in the sediment transfer connectivity. Such lower connectivity is indicated by the low SDRs of these subbasins in SIM 3, which does not account for the land use effect, and suggests the presence of geomorphic sediment buffers (Fryirs,

2013). The different topographic connectivity of the southeastern and northwestern regions reflects the different geomorphology of these two parts of the basin. In fact, the southeastern region of the basin is characterized by a predominantly Last Glacial Maximum landscape with wide valleys and major instabilities, which are in most cases not directly connected to the river network (Schwab *et al.*, 2008; Van Den Berg *et al.*, 2012; Clapuyt *et al.*, 2019). On the other hand, the northwestern part of the basin, i.e. tributaries T4 and T5, shows a rejuvenating landscape where recent fluvial dissection created narrow and deeply incised valleys with a strong coupling between hillslopes and channels (Schlunegger and Schneider, 2005; Norton *et al.*, 2008).

The reduction of sediment transfer connectivity by spatially distributed surface erodibility can be attributed to the assumption in the sediment module that the sediment discharge always satisfies the overland flow transport capacity. Based on this assumption, a spatially variable α allows, on the one hand to modulate the sediment mobilization in space and, on the other hand, to define preferential areas of sediment deposition and therefore sediment connectivity. By associating a lower transport capacity to forests, their role as sediment buffers blocking sediments will emerge. Vice versa, high α values in crop areas will mean the absence of obstacles to sediment flux. Therefore, the smaller sediment transfer connectivity of SIM 1 and 2 compared to SIM 3 and 4 reflects the location of sediment buffers (i.e. forests) with respect to the channel network. In fact, in most of the basin, forested areas surround channel headwaters, thus disconnecting the sediment sources on the hillslopes and mountain flanks from the river network (see e.g. Clinnick, 1985; Parkyn *et al.*, 2005; Schoonover *et al.*, 2006; Mekonnen *et al.*, 2015).

3.5.3 Sediment load and connectivity

The analyses presented in the previous sections focus on the driving processes of sediment mobilization and transfer across the basin and the reasons for the reduction in SDR with variable erosion drivers. In this section we analyse how their balance determines the sediment load at the outlet.

In the distributed surface erodibility simulations (SIM 1 and 2) a reduced sediment yield (Y) is observed at the basin outlet determined by a reduction in both sediment production (P) and sediment transfer connectivity (expressed by the SDR) with respect to uniform erodibility simulations (SIM 3 and 4):

$$\downarrow Y = SDR \downarrow \cdot P \downarrow . \tag{3.6}$$

In the distributed precipitation simulations (SIM 1 and 3) instead, an increased sediment yield at the basin outlet is observed compared to uniform precipitation simulations, which results from a combination of a smaller SDR and a much greater sediment production across the basin. The increase in sediment yield indicates that the greater sediment production dominates over the decreased sediment connectivity:

$$\uparrow Y = SDR \downarrow \cdot P \Uparrow . \tag{3.7}$$

This result means that localized sediment source areas are activated by the very high erosive power of localized precipitation captured by distributed simulations. Their signal reaches the outlet despite the system being globally less efficient in evacuating the eroded sediments. These hotspots of erosion are generated where precipitation falls with a high intensity, soil saturation is reached soon during storms, eventually favoured by shallow soils, and therefore hydrological and sediment flux connectivity are locally high.

In a hydrological modeling experiment conducted with TOPKAPI-ETH on the same catchment, Paschalis *et al.* (2014) demonstrated the dependence of the discharge peak on the clustering of high soil moisture areas. Our results show that the high soil moisture areas may also define the sediment

signal. This finding also suggests that a large proportion of the sediment yield can be supplied by just few localized sediment sources (e.g. Pelletier, 2012). The role of soil moisture in producing high sediment concentrations has also been highlighted by Dominic *et al.* (2015) and Brasington and Richards (2000), who attribute the peaks of SSCs to the connection of remote sediment sources during the wetting up of the catchment.

Given the relevance of soil moisture spatial distribution for runoff generation, we also expect event sediment yields to be more affected by precipitation spatial variability, i.e. precipitation intensity, at low initial soil moisture than at high initial soil moisture, as is suggested by Fig. 3.10b. This is further supported by findings of Paschalis *et al.* (2014) and Shah *et al.* (1996) which indicate that higher initial basin saturation reduces the dependency of runoff on precipitation spatial distribution. However, we also stress that in our study the relatively small difference between the sediment load distributions of low and high SM_0 events and the tendency to overestimate flow in low SM_0 events, do not allow for a clear conclusion.

3.6 Conclusions

We presented a new spatially distributed soil erosion and suspended sediment transport module integrated into the computationally efficient physically based hydrological model TOPKAPI-ETH. The model allows for continuous long-term, high temporal and spatial resolution simulations of erosion and sediment transport in mesoscale basins, and it is based on the physically driven processes of overland flow on hillslope and in channels. With the aim of exploring the impacts of two key spatially variable erosion drivers on suspended sediment dynamics, we conducted a series of numerical experiments on a mesoscale river basin. We compared the effects of spatially variable rainfall and surface erodibility with combinations of uniform and variable spatial distributions of these drivers.

Our results show that, first, the proposed model can reproduce part of the scatter of the observed SSC-Q relation, which is generated by spatially and temporally variable meteorological inputs and spatial heterogeneities of the physical properties of the basin, leading to a multitude of possible flow and sediment pathways. At the same time, our results suggest that other processes are also relevant to capture the scatter, such as localized sediment sources and the inherent randomness of sediment production and transfer, which are not included in our model.

Second, we found that spatial variability in both drivers favors the clustering of sediment source areas and reduces their overall connectivity to the river network, by capturing the buffering effect of forests and low slope areas. At the same time, spatially variable surface erodibility reduces sediment production, while a spatially variable precipitation increases sediment production by high rates of erosion in areas of high rainfall and overland flow intensity.

Third, we found that the combination of the effects of spatial variability on sediment production and connectivity determines an overall lower sediment yield for distributed surface erodibility, due to reduced sediment production and to buffering effects, and a greater sediment yield for distributed precipitation, due to locally very high soil erosion. This last result is due to areas of high soil moisture in the catchment that are easy to saturate, which produce high local sediment inputs and catchment loads in spatially variable simulations.

Although our findings were obtained with reference to the specific climatic and geomorphologic features of the Kleine Emme catchment, we think they indicate the general importance of resolving the spatial variability in sediment mobilization and transfer processes when modelling sediment dynamics at the basin scale. The model we presented is particularly suitable for applications at medium and large scales, where gradients in climatic and physiographic characteristics represent a key control on sediment mobilization and transfer. Moreover, this model offers a valuable tool for

investigating future scenarios of precipitation and land cover, which are expected to take place due to climate change or human land use management.

Data availability

DEM, soil and land use maps, discharge and suspended sediment concentrations data and simulation results are available at https://doi.org/10.3929/ethz-b-000358874. Meteorological input data can be requested at https://gate.meteoswiss.ch/idaweb/login.do.

Acknowledgements

The study was funded by the DAFNE project, an Horizon 2020 programme WATER 2015 of the European Union, GA no. 690268. We thank Fritz Schlunegger (University of Bern) for sharing his knowledge of the study basin, Enrico Weber (ETH Zurich) and Scott Sinclair (ETH Zurich) for technical support during the development of the model.

Author contributions

G. Battista developed the model and carried out the simulations and the analyses of the results. P. Molnar and P. Burlando contributed to the conceptualization of the model and to the discussion of the results. G. Battista prepared the paper with contributions and edits from all coauthors.

CHAPTER 4

Modelling localized sources of sediment in mountain catchments for provenance studies

Published in *Earth Surface Processes and Landforms*, authored by Giulia Battista, Fritz Schlunegger, Paolo Burlando and Peter Molnar.

Abstract

A hydrology-sediment modelling framework based on the model Topkapi-ETH combined with basin geomorphic mapping is used to investigate the role of localized sediment sources in a mountain river basin (Kleine Emme, Switzerland). The periodic sediment mobilization from incised areas and landslides by hillslope runoff and river discharge is simulated in addition to overland flow erosion to quantify their contributions to suspended sediment fluxes. The framework simulates the suspended sediment load provenance at the outlet and its temporal dynamics, by routing fine sediment along topographically-driven pathways from the distinct sediment sources to the outlet. We show that accounting for localized sediment sources substantially improves the modelling of observed sediment concentrations and loads at the outlet compared to overland flow erosion alone. We demonstrate that the modelled river basin can shift between channel-process and hillslope-process dominant behaviour depending on the model parameter describing gully competence on landslide surfaces. The simulations in which channel processes dominate were found to be more consistent with observations, and with two independent validations in the Kleine Emme, by topographic analysis of surface roughness and by sediment tracing with ^{10}Be concentrations. This research shows that spatially explicit modelling can be used to infer the dominant sediment production process in a river basin, to inform and optimise sediment sampling strategies for denudation rate estimates, and in general to support sediment provenance studies.

Battista G, Schlunegger F, Burlando P, and Molnar P, 2020. Modelling localized sources of sediment in mountain catchments for provenance studies. *Earth Surface Processes and Landforms*, 45(14): 3475-3487. https://onlinelibrary.wiley.com/doi/full/10.1002/esp.4979

4.1 Introduction

Suspended sediment load is generated by several types of mobilization processes that act on hillslopes and in channels, such as landslides, debris flows, overland flow erosion, river bed and bank erosion, the signal of which is filtered by the transport processes in the river network (e.g. Jerolmack and Paola, 2010; Bracken *et al.*, 2015). Given the strong nonlinearity and stochasticity of the involved processes, the magnitude of sediment load at a river basin outlet and its provenance, i.e. the origin of the sediment delivered to the outlet from different sources, are very difficult to predict (e.g. Roering *et al.*, 1999; Phillips, 2011). At the same time, such information is of fundamental importance to identify the locations of strongest soil erosion and sediment production, and to determine the downstream effects of the mobilized sediment.

A widely used approach in sediment provenance studies are fingerprinting methods, which allow quantification of the relative contributions of sediment sources to the outlet sediment load, by means of measurable and conservative sediment properties (Haddadchi *et al.*, 2013; Walling, 2005). Fingerprinting methods have been used to demonstrate the blocking of parts of the catchment from sediment production (e.g. Stutenbecker *et al.*, 2018, 2019), the role of valley gradient in the hillslope-channel geomorphic coupling (e.g. D'Haen *et al.*, 2013) and the correlation between rainfall properties and sediment export (e.g. Navratil *et al.*, 2012). However, these methods only provide limited information about the actual sediment pathways from source to the outlet and the temporal dynamics of the sediment load composition.

Information about sediment provenance is also essential for denudation rate studies based on cosmogenic radionuclide (CRN) dating. CRN concentrations in river bed samples are used to estimate catchment-average long-term denudation rates, under the assumptions that a sediment sample taken at the river outlet is representative of the long-term erosion rates of the upstream part of the basin, and that the different areas of the basin are represented in the sample proportionally to their erosion rates (von Blanckenburg, 2005; Yanites *et al.*, 2009). These conditions are especially difficult to be satisfied in mountainous environments, where soil erosion is highly episodic and localized, often dominated by mass movements, and where sediment production from small areas can temporarily dominate the basin sediment load (e.g. Korup *et al.*, 2004; Evrard *et al.*, 2011; Delunel *et al.*, 2014; Cruz Nunes *et al.*, 2015). Therefore, information about preferential sediment production areas and the hydrological conditions that activate them is key to correctly interpret CRN concentrations in river bed samples in mountainous environments.

One way to quantify the activation of localized sediment sources by time-dependent overland and channel flow, and to track sediment from origin to outlet, is by physically-based spatially-distributed hydrological and sediment transport modelling (de Vente *et al.*, 2006; Kim and Ivanov, 2014; Tsuruta *et al.*, 2018; Battista *et al.*, 2020a). Research has shown that widely used conceptual approaches to spatial erosion estimation, such as RUSLE (Renard *et al.*, 1997) and WaTEM/SEDEM (Van Rompaey *et al.*, 2001) fail in catchments where landslides, bank and gully erosion are expected to play an important role in sediment mobilization (Van Rompaey *et al.*, 2005; Borrelli *et al.*, 2014, 2018). Some spatially-distributed models already include localized mass wasting processes, e.g. landslides, as a sediment source in addition to diffuse hillslope erosion processes (e.g. Bathurst and Burton, 1998; Doten *et al.*, 2006; Coulthard *et al.*, 2013). However, they do not explicitly track the sediment produced by the different sediment sources in space and time and therefore cannot reconstruct the sediment provenance at the outlet.

The aim of this work is to provide an approach that combines spatially explicit hydrology-sediment modelling with detailed knowledge of localized sediment sources, in order to track sediment produced by them to the outlet. In particular, (1) we combine a recently developed distributed hydrology-sediment numerical model (Battista *et al.*, 2020a) with detailed basin geomorphic mapping of main sediment production areas in a pre-Alpine river basin, (2) we show with this

model how the relative contributions of landslide, hillslope and channel production processes to the fine suspended sediment load at the outlet are affected by parameter choices, (3) we use the model together with surface topographic analysis of landslide areas and measured CRN concentrations in the production zones as a tracer, to independently validate the sediment load composition in the study catchment, and (4) we discuss how the time-dependent modelling of sediment load composition can be used to guide the sampling of CRN for denudation rate estimates and complement fingerprinting approaches.

The hydrology-sediment model is the two-dimensional high-resolution catchment hydrology model TOPKAPI-ETH (Paschalis *et al.*, 2014; Fatichi *et al.*, 2015) with a new suspended sediment module recently introduced by Battista *et al.* (2020a). The latter showed that high suspended sediment concentrations in the same study catchment were difficult to model by only accounting for diffuse overland flow erosion, and suggested the need to include mass wasting processes with a threshold behaviour. In this work we introduced sediment mobilization from landslides and channel inner gorges as additional erosion processes and fine sediment sources. We introduced a new parameter for sediment mobilization by overland flow on landslide surfaces, the so-called gully competence parameter, to regulate the relative contribution of landslides and incised areas to total sediment yield. We show how this parameter can potentially be estimated from surface roughness derived from a high resolution DEM or by measurements of a sediment source tracer such as the ^{10}Be concentrations. We close the paper with a discussion of how this approach can guide optimal riverbed sediment sampling strategies of CRN for denudation rate estimates, and in combination with fingerprinting methods can increase our understanding of the sediment dynamics in a mountain environment.

4.2 Data and Methods

4.2.1 Catchment geomorphic mapping

The case study basin is the Kleine Emme, a 477 km^2 pre-Alpine basin located in central Switzerland. The basin has been moderately geomorphically active and is characterized by several inner gorges and knickpoints, expressions of erosional waves generated by the lowering of the base level of the river network following the Last Glacial Maximum (Schlunegger and Schneider, 2005; Van Den Berg *et al.*, 2012; Dürst Stucki *et al.*, 2012). In the gorges, deep river incision in the valley floor generates steep river banks characterized by frequent debris flows and bank failures, delivering abundant regolith to the river. The exposure of bedrock in these gorges indicates an efficient and supply-limited sediment transport regime in the channels (Schwab *et al.*, 2008). On the hillslopes, several mass movements like earthflows and landslides are present. The sediment produced by these processes is stored on the hillslopes for potentially long time periods and is only delivered to the river network when short-lived and rare episodes of hillslope-channel coupling take place, consisting mostly of superimposed debris flows (Schwab *et al.*, 2008; Clapuyt *et al.*, 2019). This mechanism indicates a transport-limited regime on the hillslopes.

We identified the areal extent of the localized sediment sources by geomorphic mapping. Landslides and earth flows (*LS*) were identified in the Geological Atlas of Switzerland (GeoCover V2) and verified with a high resolution 2 m LIDAR DEM (SwissAlti3d). Slopes from the LIDAR DEM were used to manually map the extent of areas deeply incised by the river, referred to as incised areas (*I*) (see map in Fig. 4.1). The *LS* and *I* areas were considered as potential hotspots of fine sediment production as they have abundant clay, silt and fine sand available for transport, and are localized as they cover only 16% of the entire catchment area.

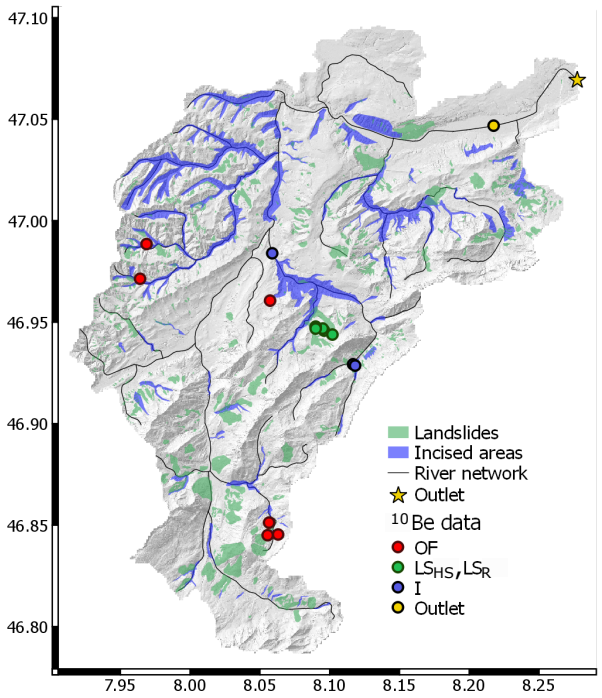

FIGURE 4.1: Map of the landslides and incised areas in the Kleine Emme river basin. The dots indicate the location of the ^{10}Be samples that were used to derive a representative concentration for sediments mobilized by overland flow erosion (OF), sediment pickup from landslides (LS_R and LS_{HS}) and incised areas (I) (see section 4.2.5). In yellow are indicated the location of the ^{10}Be sample at the outlet (dot) and the basin outlet hydrometric station (star).

4.2.2 Modelling concept for localized sediment sources

The hydrology module in Topkapi-ETH is physically based and fully distributed, i.e. raster-based, and it simulates runoff on hillslopes and in the channels, and subsurface flow in a multi-layered soil, from climatic inputs (precipitation, air temperature, cloud cover) and watershed surface and subsurface properties (DEM, soils, vegetation cover). It includes all relevant hydrological processes in alpine environments, such as infiltration and saturation excess runoff formation, soil moisture limited evapotranspiration, snow accumulation and melt, etc. For more model details see Fatichi *et al.* (2015). The sediment module in Topkapi-ETH simulates erosion by overland flow on the hillslopes (OF process) and is based on a transport capacity approach, where at cell level the sediment production rate (erosion) adjusts to the local transport capacity T_c:

$$T_c = \alpha \cdot q_{OF}^{1.4} \cdot S^{1.4}, \tag{4.1}$$

where T_c is the specific sediment transport capacity of overland flow per unit area [kg m^{-2} s^{-1}], q_{OF} is the specific overland flow [m^2 s^{-1}], S the local slope and α [ks s$^{0.4}$ m$^{4.8}$] is a surface erodibility parameter. The spatial distribution of α is given by the C (land cover and management) and K (soil erodibility) factors in the RUSLE equation (Renard *et al.*, 1997), and its magnitude was calibrated with observed suspended sediment concentrations (SSCs) at the river basin outlet (Battista *et al.*, 2020a).

In the present work, we introduced additional localized sediment sources, i.e. landslides and incised areas, as potential hotspots of fine sediment production. We assumed that mobilization takes place by means of three new processes supported by these hotspots: sediment pickup from

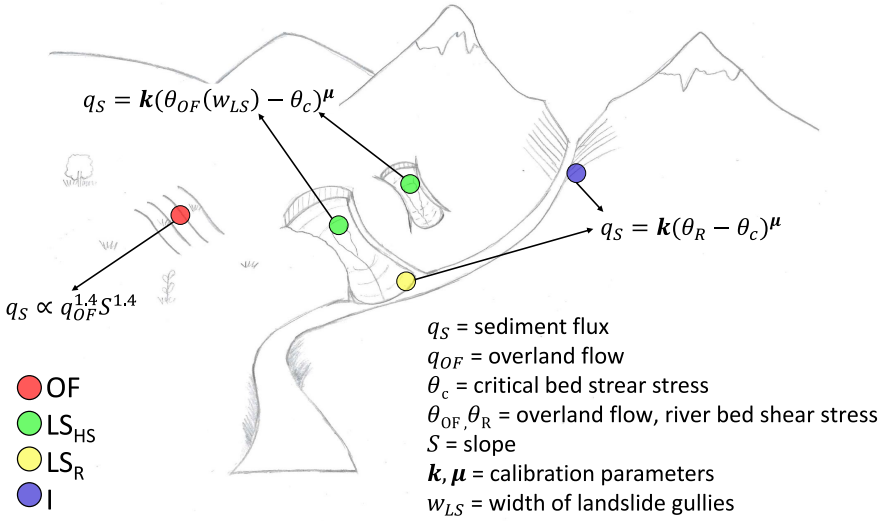

FIGURE 4.2: Schematic description of the model. Sediment mobilization is possible through 4 processes: diffuse overland flow erosion (OF), sediment pickup from the body of landslides by hillslope overland flow (LS_{HS}), from the toe of landslides by river flow (LS_R) and from incised areas (I). LS_{HS}, LS_R and I are activated when applied bed shear stress exceeds a threshold. On landslide surfaces the applied bed shear stress is a function of the gully width (w_{LS}).

incised areas (I), from the toe of landslides by action of the river flow (LS_R) and from the body of landslides by action of hillslope overland flow (LS_{HS}) (Fig. 4.2).

Sediment was assumed to be mobilized from the incised areas I by action of the discharge in the inner gorges, when it exceeds a critical value. Such threshold behaviour represents the activation of debris flows and bank failures that supply sediment from hillslopes to the channel. Sediment was considered to be always available, when the critical bed shear stress in the river is exceeded.

The landslide processes (LS_R and LS_{HS}) were also assumed to have a threshold behaviour, in order to represent the episodic activation of the hillslope-channel coupling. In the light of the transport limited character of sediment flux on the hillslopes, we assumed that the sediment storage of landslides was also unlimited. We observe that in the basin there are landslides directly connected to the river network, which can be emptied by both LS_R and LS_{HS}, and landslides disconnected from the river network, which are only emptied by LS_{HS}. The disconnected landslides deliver sediment to the channel only if the overland flow bed shear stress is sufficiently high along the flow path to the nearest channel cell, and therefore have a transient functional connectivity to the river network.

The sediment input from landslides and incised areas takes place when applied shear stresses exceed a threshold, with the same sediment transport formula applied to all three processes (Fig. 4.2):

$$q_s = k \cdot (\theta - \theta_c)^{\mu} \tag{4.2}$$

where q_s [m^2/s] is the specific sediment flux, θ is the dimensionless bed shear stress, θ_c the dimensionless critical bed shear stress and k and μ are parameters that regulate the sediment flux. The parameters k and μ depend on grain size, sediment mass density and the magnitude and non-linearity of the morphological response following the triggering of debris flows, bank collapses, and the activation of hillslope-channel coupling, and must be calibrated. Following a sensitivity analysis we assumed θ_c=0.05 and constant in this study. The dimensionless bed shear stress θ is the key hydraulic factor that makes q_s different on landslides, in channels and incised areas, despite the same parameters k and μ in Eq. 4.2 (see Sect. 4.2.3).

The routing of sediment on the hillslopes and in the channels takes place in parallel from all sources. Overland flow (OF) erosion and sediment transport takes place on all hillslope cells provided the hydrological forcing $q_{OF} > 0$. Sediment is routed along the hillslope flow paths, it can be deposited if the transport capacity in Eq. 4.1 is exceeded, and is input into the river network once a channel cell is reached. Extra sediment is mobilized on the hillslopes on landslide surfaces (LS_{HS}) when the overland flow shear stress exceeds the critical value θ_c (Eq. 4.2) and this sediment is input into the river network if transport capacity allows it. Rivers receive extra sediment input when they cross incised areas (I) or the toes of landslides directly connected to the river network (process LS_R) and the streamflow bed shear stress exceeds θ_c (Eq. 4.2).

In the channels, fine sediment produced from all four sediment sources (OF, LS_{HS}, LS_R, I) is routed as suspended load using an advection solution, neglecting diffusion and the possibility of sediment deposition. The sediment flux at any point in the river network consists of the sum of the four sediment fluxes at any given time step. The hypothesis of pure sediment advection neglects the recycling and mixing processes within the river network and is motivated by the efficient and supply-limited transport in the river network of the study basin (see Sect. 4.2.1). On the contrary, the possibility of deposition and re-mobilization of the eroded sediment on the hillslopes implies that the delivery of hillslope sediment by overland flow into the channels can be instantaneous during large rainfall events, or spread over long time periods when sediment undergoes many erosion-deposition cycles (see Battista *et al.*, 2020a).

Finally, we note that, because of the moderate geomorphic activity of the basin and the decadal-scale simulation horizon, we assumed that landslides and incised areas are fixed features in the basin and we did not consider the generation of new landslides or inner gorge sources at the timescales of our simulations.

4.2.3 Gully competence parameter

To compute the bed shear stress for hillslope and river cells, it is necessary to know the width of the flow confinement. In our study basin, the width for river cells was known from cross-section measurements provided by the Swiss Federal Office for the Environment (FOEN) along the river network. For hillslope cells, OF erosion by surface runoff with rate T_c takes place over the entire width of the cells (Δx). However, landslide bodies can be heavily gullied, changing the active flow width of hillslope cells located on landslides. Therefore, a new parameter was needed to define the active cell width where erosion action and sediment transport take place.

We described the effect of overland flow channelization on the landslide body by assuming that the gullying of a landslide cell is represented by an equivalent width w_{LS} of a gully that is always deep enough to contain all the overland flow on the cell ($w_{LS} \leq \Delta x$). We introduced a parameter for gully competence λ, which represents this flow concentration:

$$\lambda = \frac{\Delta x}{w_{LS}}. \tag{4.3}$$

Low values of λ ($w_{LS} \approx \Delta x$) mean that gullies on the landslide surface are wide and shallow, and therefore have a low competence for sediment transport, because flow is not concentrated and shear stress is low – this is a poorly gullied landslide (PGL). High values of λ ($w_{LS} << \Delta x$) represent a surface with narrow, deep and competent gullies, where the flow is concentrated and shear stress is large – this is a strongly gullied landslide (SGL).

It is expected that λ has an effect on the partitioning of the sediment flux between landslides and incised areas. In our simulations we tested two end-member values $\lambda = 1$ ($w_{LS} = \Delta x$) and $\lambda = 100$ ($w_{LS} = 1$ m, $\Delta x = 100$ m) as scenarios, and we present a possible way to estimate λ from the statistical distribution of the surface roughness of landslide surfaces. To this end, we computed

the standard deviation σ_z of elevations from a high resolution 2 m LIDAR DEM in areas of 6×6 m over the extent of each landslide. Given that the surface roughness on gully banks is higher than on the other parts of the landslide surface, high values of σ_z in the frequency distribution indicate the presence of gullies on the surface. We selected an example of a poorly gullied landslide and a strongly gullied landslide in the Kleine Emme and we assumed their σ_z frequency distributions to be representative of a $\lambda = 1$ situation, and a $\lambda = 100$ situation, respectively. To infer the λ end-member value that better represents the gully development across the whole basin, we compared the σ_z frequency distributions of the PGL and SGL to that of all landslide surfaces in the basin and chose the end-member that better matches the two distributions.

4.2.4 Model calibration and simulations

The hydrology-sediment model was set up for the period 2004–2016 with a spatial resolution of Δx=100 m and a time step of Δt=1 hour. The hydrological component was calibrated on streamflow measured at three stations in the basin for the same period, using as inputs hourly measurements of sunshine duration, air temperature, and precipitation measured at rain gauges and combined with the spatially distributed daily RhiresD dataset (MeteoSwiss). Overall, the model performed well in reproducing the hourly streamflow, e.g. reaching a correlation coefficient r=0.84 and model efficiency ME=0.69 at the outlet (Battista *et al.*, 2020a).

The α parameter of the overland flow component in Eq. 4.1 was calibrated by considering only the OF process and fitting the modelled and observed SSC-Q clouds of point and the frequency distribution of SSCs up to the 85th quantile, i.e. ignoring the extremes. SSCs measurements are available at the outlet for the simulated period with a measurement frequency of two samples a week from the Swiss Federal Office for the Environment (FOEN). See Battista *et al.* (2020a) for more details on the calibration of the OF process.

In this work, we kept the α parameter unchanged and calibrated the k and μ parameters (Fig. 4.2 and Eq. 4.2) by maximizing the coefficient of determination R^2 and the model efficiency ME in predicting all observed hourly suspended sediment loads, without any limitation on the quantiles. Given the two end-members for λ, calibration of k and μ was performed twice: for $\lambda = 1$ in SIM A (poorly gullied landslides), and for $\lambda = 100$ in SIM B (strongly gullied landslides).

The simulated annual suspended sediment load was compared with two estimates of sediment load derived from observations, based on two different methods to extrapolate an annual load from the low temporal resolution SSC measurements available. The first (lower) estimate is based on yearly SSC-Q rating curves fitted to each year of hourly observations, and used to infer the missing hourly SSCs (Qs^{OBS}_{MIN}=7.41 10^4 t/y), while the second (higher) estimate is based on an estimate of daily load from the observed SSCs only and gives more weight to the single SSC-Q observation pairs (Qs^{OBS}_{MAX}=2.83 10^5 t/y, Hinderer *et al.* (2013), see FOEN (2010) for details).

Given the effect of λ in regulating the sediment input from LS_{HS} processes, SIM A and SIM B are expected to show different provenance of the sediment load at the outlet. Therefore, we performed a sensitivity analysis of λ, k and μ parameters to compare the effect of each parameter on the sediment load provenance at the outlet. Taking SIM A as a reference, we varied λ within the range [1,100], and k and μ within the ranges provided by their calibrated values for SIM A and SIM B.

4.2.5 ^{10}Be concentration data

To corroborate the estimate of λ obtained in Sect. 4.2.3, we applied sediment tracing in the model by using measurements of ^{10}Be concentrations available across the basin in different morphologies and at the outlet.

Mobilization process	^{10}Be Concentration [10^4 at/g_{Quartz}]
OF	6.16 ± 1.72
LS_{HS}, LS_R	1.60 ± 0.75
I	0.69 ± 0.58

TABLE 4.1: Estimated representative ^{10}Be concentrations of sediments mobilized by the four sediment production processes. LS_{HS} and LS_R have the same concentration because they mobilize sediments from the same source. The reader is referred to the Appendix B for details about the derivation.

Because ^{10}Be concentrations on the surface are inversely proportional to the long-term erosion rates, they are expected to label the sediments mobilized by different processes with a different concentration. From data of in-situ produced CRN rates available from the literature in the basin (Clapuyt *et al.*, 2019; Van Den Berg *et al.*, 2012; Norton *et al.*, 2008; Casagrande, 2014), we selected samples on landslide surfaces, in headwater channels, and in a subbasin including incised areas, to derive a concentration representative of each sediment production process simulated in the model. The details of the computation of the representative concentrations are reported in the Supporting Information. The location of the samples is shown in Fig. 4.1 and the resulting ^{10}Be concentrations associated with the production processes are reported in Table 4.1. By assigning these concentrations to the corresponding modelled sediment fluxes at the outlet, we were able to derive a time series of ^{10}Be concentration at the outlet for SIM A and SIM B.

We analysed the frequency distributions of simulated ^{10}Be concentrations in the suspended sediment under SIM A and SIM B to highlight how differences in sediment production sources and their activation will impact the time-dependent mixing of sediment at the outlet. We compared these distributions with a single river bed ^{10}Be sediment sample taken close to the outlet by Wittmann *et al.* (2007), to assess which of the two simulations better represents erosion processes in the study basin.

Finally, we discuss the implications of the modelled temporal fluctuations of ^{10}Be concentration for the sampling of river sediment that is representative of long term denudation rates. To this end, we also used the model results to investigate how the sampling location in the cross section might affect the representative value of the sediment transported in the river at that location. In particular, we computed the variability of the modelled ^{10}Be concentration expected in river bed samples taken at different elevations on the river bed. To do so, we first identified the water depth that fully covers the mobile part of the bed based on the outlet cross section profile provided by FOEN (the banks of the channel are protected and fixed). Second, from this water depth we derived the range of discharges during which sampling is possible, given the water level h-Q relationship at the outlet cross section (also provided by FOEN), and we computed the water depths corresponding to the 5th , 25th, 50th and 75th percentiles of this range of discharge. Finally, we filtered the modelled ^{10}Be concentration distribution with the modelled discharges that reach or exceed these water depths. These are the concentrations potentially deposited by the flow on the river bed above the corresponding water levels (h_5, h_{25}, h_{50} and h_{75}). The described approach assumed that deposition is independent of the grain-size and flow conditions.

4.3 Results

4.3.1 Sediment sources and simulated SSCs

The results of the two calibrated simulations SIM A ($\lambda = 1$) and SIM B ($\lambda = 100$) are presented in Fig. 4.3 in terms of modelled SSCs against discharge. In Fig. 4.3 we associated a color to each of the sediment production processes and then filled each Q-SSC dot by mixing these colors proportionally to the relative contribution of each source. Therefore, the color coding indicates the process, or the combination of processes, generating each hourly SSC. The overland flow process OF is the dominant sediment production process at lower discharges, generating the lower modelled SSCs (red markers). At higher flows, the threshold processes I and LS_{HS} (blue and green markers) become the dominant sediment production processes. The highest SSCs are generated in SIM A by sediment pickup from incised areas (I), and in SIM B from the body of landslides (LS_{HS}), and this is reflected in the composition of the yearly load reported in Table 4.2, where I contributes 81% of the total sediment mass in SIM A and LS_{HS} contributes 98% of the total sediment mass in SIM B. This result indicates that the different parameterization of SIM A and B has the effect to redistribute the sediment provenance between these two dominant sources. The calibrated parameters of the hydrology-sediment model for both simulations and the modelled annual sediment loads are listed in Table 4.2.

The model performance is presented in Table 4.3 by evaluating the fit of observed and modelled hourly sediment flux Q_s, SSC variability, and annual sediment yield. It is interesting to note that the two calibrated simulations produced almost equally good values of the goodness-of-fit metrics. In both simulations, the coefficient of determination R^2 and the model efficiency ME of the hourly loads Q_s are rather low in terms of their absolute values (Moriasi *et al.*, 2007), however, considering the simplified representation of the suspended sediment transport in the channels and that similar models show R^2 of about 0.7 and ME between 0.5 and 0.9 for daily or monthly temporal resolutions (Francipane *et al.*, 2012; Betrie *et al.*, 2011; Tsuruta *et al.*, 2018), the results can be considered relatively good in the framework of this type of models. The percentage of SSCs falling within the [5,95]th and [25,75]th percentiles of observations quantifies the fit between the modelled and observed SSC-Q relation and its scatter, and indicates that both simulations almost perfectly captured the observed variability. The comparison of the modelled mean annual sediment loads with the higher estimate $Q_{s_{MAX}}^{OBS}$ from observations (Hinderer *et al.*, 2013) gives very good results, with slight underestimation (-22%) by SIM A and slight overestimation (+33%) by SIM B.

The almost equal performance of the two simulations suggests that a good fit with the observations may be achieved by very different combinations of sediment source activation and that it may not be possible to identify the dominant sediment sources based on the sediment dynamics properties only. This limitation could be in part related to the low temporal resolution of the SSC observations in the study basin, which does not allow to fully characterize the SSC-Q relation, and therefore to discriminate between the two solutions. However, this quality of SSC data is typical in many monitored catchments and as a consequence the physical meaningfulness of the parameters, especially λ, needs to be validated with an independent analysis.

4.3.2 Sensitivity analysis

The results of the previous section indicate how the different parameterisations of SIM A and B redistribute the provenance of the outlet sediments among the different sources. In this section we investigate the role of each parameter λ, μ and k in determining the distribution of sediment provenance. To do so, we carried out a sensitivity analysis of SIM A to these parameters in the ranges defined by the calibrated values of SIM A and B (see Table 4.2).

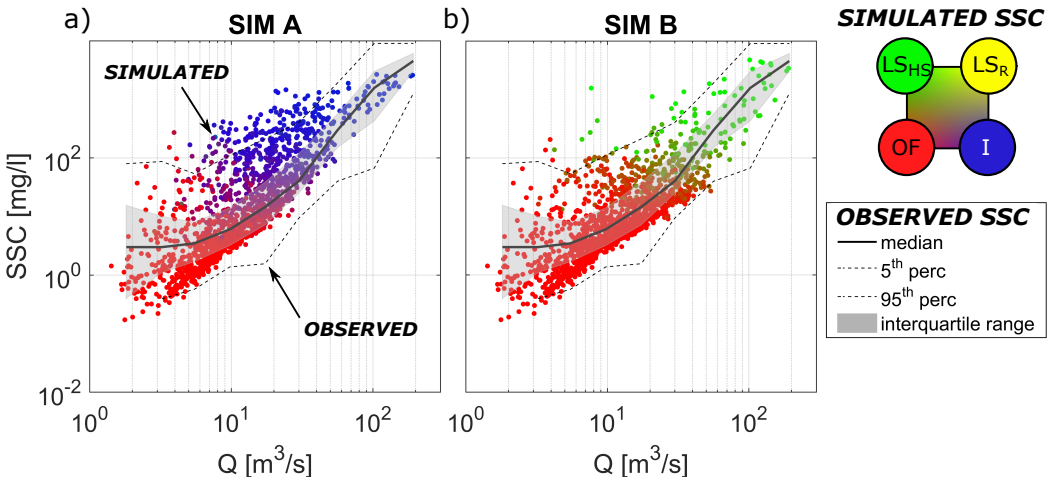

FIGURE 4.3: Calibrated simulations. Modelled hourly SSCs at the outlet (colored dots) for SIM A (λ=1) and SIM B (λ=100) are compared with the median (continuous line), the interquartile range (shaded area) and the 5th and 95th percentiles (dotted lines) of the observation. The color of the modelled SSCs represents the sediment mobilization process, or the combination of processes, producing each concentration.

	Calibrated parameters			Yearly load	Composition of yearly load			
	λ [-]	k [kg m^{-1} s^{-1}]	μ [-]	Q_s [10^5 t/y]	$Q_s(OF)$ [%]	$Q_s(LS_R)$ [%]	$Q_s(LS_{HS})$ [%]	$Q_s(I)$ [%]
SIM A	1	0.023	2.5	2.21	7.73	11.27	0	81
SIM B	100	9.17e-6	6	3.76	4.54	0	95.45	0.01

TABLE 4.2: Values of the calibration parameters k and μ, modelled yearly load Q_s, and percentages of its composition for simulations SIM A and SIM B.

	Hourly Q_s		Scatter fit [%]		Yearly load error [%]	
	R^2	ME	5-95th	25-75th	Q_s - $Q_{s_{MIN}}^{OBS}$	Q_s - $Q_{s_{MAX}}^{OBS}$
SIM A	0.47	0.32	89	49	198	-22
SIM B	0.48	0.40	93	51	407	33

TABLE 4.3: Model performance. R^2 and model efficiency (ME) of the simulated hourly sediment load, percentage of simulated SSCs that fall within the [5,95]th and [25,75]th percentile of the observations and relative error of the modelled annual sediment yield compared with two estimates of annual load from observations (see text for explanations).

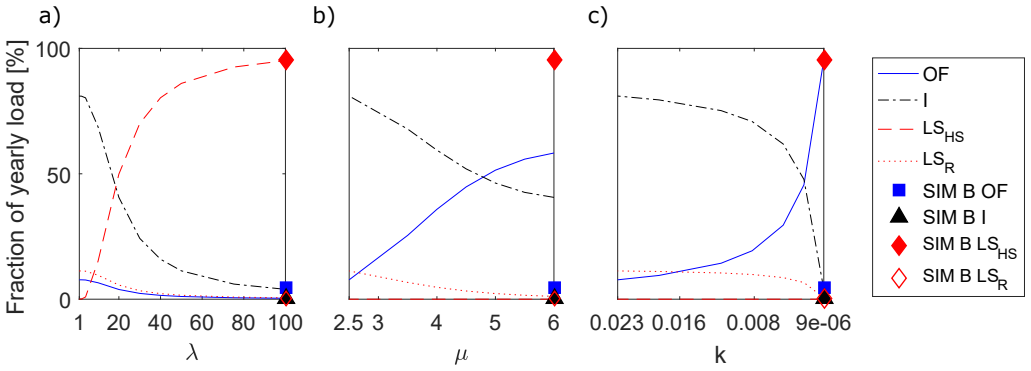

FIGURE 4.4: Sediment load composition in the sensitivity analysis simulations. The percentage of yearly load generated by each sediment production process is plotted as a function of the studied parameter. On the left side of the x-axis, λ, μ and k have the values of calibrated SIM A, and on the right side the values of calibrated SIM B. The lines are the fractions of yearly load in a simulation that has the same parameters as SIM A, except for the parameter on the x-axis. Note the reversed axis in (c). The blue square, black triangle, filled and empty red diamond indicate the fractions of yearly load of SIM B.

The fraction of the mean yearly suspended sediment load generated by each sediment mobilization process as a function of the studied parameters is shown in Fig. 4.4. On the left side of the x-axis of the plots, λ, μ and k have the values of calibrated SIM A, and on the right side the values of calibrated SIM B. The lines are the fractions of yearly load in a simulation that has the same parameters as SIM A, except for the parameter on the x-axis, and the symbols (square, triangle and diamonds) indicate the partitioning of sediment load in SIM B.

Fig. 4.4 shows that μ and k mainly affect the ratio between threshold (I, LS_R and LS_{HS}) and continuous (OF) processes, while λ strongly affects the hillslope (LS_{HS} and OF) to channel (I and LS_R) process ratio, by increasing the LS_{HS} contribution as it grows. We observe that SIM A with λ=100 closely captures the SIM B yearly load partitioning (square, triangle and diamonds) even if the μ and k parameters have not been changed (Fig. 4.4a). On the contrary, the composition achieved by SIM A with μ and k of SIM B is very different from SIM B composition. This result indicates that among the three main model parameters, λ has a dominant role in determining the sediment load composition at the basin outlet. In other words, it is the key parameter that redistributes sediment provenance towards incision areas, in the poorly gullied case (SIM A), and landslide surfaces, in the strongly gullied case (SIM B).

4.3.3 Landslide surface roughness to quantify gully competence

The first independent validation of the two end-member simulations SIM A and SIM B is by estimating the gully competence parameter λ directly from topographic analysis of landslide surfaces. The surface roughness of two selected landslide surfaces measured by the local standard deviation of the topographic height σ_z is shown in Fig. 4.5. The spatial maps clearly show that the poorly gullied landslide (PGL, top) has less rill and gully formation and a much lower roughness measured by lower mean σ_z, variance and more skewed distribution, while the strongly gullied landslide (SGL, bottom) has very significant and deep gullies distributed over the surface and a much higher roughness measured by higher σ_z, variance, and a less skewed distribution.

To assess if the entire basin of the Kleine Emme is more like PGL or SGL, we computed the frequency distribution of σ_z and its basic statistics over all landslide surfaces in the catchment based on the 2 m resolution Lidar DEM. Our hypothesis is that if a better overlap exists for PGL, the simulation SIM A ($\lambda = 1$) would be a more accurate description of the sediment processes

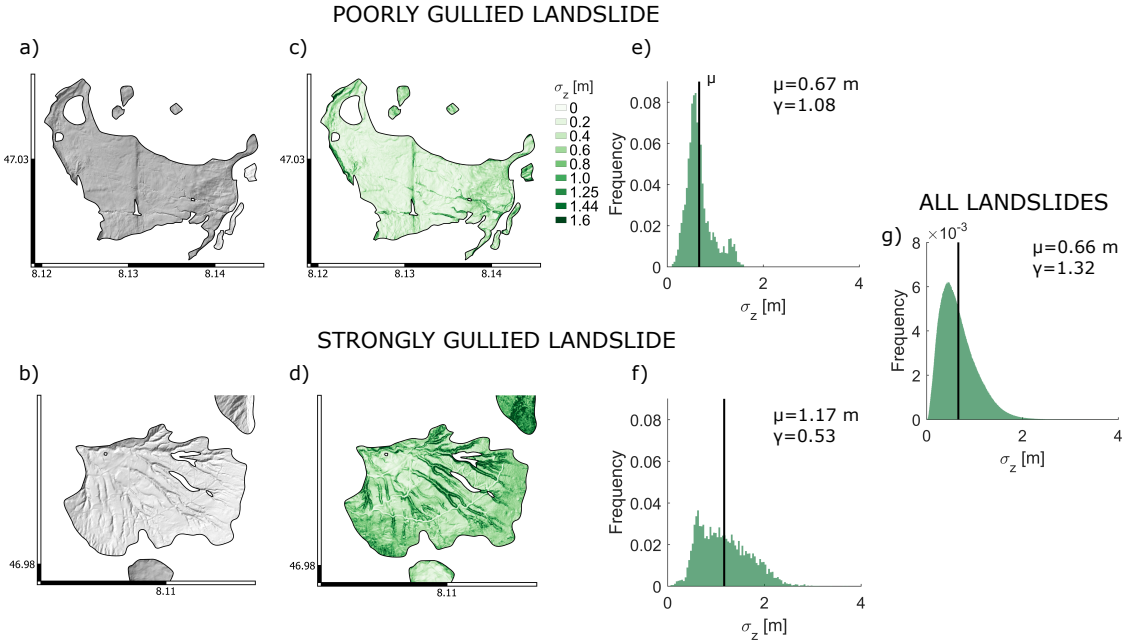

FIGURE 4.5: Quantification of gully development on landslides surfaces. (a, b) Hillshade of the 2 m resolution Lidar DEM (SwissAlti3D), (c, d) surface roughness σ_z computed as the standard deviation of elevations in the Lidar DEM and (e, f) frequency distribution of σ_z, its mean μ and skewness γ for a poorly gullied landslide (top row), and for a strongly gullied landslide (bottom row) in the study basin. (g) shows the σ_z frequency distribution of all landslide surfaces in the basin.

in the basin, while if a better overlap exists for SGL, then simulation SIM B ($\lambda = 100$) would the better choice. The frequency distribution of σ_z for all landslides is shown in Fig. 4.5g, and it is clearly more similar to the PGL σ_z distribution (D Kolmogorov-Smirnov(PGL)=0.22, D Kolmogorov-Smirnov(SGL)=0.58). We conclude that landslide surfaces in the Kleine Emme have weakly developed gullies and SIM A is a better end-member parameterisation, giving more weight to the role of incised rivers in inner gorges as a sediment source.

We note that the surface roughness is, however, high in other steep regions too, like the landslide scarp. This adds spuriously high σ_z in the frequency distribution of the PGL and of the global distribution, while the SGL does not present such features. Removing the spurious σ_z would reduce the mean σ_z and the skewness of the PGL and of the global σ_z distribution, thus differentiating them even more from the SGL, and is therefore not expected to change the results of this comparison.

4.3.4 ^{10}Be as a sediment tracer

The second independent validation of the two end-member simulations SIM A and SIM B is by using ^{10}Be concentrations as a sediment tracer. Time series of modelled ^{10}Be concentrations in the suspended sediment in transport have been derived by associating the representative concentration of each sediment production process to the corresponding sediment flux at the outlet and computing an average ^{10}Be concentration. They are presented in Fig. 4.6a for SIM A and 4.6c for SIM B for one representative year. As it is expected for basins dominated by mass movements, the ^{10}Be tracer shows strong temporal fluctuations driven by the flow rate. Higher flow rates activate the threshold processes in LS_R, LS_{HS} and I, generating pulses of lower ^{10}Be concentrations. The amplitude of the fluctuations is greater in SIM A because of the lower ^{10}Be concentration in the incised areas compared to landslides. The frequency distribution of ^{10}Be concentrations in the

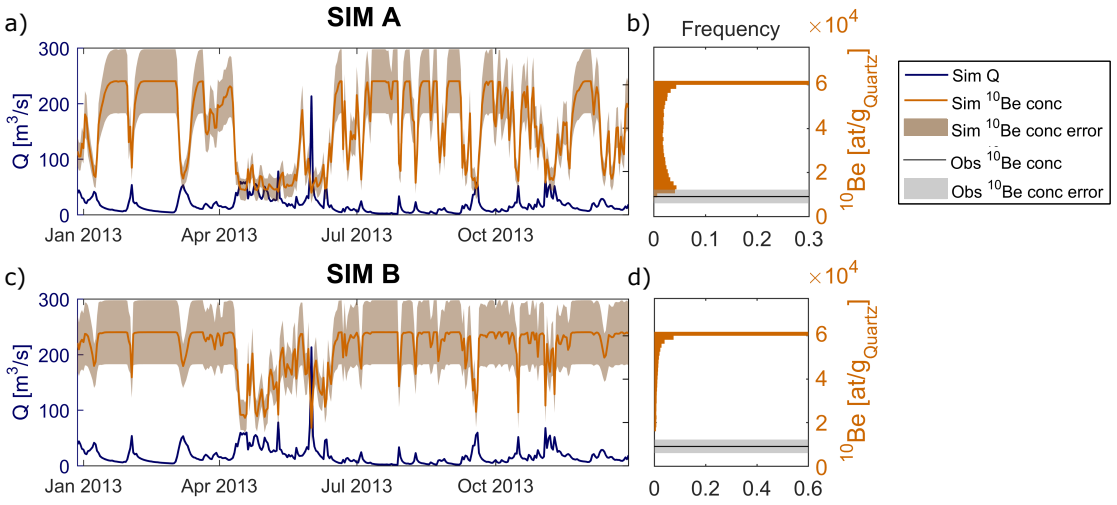

FIGURE 4.6: Modelled and observed ^{10}Be concentration at the outlet. (a, c) Time series of daily flow and ^{10}Be concentration with its uncertainty derived from the modelled sediment load composition for one representative year. (b, d) Frequency distribution of the hourly ^{10}Be concentrations for the simulation period 2004–2016 compared with a single observation of concentration at the outlet by Wittmann *et al.* (2007).

entire simulation period (Fig. 4.6b and 4.6d) is bimodal in SIM A, with a peak at the highest concentrations representing the overland flow erosion process, and at the lowest concentrations, generated by the sediment mobilized from the incised areas and the landslide toes. The clustering of concentrations around two frequency peaks in SIM A, compared to the single peak distribution of SIM B, suggests that the hydrologic conditions that mobilize the sediments from incised areas and from the toes of the landslides are more similar to each other than those that mobilize sediments from the body of landslides. This can be explained by more variable hydrologic (surface runoff) conditions on the hillslopes than in the channel.

In Fig. 4.6b and 4.6d the modelled ^{10}Be concentrations in suspended sediment are compared to a single river bed sample concentration by Wittmann *et al.* (2007). The observed ^{10}Be concentration at the outlet from Wittmann *et al.* (2007) falls at the low concentration end of SIM A frequency distribution, but outside of the range of SIM B simulated frequency distribution. This supports the hypothesis that SIM A is more likely to be compatible with the ^{10}Be observation, and therefore indicates low values of λ, in the vicinity of 1, as a more representative parameterization of the sediment production and transport processes. The simulated distribution of ^{10}Be concentrations compared to the observation would suggest that the sample by Wittmann *et al.* (2007) is representative of extreme flow conditions. However, we will discuss in Sect. 4.4.2 the difficulties associated with such a comparison and its interpretation.

Finally, we explore how well a sediment sample taken on the river bed represents the sediment transported in the river at that location, depending on the sampling location in the cross section. We show in Fig. 4.7 that if the suspended sediment was partially deposited on the river bed as a function of the inundation frequency, there would be a gradient in river bed sediment ^{10}Be concentration with increasing height above the thalweg. Both in SIM A and SIM B, the mean concentration on the river bed decreases with the height, as higher parts of the river bed and bank are only inundated by larger discharges, which are likely to carry high sediment loads from incision areas and landslides with lower ^{10}Be concentrations. The variability of concentrations in sediment deposited on the bed decreases with river bed height in SIM A, while it increases in SIM B. This is indicative of the fact

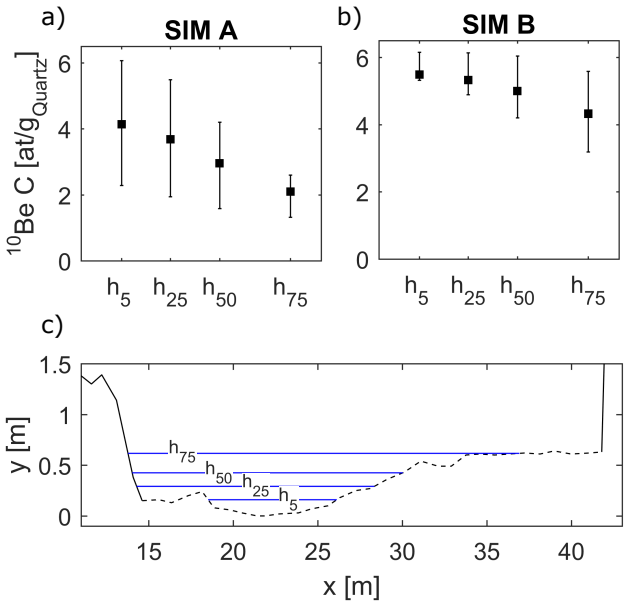

FIGURE 4.7: Distribution of ^{10}Be concentration in potentially deposited sediment in a cross section. (a, b) Mean (square) and interquartile (wiskers) range of the modelled ^{10}Be suspended sediment concentration transported when the water level exceeds h_5, h_{25}, h_{50} and h_{75} (corresponding to the 5th, 25th, 50th and 75th percentiles of the flow distribution). (c) Elevation profile of the outlet cross section with the water depths in blue. The continuous lines indicate a fixed protected bed, the dotted line the mobile bed.

that a wider range of discharges is responsible for sediment mobilization from the localized sources in SIM B, compared to SIM A.

4.4 Discussion

4.4.1 Importance of localized production processes in mountain basins

The implementation of sediment mobilization from localized high sediment production areas with a threshold activation and a strongly non-linear transport rate in a hydrology-sediment model allowed us to reproduce the full range of observed SSCs, the variability in the observed SSC-Q relation, and the annual sediment load at the outlet of the Kleine Emme catchment (Fig. 4.3 and Table 4.3). This represents a substantial improvement in the model performance compared to only including diffuse overland flow erosion in Battista *et al.* (2020a), which resulted in an underestimation of the high sediment concentration pulses and the total sediment yield. This raises the possibility that many other distributed physically-based erosion and sediment transport models based on overland flow alone are probably not suitable for applications in mountain areas, where mass wasting and localized sources dominate the sediment production.

Some evidence for this can be found in the literature. WATEM/SEDEM and RUSLE are based on overland flow erosion and have been found to perform poorly in mountain catchments (Van Rompaey *et al.*, 2005; Borrelli *et al.*, 2014, 2018). Already in the early work of Benda and Dunne (1997), stochastic sediment input from landslides and debris flows was proposed to be an important part of the sediment budget in river network models. de Vente *et al.* (2006) applied a suspended sediment yield semi-quantitative model to 40 catchments including mountainous environments, and found that the model performance substantially increased when the presence of landslides

was accounted for. Several authors have indeed proposed modelling frameworks to simulate the dynamics of such localized sources in mountain environments with different approaches and degrees of complexity (e.g. Wichmann *et al.*, 2009; Bennett *et al.*, 2014; Taccone *et al.*, 2018).

The approach presented here allows, furthermore, to track the sediment produced by the different sources in space and time, and therefore to understand when and why certain sources dominate in the model. For example, the dominant sediment production from incised areas in SIM A is the result of a channel-process dominated system, while SIM B represents a hillslope-process dominated system because most of the sediment load is sourced from the landslide bodies. While the sediment mobilization Eq. 4.2 in our model is the same for all three localized sediment production processes, the gully competence parameter λ on landslides allows to differentiate between the frequency of activation of hillslope and channel processes. In SIM A and SIM B we have considered the two extreme values of λ and, coherently, we obtained respectively very low and very high ratios of hillslope to channel process contributions. We conclude that a more realistic λ for the study basin would probably be an intermediate value between the two end members, and with our analysis we can estimate whether this value should lie close to λ=1 or λ=100.

Poor gully development on landslide bodies and the comparison of modelled time series of ^{10}Be concentrations with measurements, suggest that SIM A is more representative of the Kleine Emme basin than SIM B (see Fig. 4.5 and Fig. 4.6). Therefore, low values of λ are more suitable to parameterize the study catchment, suggesting that channel processes of sediment production are possibly more important than hillslope processes in this catchment. This result is consistent with field observations by Schwab *et al.* (2008), who proposed that in the Kleine Emme the connectivity between landslides on the hillslopes and the river network only takes place occasionally by activation of debris and earth flows. Clapuyt *et al.* (2019) also argued that this coupling is switched on only rarely and for short periods of time and therefore the contribution of hillslope-generated sediments to the annual sediment load is negligible most of the time. The hypothesis of dominant channel sediment production processes in the Kleine Emme basin is supported by qualitative geomorphological observations, such as the presence of river cut terraces and the lack of significant main river adjustment at the confluence of small tributaries. Finally, the presence of multiple gorges with upstream migrating knickpoints also suggests that they act as a significant source of sediment (Schwab *et al.*, 2008; Schlunegger and Schneider, 2005; Van Den Berg *et al.*, 2012; Dürst Stucki *et al.*, 2012).

4.4.2 Implications for the use of CRN data and for provenance studies

The parallel routing of mobilized sediment from different sources to the outlet allows us to produce a transient mixing of sediment that is driven by the space-time variable hydrological regime, i.e. surface runoff. We used ^{10}Be as a sediment tracer in this regards to simulate time series of ^{10}Be concentration at the outlet (Fig. 4.6). ^{10}Be concentrations can be used to derive denudation rates. However, we caution against the use of such modelled concentrations to derive catchment-wide denudation rates for three main reasons: (1) CRN-derived denudation rates are inferred from riverbed sediment samples, while we do not simulate a river bed sediment storage and only simulate the concentration of fine sediment in transport. This also implies that fluvial mixing is not simulated, while this has been demonstrated to be an important factor to smooth out temporal fluctuations of CRN concentrations (Yanites *et al.*, 2009). (2) Our model is suitable for decadal time scales only, and does not account for the formation of new landslides, activation and extension of new inner gorges, knickpoint migration, etc., on longer time scales. On the contrary, denudation rates derived from CRN concentrations integrate time scales of 100-10^5 years and therefore also include these processes. (3) Representative ^{10}Be concentrations attributed to the sediment production processes in our model (see Table 4.1) as a tracer are imperfect, as they are derived from a limited number

of samples non-uniformly distributed in space (Fig. 4.1). Moreover, in the interpolation of the sample concentrations we neglected the dependence of ^{10}Be concentration on elevation and grain size (Lukens *et al.*, 2016; Van Dongen *et al.*, 2019) (see Appendix B). These limitations introduce an uncertainty in the modelled ^{10}Be concentrations at the outlet.

Nevertheless, compared to models specifically developed for CRN dynamics at 10^5–10^6 years temporal scales (Niemi *et al.*, 2005; Yanites *et al.*, 2009), our model includes explicit spatial dependencies along flowpaths and is characterized by a high temporal resolution (hourly). This can provide insights into the short term dynamics of CRNs and help to guide the collection of samples representative of long-term catchment-average denudation rates in mass-movement dominated basins.

In the first place, results like those in Fig. 4.6 can be used to identify the most suitable hydrological conditions for sampling. They allow one to discriminate between hydrological conditions leading to a suspended sediment load dominated by one single process, and those producing instead a mix of sediment sources. Samples for CRN concentration measurements are usually taken from river bed sediment, however in some conditions the provenance of the suspended sediment load can be taken as a proxy for the variability in the fine fraction of riverbed sediments. This is the case for example in the Kleine Emme, where the sediment storage capacity of the river bed is estimated to be small and the residence time of the fine sediment in the basin to be short. Here, we expect the actual smearing effect (Yanites *et al.*, 2009) of hillslope inputs by fluvial mixing to be rather small and, in the period following a large flood, the streambed sediment to be composed mostly of localized source sediment. A sample of such sediment is neither representative of long-term erosion rates, as it is influenced by an exceptional event, nor of catchment-averaged erosion rates, as some regions of the basin are over-represented. Therefore, the two main assumptions at the basis of denudation rate estimates from CRN concentration fail (von Blanckenburg, 2005).

Additional useful information for CRN sampling is provided by the correlation between suspended sediment ^{10}Be concentrations and river bed sampling height above the thalweg. Fig. 4.7 suggests that samples taken higher up on the river bank are likely to be over-representative of localized sediment sources activated by higher flows, therefore it is important to sample closer to the low flow channel to get a more integrated sediment source signal. At the same time, Fig. 4.7 also indicates that the location of sampling matters especially in basins where localized sources of sediments produce a clearly distinct signal for a given range of discharges (SIM A). In these basins, because the variability of potentially deposited concentration decreases with sampling elevation, the probability of observing concentrations that are over-representative of localized sediment sources at the higher locations, is higher compared to SIM B.

To summarize, two practical suggestions can be drawn to guide the sampling of ^{10}Be concentrations representative of long-term catchment-average denudation rates in mass-movement dominated basins: (1) preferring sampling during low flow conditions, while avoiding it during and immediately after high-flow events; (2) avoiding sampling from high-flow deposits by sampling as close as possible to the low flow channel.

Our modelling results predicted a wide distribution of possible ^{10}Be concentrations at the catchment outlet, in which the observation made by Wittmann *et al.* (2007) are exceptionally low. This would intuitively suggest that their sample is representative of an extreme flow event and that the actual catchment integrated erosion rate is much lower. However, there are several issues involved with such a comparison. The first issue is the uncertainty in the modelled ^{10}Be concentrations at the outlet, due to the imperfect estimate of the representative ^{10}Be concentration in the sediment sources (Table 4.1). The second is that Wittmann *et al.* (2007) sampled on the river bed and we are comparing their data with suspended sediments in transport. This implies that the observed grain size is likely to be coarser than the simulated one, and this might introduce a bias towards lower concentrations in the measurements.

Finally, we argue that the approach presented here is useful in combination with fingerprinting methods to complement sediment provenance studies, thus increasing the understanding of the sediment dynamics in river basins. On the one hand, observations of sediment provenance estimated by fingerprinting methods are needed to calibrate the model, as we have proposed by comparing the simulation results with a single measurement of ^{10}Be concentration. Time series of observations of tracers that label the different sediment sources, such as those derived by Navratil *et al.* (2012); Cooper *et al.* (2015); Uber *et al.* (2019), would substantially improve the accuracy of such calibration. On the other hand, the modelling concept can be used to generalize the observations of fingerprinting studies, which allow to reconstruct the sediment provenance only at a limited number of locations and for a limited period of time determined by the availability of field observations. The combination of such datasets with the application of our model would allow to investigate the climatic forcings that produce specific sediment load compositions, as well as to extrapolate the information about sediment provenance to other hydrological conditions and locations across the basin, besides the observed ones. At the same time, the transient routing produced by the model may also provide a physically-based concept to support the choice of statistical mixing models used in fingerprinting methods (e.g Evrard *et al.*, 2011; Blake *et al.*, 2018).

4.4.3 Limitations and further developments

We discuss in the following three main limitations of the model.

The first limitation is the confined model structure. High accuracy was used for the hydrological physical process representation, leading to space-time dependent surface runoff generation, and in identifying possible sediment sources by geomorphological mapping. On the contrary, simplified representations were chosen for overland flow erosion and threshold sediment mobilization from landslides and incised areas. The latter have as few parameters as possible while remaining physically meaningful, to avoid model over-parameterisation with only a single station with SSC observations to compare with. We recognise that other erosion models may use much more complex formulations for erosion and sediment transport, and these could be included in the future, especially for applications where more data are available. Additionally, we focus on bulk fine sediment produced in the catchment and transported in suspension only, because this is the main mode of sediment transport contribution to total yield in many alpine environments (Turowski *et al.*, 2010). Including multiple grain sizes, processes of grain size fining during transport and the interaction between bedload and suspended load would provide a significant improvement and expand the application possibilities.

Model calibration is a second limitation. We performed a manual calibration of the few parameters that needed to be defined, e.g. α, θ, k and μ, by varying a single parameter at a time. We did not vary them simultaneously with an automatic calibration procedure because of computational limitations. In our end-member based analysis, such calibration would allow a better tuning of the parameters and therefore of the contribution of the different processes to the outlet sediment load. However, it is not expected to significantly alter the results of our analysis, as we have shown that OF is only responsible for low SSCs and λ has a dominant role on the sediment contribution compared to μ and k. The added value of an automatic calibration would be to easily identify the intermediate values of λ and corresponding combinations of parameters that equally match the observed SSCs, i.e. several sediment load compositions that represent plausible balances among the sediment production processes in the study basin. To solve this non-uniqueness problem, additional sediment-specific tracing data from the sources of sediments in a basin would be needed, such as additional measurements of tracers at the outlet repeated in time. For example, meteoric ^{10}Be has also been showed to be an effective tracer of sediment production processes within a catchment, with the advantage of being quicker and cheaper than cosmogenic

^{10}Be (Reusser and Bierman, 2010). In order to further constrain the problem, process-labeling tracers like cosmogenic and meteoric ^{10}Be could be associated with tracers adding information on the soil depth of sediment provenance (e.g. ^{137}Cs) and the travel time of sediments from the source to the outlet (e.g. ^{7}Be/^{210}Pb$_{xs}$) (Evrard *et al.*, 2016). In this respect, the modelling framework also offers a possibility to propagate uncertainty, i.e. to simulate sediment fluxes with many realisations of a stochastic climate and parameter values from pre-defined probability distributions, thereby explicitly quantifying the uncertainty in the SSC predictions and partitioning it to climatic, model parameter, and tracer sources.

Finally, in further work, the role of the spatial distribution of λ and its variability in time could be explored. In this work we chose to use a constant value, to explore its role in basin scale modelling. However, Clapuyt *et al.* (2019) showed that episodic hillslope-channel coupling in specific landslide areas in the Kleine Emme basin are key in determining the seasonal sediment load contributions, even if often negligible at the annual scale. This suggests that a better representation of the hillslope-channel balance in the Kleine Emme could be obtained by using a temporally variable λ. At the same time, λ can be expected to also be spatially variable because landslide surfaces have diffferent gradients, morphologies, soils, etc. This is also indicated by the variance of the distribution of surface roughness across all landslides in the study area of this work. An example is the difference between the northwestern region of the basin (Fontanne subcatchment) characterized by narrow and deeply incised valleys and the southeastern region (Entle subcatchment), dominated by wide valley and major instabilities disconnected from the river network (Van Den Berg *et al.*, 2012; Norton *et al.*, 2008; Schlunegger and Schneider, 2005). In a further development of the model, the gully competence parameter on landslides should be adapted to represent a higher complexity and thus simulate more general relations between the size and morphologies of landslide bodies, and the different degrees of hillslope-channel connectivity.

4.5 Conclusions

We presented a hydrology-sediment modelling framework based on the model Topkapi-ETH combined with geomorphic mapping that accounts for localized processes of suspended sediment mobilization, in an application to the pre-Alpine Kleine Emme basin in Switzerland. We introduced sediment mobilization from landsliding areas and incised river gorges, by activation of threshold processes such as erosion of banks and landslide toes, in addition to overland flow erosion. Fine sediment is routed along topographically-driven pathways in parallel from all sources to the outlet. This allows us to reproduce the suspended sediment load composition and its temporal dynamics, including ^{10}Be concentrations as a sediment tracer. The main outcomes of the work are as follows:

(1) The modelling framework with additional concentrated sediment sources from landslides and incised areas allowed us to improve the simulation of observed suspended sediment concentrations and annual sediment load at the outlet, compared to modelling overland flow erosion alone. Such localized sources activated only episodically by surface runoff on hillslopes or high discharge in rivers are very important in the sediment budget of the studied basin.

(2) We quantified two end-members of modelled sediment provenance that could explain the observed SSCs at the outlet of the basin: channel-dominant processes from incised areas, and hillslope-dominant processes from landslide surfaces. In our model, the competition between these two processes is a function of the parameter of gully competence, which adjusts the hillslope sediment production rate on landslide surfaces.

(3) By independent validation of the model with topographic analysis of surface roughness and sediment tracing with ^{10}Be concentrations, it was possible to infer the dominant sediment production processes in the basin. In the study case, we found that the end-member assuming poor

landslide surface gullying and giving more weight to channel processes is more consistent with observations.

(4) The modelled temporal dynamics of sediment load composition provides useful information for guiding sediment sampling for CRN basin denudation rate estimates. Such information can be summarized into the following suggestions: (a) preferring sampling during low flow conditions, while avoiding it during and immediately after high-flow events; (b) avoiding sampling from high-flow deposits by sampling as close as possible to the low flow channel.

This research shows that inputs of localized rich sediment sources activated episodically by hydrological processes can be very important for sediment budgets in mountain basins and should be taken into account when modelling their sediment dynamics. It also shows that transient mixing of sediment from these sources by hydrologically driven runoff generation is to some degree predictable with numerical models. Finally, the proposed framework can be used to generalize the information of sediment apportionment derived by fingerprinting measurements, by linking it to climatic variables and hydrological conditions.

Acknowledgments

This work was founded by the DAFNE project, an Horizon 2020 programme WATER 2015 of the European Union, GA no. 690268. We thank the Swiss Federal Office of Topography for providing the SwissAlti3d DEM (https://shop.swisstopo.admin.ch/en/products/height_models/alti3D) and the GeoCover V2 map (https://shop.swisstopo.admin.ch/en/products/maps/geology/GC_VECTOR), and the Swiss Federal Office for the Environment for providing the cross section measurements.

Author contributions

G. Battista developed the model and carried out the simulations and the analyses of the results. P. Molnar, F. Schlunegger and P. Burlando contributed to conceptualizing the model, planning the simulation and interpretation of the the results. G. Battista prepared the manuscript with contributions and edits from all coauthors.

CHAPTER 5

Sediment supply effects in hydrology-sediment modelling of a pre-Alpine basin

Submitted for publication in *Water Resources Research* on the 7th December 2020, authored by Giulia Battista, Fritz Schlunegger, Paolo Burlando and Peter Molnar.

Abstract

In mountain river basins, sediment availability on hillslopes and in channels is key to predict the sediment response to hydrological forcing. However, quantification of sediment availability and its variability in time is challenging, because sediment supply is often strongly stochastic and dominated by mass wasting. In this paper, we introduced a variable landslide sediment supply as a function of topography, hydrology, and hillslope activity in the hydrology-sediment model TOPKAPI-ETH. We used the model to analyse the dynamics of sediment storage in a mesoscale pre-Alpine basin. We simulated a range of transport- and supply-limited conditions to quantify the variability of suspended sediment concentrations and load, and the seasonal dynamics of sediment storage. We show that supply limitation dampens the natural variability of the hydrological and sediment transport processes, and therefore reduces the scatter of the suspended sediment rating curve. By comparing the model results with observations, we demonstrate that alternation of low and high sediment availability favours sediment load variability at the outlet. The temporal dynamics of sediment storage depends on the hillslope activity, and the balance between sediment supply by landslides and evacuation by runoff. When the export flux is comparable or greater than the recharge flux, the storage shows seasonal fluctuations with a maximum in late winter or spring, and sediment starvation in summer. By representing the dynamics of both inputs and outputs of the sediment storage, the proposed model provides a physically based tool to isolate the effect of transport- and supply-limited conditions in basin sediment response.

Battista G, Schlunegger F, Burlando P, and Molnar P. Sediment supply effects in hydrology-sediment modelling of an Alpine basin. *Water Resources Research*, under review.

5.1 Introduction

Damages caused by flooding in Europe amount to a cost of about 5bn dollars every year, and are showing an increasing trend in the recent decades due to the effect of climate change (Kron *et al.*, 2019). Mountain areas are particularly vulnerable to such damages, because high intensity precipitation events can be associated with substantial mobilization of sediment (e.g. Rickenmann *et al.*, 2016). Mobilization of exceptional volumes of sediment not only creates problems of upland erosion, but also delivers high sediment loads to the river network, which puts at risk downstream areas. Therefore, it is key to be able to predict the sediment response of a river basin to precipitation events. However, the high stochasticity in sediment mobilization and transport processes makes such prediction very complex. In fact, the stochasticity generates strongly scattered rating curves of suspended sediment concentration (SSC) against discharge (Q) in most river basins, implying a large uncertainty in the estimates of sediment load (e.g. Horowitz, 2003; Doomen *et al.*, 2008).

The amount of sediment available for mobilization on the hillslopes and in the channels (i.e. in the sediment reservoir of the basin) at the moment of the rainfall-runoff erosion event is key to determine the sediment response of a river basin (Jakob *et al.*, 2005; Bennett *et al.*, 2014). However, the quantification of basin sediment reservoir and its temporal evolution is very challenging, because it results from the combination of processes of recharge and emptying. Sediment supply is provided to the reservoir by mechanisms such as rock weathering, soil creep, and mass wasting including landsliding, while overland flow on the hillslopes and river flow in the channels evacuate the sediment from the reservoir. In non-glaciated mountain river basins, the sediment supply is often dominated by landslides and therefore can be strongly intermittent (Korup *et al.*, 2004; Hovius *et al.*, 2002). Previous research demonstrated that sediment supply by landsliding is dependent on soil moisture, with more frequent slope failures on wet soils (Iverson and Major, 1987; Coe *et al.*, 2003; Schwab *et al.*, 2007; Coe, 2012; Handwerger *et al.*, 2019a). Some field studies quantified inputs and outputs of the basin storage and proposed a seasonal behaviour to explain its temporal variability (Schuerch *et al.*, 2006; Berger *et al.*, 2011; Fuller and Marden, 2010). However, a comprehensive description of the process of sediment storage is difficult to achieve by means of field observations, because they are limited in spatial and temporal quantification of the sediment fluxes. An alternative approach consists in the implementation of temporally variable sediment supply by landslides into spatially distributed modelling of sediment transport.

In this paper, we introduce a soil moisture dependent sediment supply by landslides in the numerical model of hydrology and sediment transport TOPKAPI-ETH, to study the temporal dynamics of material storage within a basin and its effect on suspended sediment load. Such a model captures the dual effect of precipitation on the basin sediment reservoir: as a driver of recharge by wetting the soil, and of export by generating overland flow and river discharge. We further introduce the dependence of sediment supply on a parameter that controls the activity of landsliding on hillslopes and thus the recharge rate of material stored in a basin. Through this parameter it is possible to generate different scenarios of sediment availability. The model allows us to simulate the dynamics of sediment storage on an hourly scale for decadal time windows, and under different scenarios of hillslope activity.

We applied the model to a pre-Alpine river basin to explore the following research questions:

1) How does basin sediment availability reflect in suspended sediment variability at the outlet?

2) What is the effect of hydrology on the seasonality of basin sediment availability and suspended sediment load?

3) Do we see signatures of sediment supply limitation in sediment measurements?

To answer these questions, we performed a series of numerical simulations assuming different intensities of hillslope activity in order to generate both transport- and supply-limited conditions.

We studied the variability of sediment reservoir across the seasons and different degrees of supply limitation, and explored their effects on the suspended sediment load at the outlet. The simulated seasonality of sediment dynamics was compared with the sediment loads measured in the study basin. We reproduced temporally variable supply and transport limited conditions by bootstrapping the simulations, and compared the results with measurements of hourly suspended sediment concentration in six Alpine and pre-Alpine river basins. We completed the analysis by looking at the spatial distribution of sediment availability, and how this affects the contributions from the different sediment sources.

5.2 Study basins

The Kleine Emme basin

The modelling investigation was conducted on the Kleine Emme river basin, a mesoscale river basin (477 km^2) located in the Swiss pre-Alps. It has a mean elevation of 1054 m a.s.l. and covers an elevation range between 430 and 2300 m a.s.l., the mean annual precipitation is 1650 mm yr^{-1} and the mean annual discharge at the outlet 13.3 m^3 s^{-1}, which corresponds to about 880 mm yr^{-1} (see Table 5.1). The basin has been object of several hydrological and geological investigations. Pappas *et al.* (2015) and Paschalis *et al.* (2014) calibrated the hydrological component of the TOPKAPI-ETH model here. Geological studies highlighted that during the Last Glacial Maximum (LGM) ice only covered the south-eastern region, while leaving the north-western region ice free, and this resulted in a diverse morphology across the basin (Schlunegger and Schneider, 2005; Schwab *et al.*, 2008; Dürst Stucki *et al.*, 2012; Van Den Berg *et al.*, 2012; Clapuyt *et al.*, 2019). The landscape in the SE is characterized by hanging valleys and gorges that incise into the thick glacial deposits, while a smoother topography and a higher drainage density is observed in the NW.

Potential sources of sediment in the basin are represented by landslides and deeply incised areas, such as inner gorges. The mapping performed by Battista *et al.* (2020b) identified 551 landslide bodies covering 7.6% of the entire area. Such mapping also indicates that the greater and thicker landslides are located in the SE, where glaciogenic material is abundant. Schwab *et al.* (2008) and Clapuyt *et al.* (2019) indicated that in the Entle subbasin (SE region) landslides act as sediment factories, because here soil creep produces loose sediment at greater rates than elsewhere, and contribute to the sediment flux only sporadically when debris flows connect them to the channel. Finally, the slip rates of the Schimbrig landslide (Entle subbasin) have been measured by Schwab *et al.* (2007) and described with a Bingham plastic model.

To complement the mapping of landslides carried out by Battista *et al.* (2020b), the slope and thickness of landslides have been derived in this work from a high resolution 2m DEM (SwissAlti3d) and from the thickness model of unconsolidated deposits, respectively. Both datasets have been provided by the Swiss Federal Office of Topography. The location, extent and thickness of these landslides is shown in Figure 5.1a, where those that will have a key role in the simulated sediment production have been labelled and will be discussed later. Figure 5.1b shows the properties of such landslides, in terms of their mean slope, thickness, areal extension (number of cells of the discretized domain occupied by each landslide) and connectivity to the river network (sum of the river network cells overlapping or adjacent to each landslide).

In the basin, measurements of hourly discharge at three gauging stations, bi-weekly suspended sediment concentrations at the outlet, and monthly and annual estimates of suspended sediment load are available from the Swiss Federal Office for the Environment (FOEN). Data of hourly air temperature, sunshine duration and precipitation, and maps of the precipitation spatial distribution (RhiresD gridded data) (Frei and Schär, 1998; Schwarb, 2000) have been provided by MeteoSwiss.

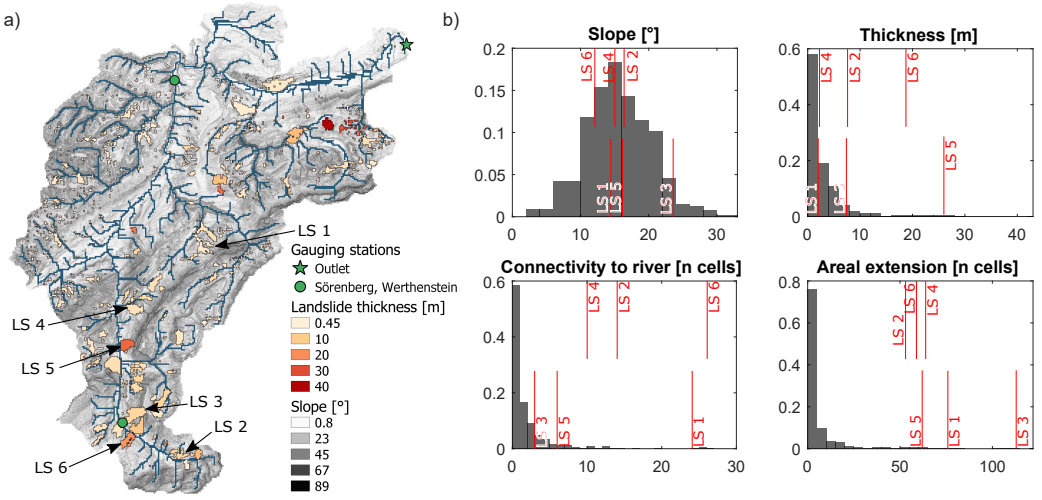

FIGURE 5.1: Landslides in the Kleine Emme river basin. (a) The location and thickness of landslides are shown on the map of the basin slope derived from the 2 m LIDAR DEM (SwissAlti3d). Some of the main landslides that will have a key role in the simulated sediment production have been labelled. The overlap between the landslides and the discretized river network (blue) used in the numerical model gives the connectivity of landslides. The green dots and star indicate the location of the gauging stations. (b) The properties of the labelled landslides are summarized in the histograms in terms of their mean slope, thickness, connectivity to the river network and areal extension.

Basins for comparison with the Alpine context

To put the model application on the Kleine Emme into an Alpine context, the model results were compared with hourly suspended sediment measurements in other Alpine and pre-Alpine river basins of comparable size (Table 5.1). To this purpose, we considered the Emme basin to the west of the Kleine Emme basin with a similar mean altitude and basin characteristics; the Thur basin on the northern margin of the Alps with a similar mean elevation; and additional basins (Ticino, Linth, Aare, and Reuss) that are situated within the Alps and have mean elevations higher than 1700 m a.s.l., and even 2100 m a.s.l. (Aare). The highest basins (Reuss, Aare and Linth) are partially covered by glaciers, which affect their hydrological and crucially their sediment supply regime.

These altitudinal ranges will have a consequence on the pattern of SSCs because a large portion of these basins is situated above the Equilibrium Line Altitude (ELA, c. 1600-2200 m a.s.l.) of the Last Glacial Maximum (LGM) c. 20'000 years ago. As revealed by Schlunegger and Norton (2013), Delunel *et al.* (2020) and Salcher *et al.* (2014), landscapes above this elevation expose oversteepened bedrock and lack a thick and regionally extensive till cover, whereas basins below the LGM ELA are soil mantled and covered with thick glacial till, which are the sources of landslides. These landscape properties affect the sediment availability of the river basins, and are indicated by the authors as the reason for the stochastic nature of soil erosion. The LGM ELA height range also corresponds to the post-LGM mean tree line altitude, thus defining the transition between different weathering regimes. Above the tree line cooler temperatures, longer snow cover, and reduced vegetation cover tend to slow down the chemical weathering, thus favoring the exposure of bare rock (Caine, 1979; Dixon and Thorn, 2005).

TABLE 5.1: Properties of the study basin and the six basins with hourly data of suspended sediment concentration used in this study (FOEN).

River	Area [km^2]	Q mean [m^3/s]	Elevation [m asl]	Slope [°]	Glaciation [%]	Length of Record	Temporal resolution
Kleine Emme at Littau	477	13.3	1054		0	2004-2016	2/week
Emme at Wiler	924	14.1	863	5.9	0	2016-2018	hourly
Thur at Halden	1085	27.8	908	8.5	0	2013-2019	hourly
Ticino at Bellinzona	1517	71.2	1679	22.5	0.2	2013-2019	hourly
Linth at Mollis	600	36.4	1743	23.4	2.9	2014-2019	hourly
Aare at Brienzweiler	555	38.8	2135	22.8	15.5	2014-2019	hourly
Reuss at Seedorf	833	44.3	2013	22.7	6.4	2013-2019	hourly

5.3 Methods

5.3.1 Hydrology-sediment model with variable recharge of the sediment reservoir

In this work we used the hydrology-sediment model presented by Battista *et al.* (2020b), which consists of a component for soil erosion on stable hillslopes and in localized sources, and a suspended sediment transport module integrated within the hydrological model TOPKAPI-ETH. The model is fully distributed and the simulation domain is discretized by a regular square grid in the horizontal dimension and by three soil layers in the vertical dimension. The hydrological component of the model is based on spatially distributed inputs of precipitation, temperature and cloud cover transmissivity, and on the topographic and surface properties of the basin. It includes a physically based representation of evapotranspiration based on Priestley-Taylor equation, groundwater as a linear reservoir, interception of rainfall by vegetation, snow accumulation and melt, and overland flow generation on the hillslopes by saturation and infiltration excess, and by exfiltration from the subsurface. Cells are connected in the horizontal direction by water fluxes in the channel, surface and subsurface, based on the steepest gradient and are solved with the kinematic wave approximation. The reader is referred to Fatichi *et al.* (2015) for a detailed description of the hydrological model.

Soil erosion is modelled by a module for overland flow erosion on stable hillslopes, and one for sediment mobilization from localized sediment sources, i.e. landslides and inner gorges. Sediment flux picked up by overland flow qs_{OF} [kg m^{-2} s^{-1}] is assumed to be always at transport capacity and proportional to the cell slope S and overland flow q_{OF} [m^2 s^{-1}]:

$$qs_{OF} = \alpha q_{OF}^{1.4} S^{1.4}. \tag{5.1}$$

Eq. 5.1 results in a nearly linear response of the sediment flux to the hydrological forcing. A spatial distribution is attributed to α [kg s$^{0.4}$ m$^{-4.8}$] based on the land use and soil properties of the basin (Battista *et al.*, 2020a). Given the transport capacity hypothesis, it is assumed that sediment availability for the overland flow process, i.e. the sediment reservoir on stable hillslopes, is unlimited.

Sediment mobilization from localized sources is assumed to take place when the bed shear stress applied by overland flow and river flow exceeds a critical value. The specific sediment flux qs [m^2/s] from the localized sources is computed as

$$qs = k(\theta - \theta_c)^{\mu}, \tag{5.2}$$

where θ is the dimensionless bed shear stress, θ_c the critical dimensionless bed shear stress, and k [kg m^{-1} s^{-1}] and μ are parameters that regulate the sediment flux. The combination of a threshold and an exponential sediment transport function results in a strongly non-linear sediment evacuation from localized areas. Since the evacuation of material by runoff in channels and on landslides establishes the coupling between the sediment factory and channel network, Eq. 5.2 makes the coupling relationships between hillslope and channelized processes non-linear.

Two types of localized sources are modelled: landslides and incised areas. Such elements are considered to be fixed features of the landscape, which are given as input maps by the user. Landslides are represented as clusters of cells, which can be either adjacent and connected to the river network, or disconnected when located on the hillslopes. Landslides directly connected to the river network can be emptied both by river flow and hillslope runoff on their surfaces, while landslides disconnected from the river are only accessed by hillslope runoff and become connected to the river network only if the bed shear stress of overland flow along the flow path remains higher than the critical value θ_c. The erosive power of overland flow on landslide surfaces is regulated by a gully competence parameter λ, which describes the width w_{LS} of the gullies on landslide surfaces relatively to the cell size of the model Δx ($\lambda = \frac{\Delta x}{w_{LS}}$) (Battista *et al.*, 2020b). Therefore, the bed shear stress of overland flow on the hillslopes in Eq. 5.2 is computed as

$$\theta_{HS} = \frac{1}{G-1} \frac{q_{OF}\, \lambda\, S}{u\, d_s}\,, \tag{5.3}$$

where u [m s^{-1}] is the flow velocity computed by the hydrological model, G the specific gravity of sediment and d_s [m] the grain size.

Sediment mobilized on stable hillslopes and landslide surfaces can reach the river network, if the transport capacity of overland flow along the flow paths allows it, otherwise it deposits on the hillslopes. Sediment that reaches or is input into the channel is advected to the basin outlet by the flow velocity, without the possibility to deposit on the river bed. The reader is referred to Battista *et al.* (2020b) for more details about the sediment module.

The new modelling element introduced in this work is a variable sediment availability in the landslide sources. On landslides, material available for erosion is considered to be made available through sliding of the landslide mass, as this mechanism is responsible for the fragmentation of material. This has also been documented for the study basin (Schwab *et al.*, 2007). Therefore, the slip rates of landslides u_{LS} define the volume of sediment available for erosion in gullies and river network, i.e. the recharge rate of the basin sediment reservoir. According to the Bingham plastic model proposed by Schwab *et al.* (2007), the sliding velocity of each landslide was assumed proportional to the soil moisture ν, thickness H [m] and slope $\hat{\alpha}$ of each landslide, and to a parameter c_{LS} representing the level of hillslope activity:

$$u_{LS} = c_{LS}\, \nu\, H^2\, sin\hat{\alpha}\,. \tag{5.4}$$

Eq. 5.4 results in a distribution of landslide velocities within the basin, which can be shifted towards lower or higher values by modifying c_{LS}, to capture a growth or reduction in the landslide activity which cannot be explained by soil moisture only. This parameter basically amplifies the moisture controls on landsliding.

Therefore, the volume of material V available at each landslide for mobilization from its surface or toe is produced by the sliding (Eq. 5.4) and emptied by river flow and overland flow (Eq. 5.2 and Eq. 5.3):

$$\frac{dV}{dt} = u_{LS} A_{LS} - \sum_{i=1}^{n_R} qs_{Ri}\, w_{Ri} - \sum_{i=1}^{n_{LS}} qs_{LSi}\, w\,, \tag{5.5}$$

TABLE 5.2: Calibrated parameters and model performance for the reference simulation SIM a. $\overline{\alpha}$ is the mean value of the spatially distributed parameter of overland flow α in Eq. 5.1. k, μ, θ_c and λ regulate the sediment flux from localized sources (Eq. 5.2 and Eq. 5.3). c_{LS} represents the level of hillslope activity in the sliding velocity u_{LS} (Eq. 5.4). The coefficient of determination R^2 and the model efficiency ME of the simulated hourly sediment loads describe the performance of the sediment component.

$\overline{\alpha}$ [kg $s^{0.4}$ $m^{-4.8}$]	k [kg m^{-1} s^{-1}]	μ	θ_c	λ	c_{LS}	R^2	ME
0.3412	9.17e-6	6	0.05	100	1e-6	0.48	0.40

where A_{LS} is the area of contact between the landslide and the river network, n_R and n_{LS} the number of river and hillslope cells where runoff mobilizes sediment from the landslide, qs_R and qs_{LS} the sediment flux from the toe and the landslide surface respectively, w_{Ri} the river width in the cell i and w the gully width on landslide.

By combining a soil moisture dependent rate of sediment supply with the modelling of runoff on hillslopes and channels, the model captures the dual role of precipitation on sediment availability: as a recharge factor by means of soil moisture v (Eq. 5.4), and as an export driver by means of river and overland flow discharge (Eq. 5.2). Furthermore, with the user-input parameter c_{LS} we introduce the possibility to simulate different long term ratios of sediment supply recharge to sediment export rates. In the model the stream has no buffering effect, because neither deposition of the mobilized sediment on the river bed nor floodplain incision are allowed. Therefore, the slip rates of landslides limit the volume of sediment available for erosion and low c_{LS} values can lead to supply limitation in the river basin. This conceptualization is summarized in Fig. 5.2.

5.3.2 Simulation of transport and supply limited conditions

The model was set up for the period 2004-2016 with a spatial resolution of Δx = 100 m and an hourly time step Δt = 1 h. The hydrological component was forced with spatially distributed hourly data of precipitation, temperature and cloud cover transmissivity, and calibrated against the hourly flow measured at three gauging stations obtaining a good performance (r=0.84 and model efficiency ME=0.69), see Battista *et al.* (2020a).

The calibration of the sediment model parameters was performed separately for the two modules. First, the overland flow erosion parameter α was calibrated by switching on only the overland flow erosion module and by fitting the simulated Q-SSC cloud of points at the outlet to the observed one excluding the extreme values, see Battista *et al.* (2020a). Then the localized sediment source module was switched on, and the μ and k parameters calibrated to best fit the observed SSCs without any limitation on the values, see Battista *et al.* (2020b). Because our aim is to explore the dynamics of the landslide sediment reservoir, we calibrated the model by setting λ=100 to simulate the highest overland flow erosivity in gullies on landslide surfaces, i.e. assuming narrow gullies with a width w=1 m in Eq. 5.3. In this phase, the availability of landslide sediment was considered unlimited, by setting c_{LS} high enough to avoid that any of the landslides exhausted their sediment reservoir during the simulation. Because of this unlimited reservoir hypothesis, we define this calibrated simulation SIM a as transport-limited. The calibrated parameters and the model performance are reported in Table 5.2.

By taking as a reference the transport-limited simulation SIM a, we performed four additional simulations (SIM b, c, d and e) where we gradually reduced the c_{LS} recharge parameter to achieve different conditions of supply limitation in the study basin. In order to explore the full range of possible sediment availability conditions, the c_{LS} value was reduced by two orders of magnitude in each simulation until the contribution of landslide sediment source to the annual load was close to

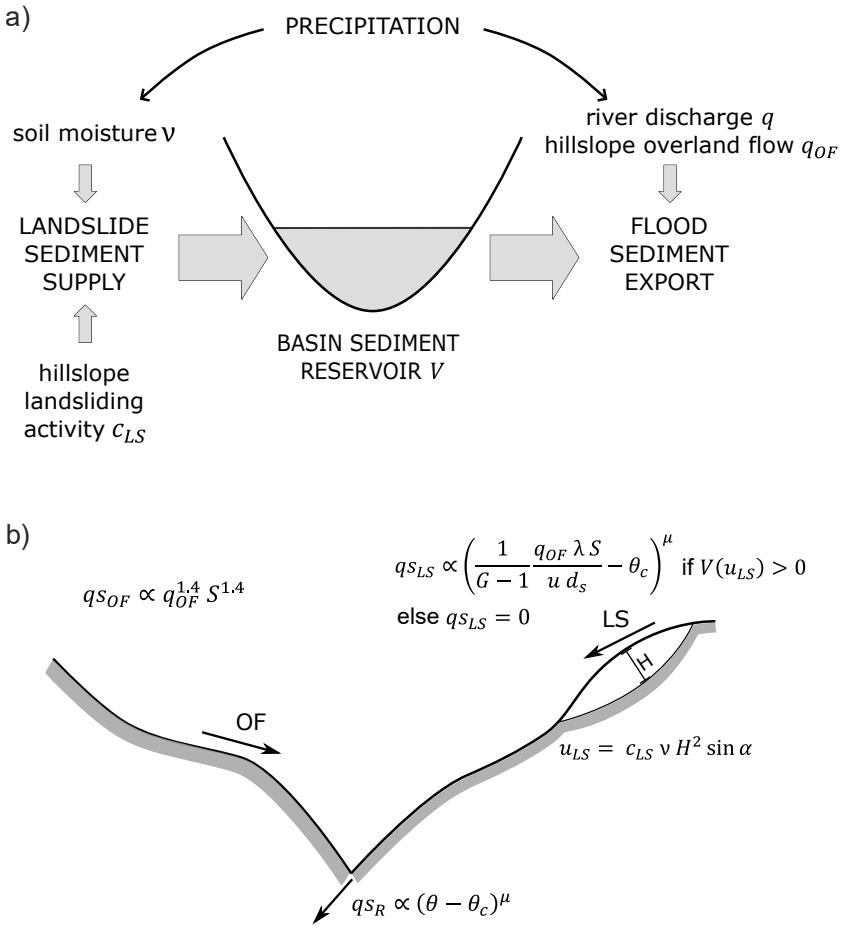

FIGURE 5.2: The TOPKAPI-ETH hydrology-sediment model simulates the temporal and spatial dynamics of the basin sediment reservoir. (a) The recharge is provided by sediment supply from landslides, which is proportional to soil moisture ν and hillslope activity c_{LS}, and the sediment export is given by river q and hillslope q_{OF} runoff. Precipitation affects both recharge and export of the sediment reservoir, by increasing the soil moisture, and by producing runoff. (b) Processes of sediment export by runoff on hillslopes and channels: overland flow q_{OF} erodes sediment on the stable hillslopes with a close-to-linear response qs_{OF}, and in gullies on landslide surfaces qs_{LS}, river flow q erodes at the toe of landslides connected to the river network qs_R. qs_{LS} and qs_R have a strongly non-linear response to the flow, provided that enough volume of material V (see Eq. 5.5) is available for transport. The material is made available by the landslide at a rate given by the sliding velocity u_{LS}, which is the mechanism responsible for the fragmentation of material.

zero. The c_{LS} parameter is assumed constant in time and uniform in space in the simulations, and its values cover a range from $1{\cdot}10^{-6}$ in SIM a to $1{\cdot}10^{-14}$ in SIM e.

5.3.3 Combined transport-supply limitations and comparison with observations

Although soil moisture has been identified as the main driver of landslide sediment supply (e.g. Handwerger *et al.*, 2019a), the internal geotechnical processes of landslide motion are not fully described by the soil moisture dynamics. For instance, sudden transitions from slow to fast moving conditions can occur, thus providing pulses of sediment supply that increase the sediment reservoir of the basin (Schumm, 1979; Benda, 1997; Fuller *et al.*, 2003; Handwerger *et al.*, 2019b). The description of such variations in hillslope landsliding activity requires a modification of the c_{LS} parameter in time. To reproduce this condition we generated time series of SSCs at the outlet by

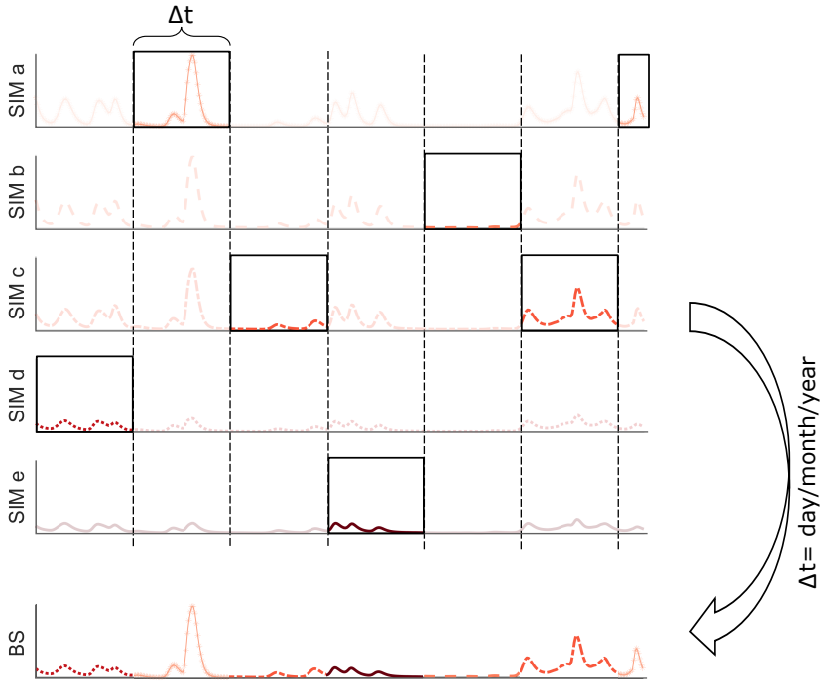

FIGURE 5.3: Bootstrapping of the simulations. Each bootstrapped time series was derived by randomly sampling for each Δt of the simulated period (2004-2016) the corresponding time series of hourly SSCs at the outlet from SIM a to SIM e. The random sampling was repeated 100 times for each value of Δt, where Δt was taken equal to one day, one month and one year. In this way, we obtained three groups of 100 bootstrapped time series (BS) of the same duration of SIM a to SIM e, corresponding to the daily (BS d), monthly (BS m) and yearly (BS y) time scales.

bootstrapping the five simulations SIM a to SIM e on daily, monthly and yearly periods, to simulate different time scales of the variability in the hillslope activity, i.e. of c_{LS}. In particular, for each simulated day, month or year of the period 2004-2016, we randomly selected the corresponding time series of hourly SSCs at the outlet from SIM a to SIM e. We repeated this random sampling 100 times for each time scale. In this way, we obtained three groups of 100 time series corresponding to the daily (BS d), monthly (BS m) and yearly (BS y) sampling time scales of the same duration of SIM a to SIM e (2004-2016 period) (see Fig. 5.3). This procedure allows us to introduce an element of stochasticity in the level of hillslope activity, while maintaining the correspondence between the hydrology and the sediment response of the basin within each day, month or year.

Finally, we compared the variability in the hourly modelled SSCs and their correlation with discharge with observations of SSCs in natural river basis. From the network of monitoring stations managed by FOEN, we selected six Alpine and pre-Alpine basins in Switzerland where hourly data of suspended sediment concentrations are available from turbidity measurements (see Table 5.1). We excluded the largest basins to keep the comparison among basins of a size similar to the Kleine Emme.

5.4 Results

5.4.1 In the sediment factory: production of sediment and supply limitation

Landslides supply material to the drainage network through sliding, which then becomes available for evacuation by runoff. Accordingly, the pattern of slip rate of landslides within a basin yields a spatio-temporal picture of the sediment reservoirs within a basin. In this section we summarize

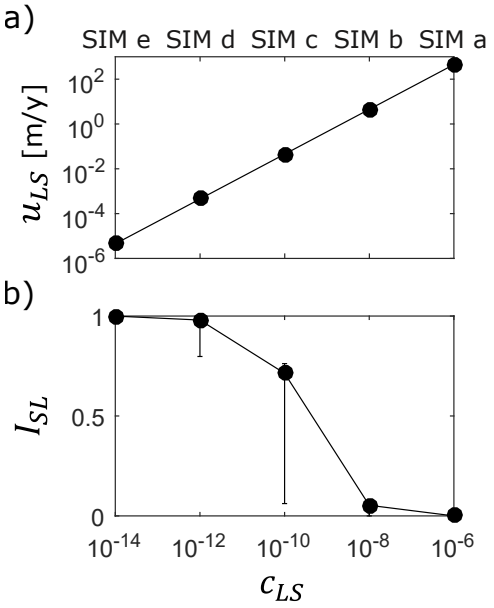

FIGURE 5.4: Landslide sliding velocity and supply limitation as a function of the c_{LS} parameter. (a) Mean u_{LS} over the entire simulation period of the spatial median and hourly sliding velocity from all landslides. (b) Index of supply limitation I_{SL} evaluated over the entire simulation period (dots), and the interquartile range of its monthly fluctuations (error bar).

the results of the five simulations SIM a to SIM e, controlled by changes in Eq. 5.4, in terms of the sliding velocities of landslides and the degree of supply limitation. The variability of landslide properties across the basin produces a distribution of sliding velocities. Therefore, in Fig. 5.4a for each simulation we report the mean over the simulation period of the median sliding velocity of all 551 landslides at each time step. The range of velocities produced by the simulations goes from extreme values (450 m/y), corresponding to a very high sediment supply to the reservoir, to almost static landslides (4.5e-3 mm/y), corresponding to very little sediment supply.

The supply limitation of each simulation is quantified as the deficit of sediment volume sourced from landslides V_{LS} in each simulation compared to the reference transport-limited simulation SIM a (Fig. 5.4b). We defined the index of supply limitation I_{SL} for the i-th simulation as:

$$I_{SL_i} = \frac{V_{LS}(SIMa) - V_{LS}(SIMi)}{V_{LS}(SIMa)} \tag{5.6}$$

The error bar in Fig. 5.4b shows the range of monthly I_{SL} fluctuations. We observe that SIM b reproduces consistently low I_{SL} across the months, i.e. predominantly transport limited conditions. On the contrary, SIM d and SIM e reproduce consistently high I_{SL}, i.e. predominantly supply limited conditions. Seasonal fluctuations are instead more pronounced in SIM c, covering a much wider range of I_{SL} values from supply limited to unlimited conditions. Overall, with this set of simulations we are able to cover the entire range of sediment availability conditions from $I_{SL} \approx 0$ to $I_{SL} \approx 1$.

5.4.2 Dynamics of the sediment reservoir

While landsliding contributes to the build up of the sediment reservoir on the hillslopes (modelled with Eq. 5.4), localized erosion by runoff in channels at the toe of the landslides and in rills on the landslides themselves (combination of Eq. 5.2 and 5.3) results in the evacuation of the sediment reservoir. The spatio-temporal development of the balance between both processes

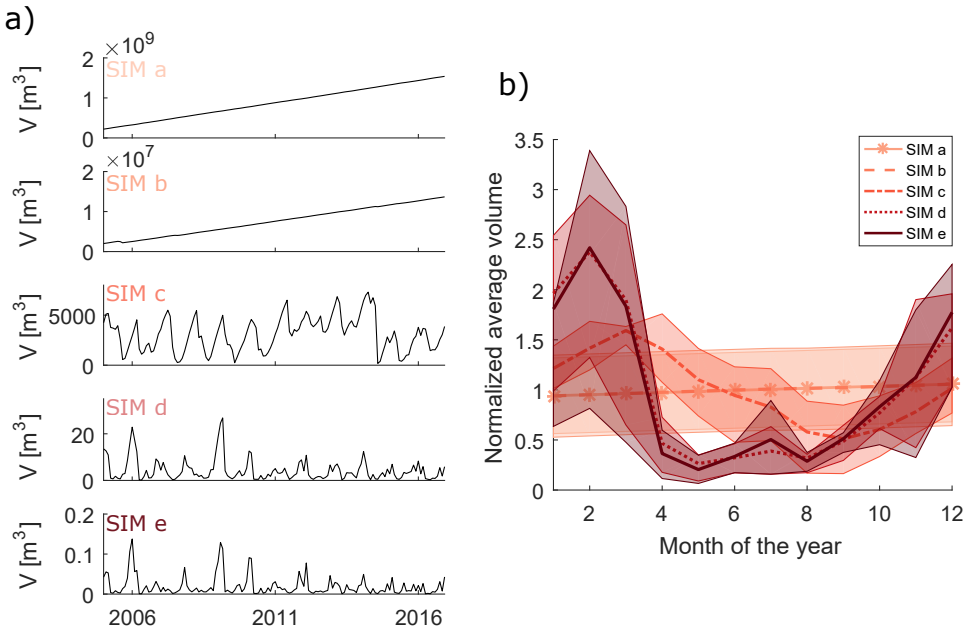

FIGURE 5.5: Temporal dynamics of sediment storage. (a) Time series of the mean monthly volume of sediment stored in the 8 most contributing landslides for SIM a to SIM e. SIM a and b show a steadily increasing volume of sediment, indicative of transport limited conditions, SIM c shows a steady state between sediment production and evacuation, and SIM d and e show predominant supply limited conditions. (b) Average monthly volume of the sediment stored in the 8 most contributing landslides, normalized by the mean volume of each simulation. The shaded areas indicate the interannual variability in terms of the interquartile range of the normalized monthly volumes.

results in a dynamic evolution of sediment storage. In particular, due to the spatial variability of precipitation, runoff and landslide properties within the basin, each landslide contributes with a different proportion to the total load. To analyse the sediment storage response to the hydrological forcing we focus on those landslides preferentially activated by runoff. We identified them by selecting the most contributing landslides in the transport limited simulation (SIM a), because in this case the contributions are determined purely by the overland flow and river shear stress distribution (combination of Eq. 5.2 and 5.3). Accordingly, we focused on 8 landslides constituting 70% of the total mobilized sediment in SIM a. In Fig. 5.5a the time series of the mean monthly volume of their reservoir is reported for SIM a to SIM e. We observe that the decrease in the volume from SIM a to SIM e corresponds to a change in the temporal dynamics too. SIM a and SIM b show a steady increase in the reservoir volume, as a result of a much greater recharge rate than export by floods. SIM c shows oscillations around the mean value for most of the simulation, and is empty only about one month a year. SIM d and SIM e also show fluctuations, but with longer periods of almost empty reservoir. The reservoir fluctuations are the result of the temporally varying balance between the process of landslide recharge, and the flushing of sediments produced by floods.

The seasonality of the stored sediment is further explored in Fig. 5.5b where the average of the reservoir volume over a year is reported for each simulation, including their interannual variability (shaded areas). To allow comparison among the simulations, the volumes have been normalized by their mean value over the entire simulation. Three seasonal behaviors of the reservoir can be identified also in this case: transport limited conditions without any seasonality (SIM a and SIM b), oscillation around the mean volume with a minimum in September (SIM c), and oscillations around

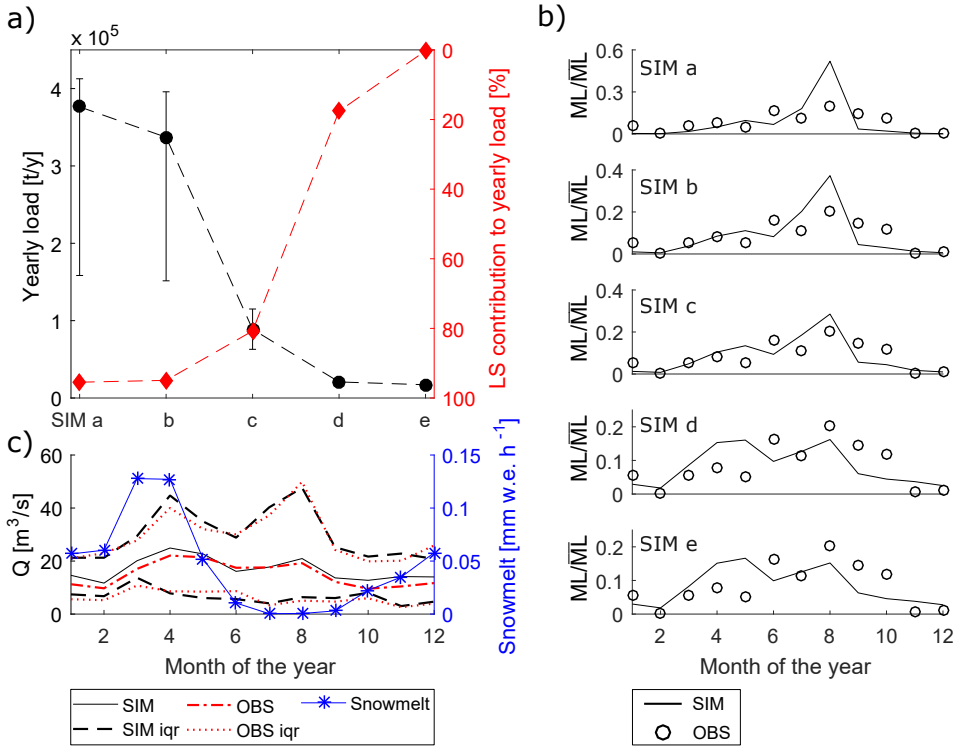

FIGURE 5.6: Sediment load and discharge at the outlet. (a) Mean annual load for SIM a to SIM e and the interquartile range of its interannual distribution (black dots with whiskers). The error bars reflect the effect of the non-linearity of the hillslope-channel coupling relationships, and patterns of SIM d and e mainly reflect the response of sediment supply by overland flow erosion, which is a nearly linear function of hydrology (Eq. 5.1). The red diamonds indicate the portion of the load produced by landslides, please note the reverse axis. (b) Simulated and observed mean monthly sediment loads (ML) at the basin outlet normalized by their 12 month average ($\overline{ML}$). The observed monthly loads have been provided by FOEN. Please note the different y-axis values. (c) Comparison of the simulated and observed mean monthly streamflow and their interquartile range (iqr), and seasonality of the simulated snowmelt.

the mean volume with a predominance of low sediment availability from April to September and a maximum value in February (SIM d and SIM e).

5.4.3 Variability in suspended sediment at the outlet

The effect of basin sediment availability on the sediment dynamics at the outlet is shown in Fig. 5.6 in terms of magnitude, variability and seasonality of the sediment load.

In Fig. 5.6a the annual sediment load is reported for each simulation, together with its interannual variability and the percentage of the total sediment load sourced from the landslides. Besides a reduction in the magnitude of the yearly load with decreasing landslide sediment supply, we also observe a decrease in its interannual variability. This results from a lack of sediment available for mobilization on the landslide bodies and at their toes, due to their slow sliding rates, and consequently to the gradual switching off the non-linear component of the hillslope-channel coupling (Eq. 5.2 and 5.3). In fact, 99.7% of the yearly load in SIM e is made up of sediment eroded by overland flow erosion (Eq. 5.1), whose response to the hydrological forcing is close to linear.

Fig. 5.6b shows the simulated and observed mean monthly sediment loads at the basin outlet. The loads have been normalized by their average over the 12 months to allow comparison of the seasonality independently of the mean simulated load. The seasonality shows two peaks, one in spring and one in late summer, which are driven by peaks in snowmelt and rainfall. While the timing of the peaks remains consistent across the simulations, the relative magnitude of the summer peak compared to the spring peak decreases significantly with increasing supply limitation. The seasonality of the observed monthly contributions is best captured by SIM c, while transport limited and strongly supply limited conditions would respectively overestimate or underestimate the summer contribution.

The observed and simulated seasonality of the sediment load differ mostly in the early summer (June), when an extra peak of sediment load is evident from the observations, and in autumn (September and October), when the simulations underestimate the observations. To investigate the sources of such discrepancy, in Fig. 5.6c we compare the observed and simulated monthly streamflow, and the monthly simulated snowmelt. Both the mean and the extremes of the monthly flow rates are captured very well by the model, especially between May and September, and therefore the performance of the hydrological model is not the cause for missing the June peak of sediment load. We also do not expect it to be the reason for the underestimation of sediment load in September and October, because in these months the simulated flow actually slightly overestimates the observations. We suggest that mass wasting events may have affected the sediment regime in these months, and therefore added a stochastic component to the flow-driven sediment response, which is not accounted for by the simulations. The effect of such events is likely to be amplified by the method applied in the extrapolation of the monthly loads from the bi-weekly sediment samples (FOEN, 2010), where in fact more weight is given to the higher observed SSCs. Moreover, the underestimation of sediment flux by the model in September and October is expected to be also caused by the simulation of direct flushing of sediment to the outlet in the river network, without the possibility to deposit it on the river bed. The lack of a reservoir of sediment in the river bed probably causes a quicker exhaustion of the modelled sediment wave than in reality.

In Fig. 5.7 we further characterize the modelled sediment dynamics by analyzing the suspended sediment concentration at the outlet of the basin, and compare it to observations from six other Alpine and pre-Alpine river basins where hourly data of SSCs are available. In Fig. 5.7a the correlation coefficient ρ of hourly water discharge and SSCs is plotted for SIM a to SIM e, the bootstrapped simulations at different time scales and the observations. For the same SSC time series, the SSC variability relative to the Q variability is quantified in Fig. 5.7b in terms of the variability index VI:

$$VI = \frac{CV(SSC)}{CV(Q)} \tag{5.7}$$

where CV is the coefficient of variation.

SIM a to SIM e predict an increasing correlation coefficient ρ and decreasing variability VI of suspended sediment concentration at the outlet with increasing supply limitation, indicating a dampening of the natural variability by effect of sediment starvation. The bootstrapped simulations show consistently lower ρ and higher VI than SIM a to SIM e, indicating the temporal variability of hillslope landsliding activity as a source of scatter. It is noticeable that the observed data of other catchments cover the entire range of ρ and VI produced by SIM a to SIM e and by the bootstrapped simulations in the Kleine Emme. The mean elevation of the river basins seems to suggest that higher elevation basins tend to have a lower correlation between SSC and Q and a higher SSC variability and therefore are more likely represented by the bootstrapped simulations, which mimic with a time-variable c_{LS}, than by models using a single c_{LS} value as in SIM a to SIM e.

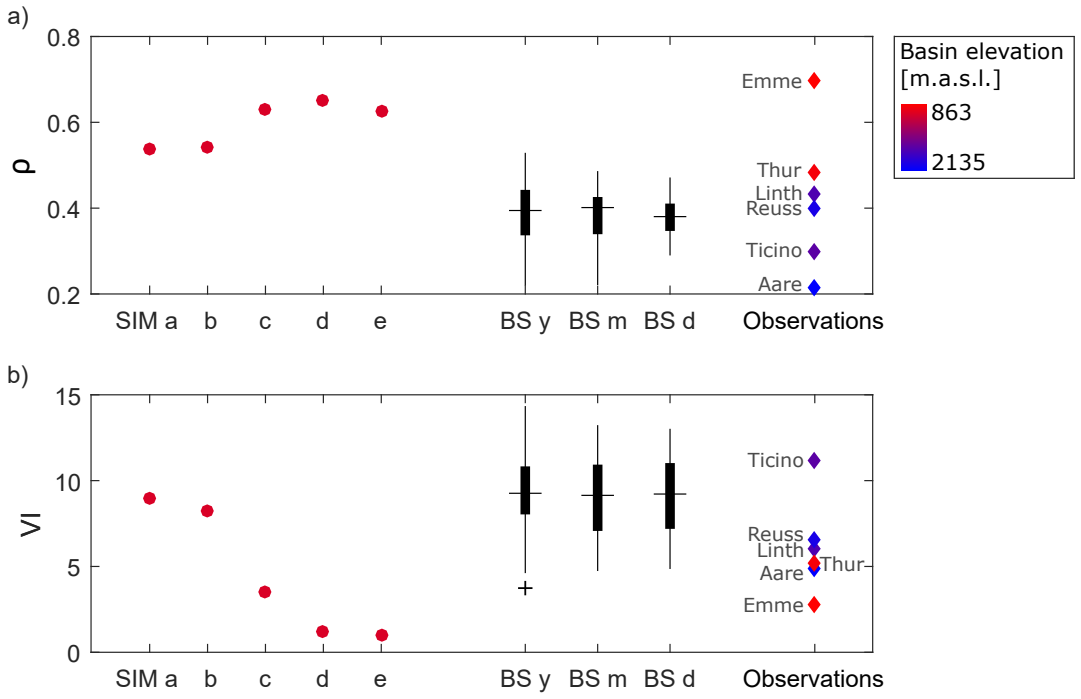

FIGURE 5.7: Variability of suspended sediment concentrations at the outlet. (a) Pearson correlation coefficient ρ between SSC and discharge at the outlet in SIM a to SIM e (dots), in the bootstrapped simulations (boxplots) at three different temporal scales (yearly BS y, monthly BS m and daily BS d) and in 6 monitored catchments in Switzerland (diamonds). b) Variability index VI of SSC in SIM a to SIM e (dots), in the bootstrapped simulations (boxplots) and in 6 monitored catchments in Switzerland (diamonds). The color coding of the diamonds and the SIM a to SIM e dots indicates the mean basin elevation.

5.4.4 Contribution of landslides as sediment sources

We complete the analysis by looking at the spatial effect of a variable landslide sediment supply. Fig. 5.8a shows the maps and frequency distribution of the mean annual contribution of each landslide to the total volume of mobilized sediment for a transport limited simulation (SIM b), a supply limited simulation (SIM d) and the intermediate condition (SIM c). Because the amount of sediment mobilized from the landslides that does not reach the channel is negligible (<3 mm of sediment deposition in 13 years in the cell with highest deposition), the contributions in Fig. 5.8a are also indicative of the landslides that mostly contribute to the sediment flux at the outlet. We notice that the landslides with the highest contribution to the sediment load are located in the south-eastern region of the basin, which is characterized by higher precipitation intensities and where the thicker and larger landslides are concentrated. The location of the dominant sediment sources changes as the sediment availability decreases, due to the exhaustion of the sources preferentially activated by hydrology, i.e. the most contributing landslides in SIM b. This also determines a shift in the frequency distribution, with a decreasing number of landslides dominating the sediment production as the supply limitation increases. In transport limited conditions, LS 1, 2 and 3 are the most contributing, because they combine high bed shear stress with high connectivity to the river (LS 1, 2), areal extension (LS 1, 2 and 3) and slope (LS 3) (see Fig. 5.1b). In intermediate conditions of sediment availability LS 2 dominates, because it is not only large and well connected to the river network, but also has a high thickness of deposits and a relatively high slope, which guarantee a

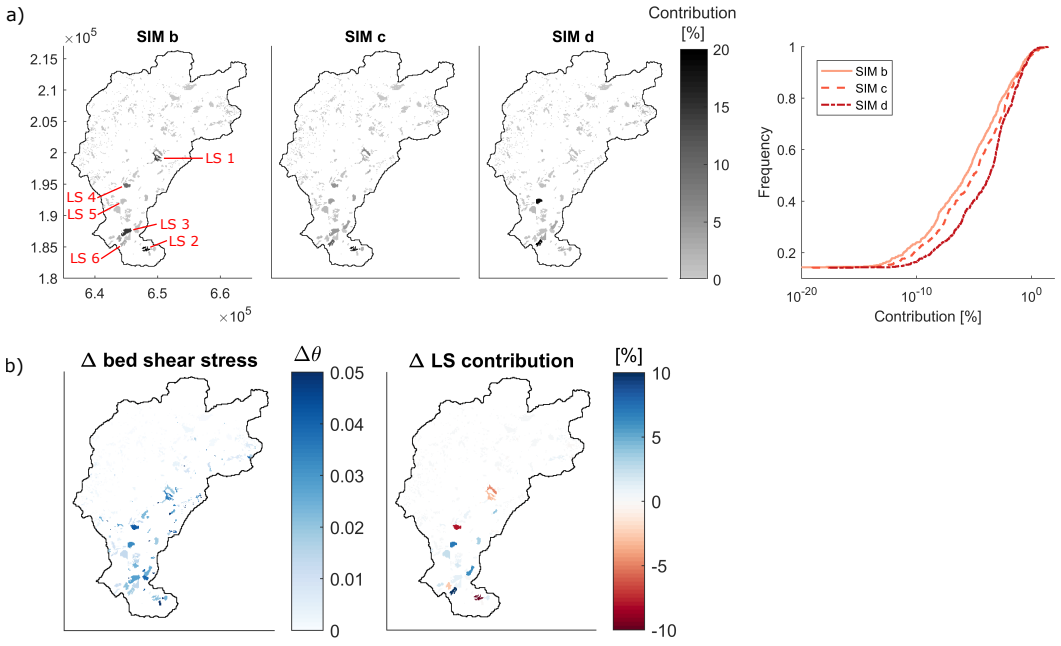

FIGURE 5.8: Contributions of the single landslides to the sediment load. (a) Maps and frequency distribution of the mean annual contribution of each landslide for SIM b, SIM c and SIM d. The properties of the landslides labelled in SIM b map are shown in Fig. 5.1b. (b) Difference between the summer and winter mean bed shear stress on landslides, and difference between the summer and winter seasonal contribution of each landslide in SIM c. A positive value indicates a greater bed shear stress or landslide contribution in summer.

high rate of sediment supply. Finally, in supply limited conditions (SIM d), LS 5 and 6 become dominant, mainly because of their very high thickness, which results in a high sliding velocity of the landslide (Eq. 5.4).

The effect of seasonal exhaustion of the sediment storage is shown in Fig. 5.8b, where the difference in the bed shear stress on landslide surfaces between summer and winter is compared to the difference in the landslide contributions for the intermediate condition SIM c. In the south-eastern part of the basin, while the bed shear stress is greater in summer than in winter, the sediment production does not increase proportionally and some landslides actually show a lower summer contribution due to a lack of sediment.

5.5 Discussion

We used the hydrology-sediment model TOPKAPI-ETH to investigate numerically the effects of sediment supply limitation on sediment load in the context of pre-Alpine basins. We assumed that the two main sources of sediment in the basin are erosion by overland flow on hillslopes and mobilization of sediment from landslides. Landslides have the greatest contribution to the modelled sediment budget, because it was assumed that the gullies on their surfaces are highly competent, and that a non-linear coupling between landslide surfaces and river network exists. We introduced a dependency of the sediment supply by landslides on the hydrology and on the activity of hillslopes. In this way the model creates a temporally variable sediment availability in the basin, and by the choice of model parameters it is possible to simulate different scenarios of sediment availability. We used this setting to study the dependency of suspended sediment dynamics both on

the seasonal fluctuations of the sediment storage driven by soil moisture and runoff variability, and on the sediment productivity of the basin depending on the hillslope activity.

In the next sections, we will address the research questions by discussing the impact of sediment availability on the variability of suspended sediment at the outlet, and the seasonality in basin sediment storage and suspended sediment load.

5.5.1 Supply limitation reduces sediment variability and shifts sediment sources

In Sect. 5.4.3 we showed that increasing supply limitation in a simulation leads to a reduced variability of suspended sediment concentrations and loads at the outlet. This is indicated by the reduction in yearly load interannual variability (Fig. 5.6), the increase in correlation between Q and SSC and the decrease in the variability of SSCs from SIM a to SIM e (Fig. 5.7). The reason for such reduced variability is the gradual switching off of sediment supply by landslides as their sliding velocity decreases. By switching off the strongly non-linear coupling of landslides and channels, the variability of the sediment response is reduced not only because the transport capacity cannot be fulfilled anymore, but also because the sediment is mobilized mainly by a close-to-linear relation to hydrology (overland flow). The implication of such a decreased variability and increased correlation is the reduction of the scatter in the SSC-Q rating curve with increasing supply limitation, and this indicates that one effect of sediment shortage can be to smooth out the natural variability given by the combination of flow variability and non-linearity of the sediment transport.

The reduction of sediment flux variability at the outlet corresponds to the exhaustion of the main sediment sources, i.e. the landslides preferentially activated by hydrology. In transport-limited conditions the landslide contributions are determined by the spatial distribution of bed shear stress, their size and slope, defining the sediment export by the overland flow on their surfaces, and their connectivity to the river network. Instead, in supply-limited conditions, the most contributing landslides are those that, besides being activated by hydrology, also have a high thickness (and slope) that determines a high supply rate. The combination of these features results in a higher contribution to the sediment load from the regions of the study catchment where precipitation is more intense, and the glacial ice cover during the LGM left a high availability of glaciogenic material on the hillslopes, and therefore a landscape dominated by wide and thick instabilities. On the contrary, smaller and shallower landslides in the non-glaciated areas result overall in minor contributions to the sediment load.

5.5.2 Stochasticity of soil erosion favors suspended sediment variability

The correlations between SSC and Q of the monitored basins clearly distinguished between low elevation basins (Emme and Thur) with a higher correlation, and high elevation basins located in the Alps with a generally lower correlation (Aare, Reuss, Linth and Ticino). Such low correlation is due to the occurrence in the observed time series of some events of sediment export with very high SSC to discharge ratios and may be explained by a strong stochasticity in the erosional processes of these basins. In fact, above the ELA of the LGM the erosional activity by glaciers produced strength-limited rock-dominated basins (Schlunegger and Norton, 2013; Salcher *et al.*, 2014), where sediment starvation is frequent and stochastic mass wasting provide pulses of sediment supply temporally increasing the sediment availability. The stochasticity of soil erosion has been associated to the steepness of basins by Delunel *et al.* (2020), who showed that it is dominant in oversteepened catchments due to the decoupling between hillslope and rivers produced by the glacial history. Therefore, the steep average slope ($>22.5°$) of the high-elevation Alpine basins considered in this study supports the hypothesis that stochasticity of erosion processes plays a key role in the sediment dynamics of these basins. For instance, this is well documented in the Aare basin where

the sediment dynamics is dominated by frequent debris flows, originating from the very steep slopes of the headwaters with colluvial and glacial deposits (Kober *et al.*, 2012).

However, not all the considered Alpine basins are also characterized by high variability indices (Aare, Reuss and Linth). In these cases the time series of SSC and discharge only show a few events with extreme SSC/Q ratios, which are responsible for lowering the correlation ρ, but their low frequency does not significantly increase the variability of SSC compared to the discharge (Eq. 5.7). This effect can be explained by the role of glacial melt, which favors a high correlation between concentrations and flow (e.g. Collins, 1989). The Aare, Reuss and Linth are indeed the basins with greatest glacial cover among those considered in this study. Therefore, in these basins the strong correlation provided by glacial melt is on the one hand perturbated by stochastic mass wasting (low ρ), and on the other hand it keeps low the variability of concentrations with respect to flow

Such different behaviours of the low and high elevation basins considered in this study are confirmed by the bootstrapped simulations. These assume a random variability of the sediment supply by landslides, and are therefore representative of the stochastic nature of soil erosion in time. The low correlation ρ between SSC and discharge, as well as the high variability index VI of the high elevation basins are better captured by the bootstrapped simulations than SIM a to SIM e. The role of stochastic sediment supply in favoring suspended sediment variability is confirmed by Horowitz (2003) and Fuller *et al.* (2003), who found that computing separate rating curves for periods of abundant and scarce sediment availability improves SSC predictions. Doomen *et al.* (2008) and VanSickle and Beschta (1983) also proposed to introduce in the sediment rating curves a parameter describing the availability of sediment to improve their performance.

Finally, the bootstrapped simulations suggest that the extreme values of sliding velocities in the transport-limited simulation SIM a are better interpreted as transient conditions, rather than permanent ones. In fact, comparable values have only been measured on very short time scales (Schwab *et al.*, 2008), after which modifications in the morphology induce feedback processes that slow down the landslide. Our conclusions are supported by other authors, who reported shifts between basin sediment availability conditions in different case studies. For instance, Fuller *et al.* (2003) found alternating multi-annual periods of transport and supply limitation in Taiwan mountain basins and attributed them to variations in the sediment supply produced by landslides. Significant variation of the sediment rating curve parameters due to the exhaustion of sediment availability were observed by Horowitz (2003) in the Mississipi, Missouri and Ohio Rivers following a major flood. Modifications in the sediment availability regimes have also been associated with human landscape modifications, such as land use change and logging (e.g. Beschta, 1978; Walling, 2008; Belmont *et al.*, 2011).

5.5.3 Hydrology produces sediment storage seasonality

Precipitation has two opposite effects on the storage of sediment in our modelling setup: on the one hand it favors input into the sediment reservoir by increasing soil moisture and therefore supply by landslides, on the other hand it favors sediment export by producing runoff, which erodes the surface and the toes of landslides. With the proposed model we are able to evaluate how these two effects balance each other during the year and at different levels of hillslope landsliding activity.

In predominantly transport limited conditions the recharge rate is much higher than the export, and therefore no seasonality can be observed in the sediment storage time series. Instead, when the two processes have a comparable magnitude (SIM c) or the export dominated the recharge rate (SIM d and e) seasonality appears. In winter, when the soil moisture is high and the flood events are limited, the recharge rate dominates the export and the sediment storage grows from late summer to spring. In spring and summer the magnitude and frequency of flood events increases and export

dominates, producing a decreasing sediment storage from April to September, or a sharp decrease in March and April followed by a period of approximately stationary empty volume.

The modelled sediment storage seasonality is supported by qualitative and quantitative observations that landslide derived sediment input to the channel is greater during the winter and spring months (Schuerch *et al.*, 2006), and that landslide deposits in the channels are present in spring but disappear by the end of the summer in Alpine basins (Berger *et al.*, 2011). Alternating periods of filling and cutting of fan channels have also been related to the sediment supply dependence on hydrology by Fuller and Marden (2010).

The modelled sediment starvation in summer affects the seasonality of the sediment flux at the outlet by significantly reducing the summer peak of sediment load compared to the transport limited case, where the sediment response reflects the hydrological forcing. The observed seasonality of sediment fluxes in the study basin suggests that sediment transport is likely affected by sediment starvation in summer, because it best compares with SIM c. Furthermore, the deviation of the observed seasonality from the simulated one indicates that random pulses of sediment inputs may affect the sediment dynamics in the case study. These would also explain some of the high observed sediment loads that do not correspond to peaks in the mean or extreme discharge.

Different sediment dynamics regimes at the seasonal level have been observed for example by Beschta (1978) and Nanson (1974), and led to the idea of introducing a dependence on the season in the sediment rating curves (Kao *et al.*, 2005). Finally, we showed that seasonal sediment source contributions are determined not only by the hydrological forcing, but also by the spatial distribution of sediment availability. In intermediate conditions of sediment availability, the landslides with a limited recharge rate could not fulfill the transport capacity of the highest flows (e.g. in summer). On the contrary, the very high thickness of some glacially conditioned landslides allowed them to respond even to the higher floods by increasing their contribution.

5.6 Conclusions

We introduced a dependency of the sediment supply by landslides on the hydrology and hillslope activity of the river basin in the TOPKAPI-ETH hydrology-sediment model. In this way, we are able to reproduce basin systems with a temporally variable sediment availability, and different degrees of supply limitation. The model was applied to a river basin representative of pre-Alpine conditions for 13 year long simulations of various scenarios. The results lead to the following main conclusions:

1) The numerical model allows us to investigate the effect of sediment availability on suspended sediment concentration variability at the basin outlet, helping to disentangle the causes of the scatter of the Q-SSC rating curve. We found that a generally low sediment availability in the river basin dampens the natural variability of SSCs, and therefore reduces the scatter of the SSC-Q rating curve. Alternation between conditions of low and high sediment availability produced by temporal variations in the hillslope activity overall increased sediment load variability at the outlet.

2) We demonstrated the effect of hydrology on the seasonality of sediment storage and suspended sediment load, and in particular on the dual role of precipitation as a driver both of sediment recharge by high soil moisture, and of its export by floods. We showed that, when the sediment supply by landslides is comparable to the flood sediment export, their temporally variable balance during the year produces sediment storage recharge in the winter months and emptying from spring to the end of summer. In supply limited conditions, sediment starvation significantly dampens the sediment load in summer, and affects the location of the seasonal sediment sources.

3) Observations of suspended sediment concentrations from six Alpine and pre-Alpine basins support the physical plausibility of the model approach. They also indicate that the high variability in the sediment concentrations of high elevation basins may be related to the sediment inputs by stochastic mass wasting, which interrupt the predominantly supply-limited conditions. In the study basin, supply limitation in summer may explain the relatively low magnitude of the sediment response to the summer floods, compared to the sediment response observed in spring.

The new feature of the TOPKAPI-ETH hydrology-sediment model allows the representation of both the input and output dynamics of the sediment storage. In this way, it is a step towards a comprehensive physically-based representation of the suspended sediment transport in pre-Alpine rivers. The novel sediment component of the model allows to represent a variety of properties of the basin to capture the natural complexity of the system, while keeping the key parameters limited in number and with a precise physical meaning. This means that, although some parameters may produce the same effect on the modelled sediment load at the outlet, the knowledge of the geomorphology of the case study helps to define their realistic range. Therefore, the parameterization can be constrained to values that are consistent with the processes they are expected to represent. The association of the model with landslide monitoring and sediment tracing would help to improve the model calibration, and would be useful to infer a frequency distribution of the c_{LS} parameter to replace the constant value used in this work with temporally variable values. Finally, the representation of the physical mechanisms of the sediment dynamics provided by the model allows to explore changes in the sediment dynamics under scenarios of future climate, related to the magnitude and variability in the dynamics of sediment availability.

Acknowledgments

This work was founded by the DAFNE project, an Horizon 2020 programme WATER 2015 of the European Union, GA no. 690268. The SwissAlti3d DEM (https://shop.swisstopo.admin.ch/en/products/height_models/alti3D) and the thickness model of unconsolidated material (https://shop.swisstopo.admin.ch/en/products/geological_models/unconsolidated_deposits) can be obtained from the Swiss Federal Office of Topography. The discharge and sediment concentration data can be requested to the Swiss Federal Office for the Environment (FOEN), and the meteorological data to MeteoSwiss.

Author contributions

G. Battista developed the model and carried out the simulations and the analyses of the results. P. Molnar, F. Schlunegger and P. Burlando contributed to conceptualizing the model, planning the simulation and interpretation of the the results. G. Battista prepared the manuscript with contributions and edits from all coauthors.

CHAPTER 6

Conclusion

6.1 Summary

This thesis explored three major sources of variability of the suspended sediment dynamics in a mesoscale pre-Alpine basin. The three main research questions addressed the role of (1) spatially variable erosion drivers, (2) localized sediment sources and (3) the sediment availability on hillslopes and in channels. To answer the research questions, I incrementally developed a new soil erosion and sediment transport component for a spatially distributed hydrological model. A new model was needed to fill a lack of spatially distributed numerical models suitable for long-term continuous simulations in medium to large river basins, ones that keep track of the sediment origin and the dynamics of sediment storage. The developed model has been applied to a representative pre-Alpine mesoscale basin with different configurations, in order to explore the sources of suspended sediment variability.

The TOPKAPI-ETH hydrology and sediment transport model
To develop such a model, I introduced three new modules in the TOPKAPI-ETH spatially distributed hydrological framework to simulate (i) hillslope erosion by overland flow, (ii) sediment mobilization from landslides and incised areas, and (iii) the dynamics of the volume of sediment available for transport in sources. Sediment mobilized from hillslopes, landslides and incised areas is routed on the hillslopes according to the transport capacity of overland flow, and then advected in the river network to the outlet. The sediment fluxes from the different sources are routed as independent waves, so that the temporal dynamics of the sediment provenance can be reconstructed at any river cell. Finally, the model allows for soil moisture dependent sediment supply by landslides and keeps track of the volume of sediment available in the sources. In this way, transport- and supply-limited conditions are explicitly distinguished. The model can be applied to medium to large scale river basins (>500 km^2) with spatial and temporal resolutions in the order of $\Delta x \approx 100$ m and $\Delta t \approx 1$ h for simulations of multiple decades.

The Kleine Emme basin
The study case is the Kleine Emme river basin, located in central Switzerland. This basin was chosen because of its diverse geomorphology, which was partly shaped by the ice cover during the Last Glacial Maximum c. 20'000 years ago, and partly by fluvial processes (e.g. Schlunegger and Schneider, 2005; Van Den Berg *et al.*, 2012). The basin has been object of several hydrological and geomorphological studies: Pappas *et al.* (2015) and Paschalis *et al.* (2014) calibrated the hydrological component of TOPKAPI-ETH here, Schwab *et al.* (2008), Schwab *et al.* (2007), Dürst Stucki *et al.* (2012) and Van den Berg and Schlunegger (2012) studied instabilities and inner gorges in the basin, and Van Den Berg *et al.* (2012), Clapuyt *et al.* (2019) and Norton *et al.* (2008) measured ^{10}Be concentrations to derive denudation rates in the subcatchments.

Below I provide a summary of the main thesis results, a discussion of the relevance of the presented research and an outlook for future model developments and applications.

6.1.1 How does spatial variability in the erosion drivers impact suspended sediment dynamics? (RQ 1)

To answer this research question, in Chapter 3 I introduced the component of hillslope erosion by overland flow into the hydrological model TOPKAPI-ETH (see Sect. 2.2.2), and used it to compare the effect of spatially variable (V) and spatially uniform (U) precipitation (P) and surface erodibility (α) on the sediment mobilization and suspended sediment transport.

I found that spatially variable drivers of erosion favour the representation of the SSC variability in the model, i.e. the scatter of the SSC-Q rating curve (Fig. 3.3). The temporal and spatial variability of precipitation contributes to SSC variability, by allowing to distinguish for example the basin response under localized intense summer events from that driven by diffuse snowmelt and winter storms. A spatially variable surface erodibility also increases the variability, when its spatial distribution enhances the heterogeneity of the basin given by the distribution of slope, elevation, aspect, and soil properties. However, the model showed a strong underestimation of the observed SSCs at high flows and therefore suggests that some sources of natural variability are still missing. I hypothesized that these are the localized sources of sediment, i.e. landscape features with a small areal extent that preferentially supply large amounts of sediment such as landslides. These sources usually have a threshold behaviour and get activated only at high flow. Their localized nature increases the spatial variability of the basin properties and therefore is expected to favour the SSC variability at the outlet.

The spatial distribution of erosion drivers was also demonstrated to be key in determining the location, productivity and connectivity to the outlet of the areas of sediment production. Although both spatially variable precipitation (VP) and erodibility (Vα) favour the clustering of sediment sources (Fig. 3.7), they have opposite effects on the sediment production (Fig. 3.8). VP favours clusters of high soil moisture, which are hotspots of overland flow and subsequent erosion, and therefore has a higher erosive power than UP (uniform precipitation). Vα also favours clusters of sediment production where the land cover is most susceptible to erosion. However, the combination of intense overland flow areas with lower erodibility areas in the study basin decreases the sediment production by Vα compared to Uα.

The connectivity to the river network of sediment production areas (Fig. 3.9) on the hillslopes was found to be reduced by VP, due to the concentration of rainfall in areas with low topographic connectivity. Vα also reduces spatial connectivity, because it accounts for the buffering effect of forested areas around first order channels, which reduce sediment input into the streams.

Overall, the spatial variability in erosion drivers produces the following effects on the sediment load at the outlet of the study basin (Fig. 3.10): (i) VP is more erosive than UP and increases the sediment load, despite a reduced connectivity of the sources to the outlet, and (ii) Vα leads to lower erosion than Uα and also decreases the source connectivity to the outlet, therefore decreasing the sediment load. Although these results are strongly dependent on the specific spatial distribution of precipitation, surface erodibility, and physical properties of the studied basin, I will discuss below the general implications of these findings (Sect. 6.2). Due to the underestimation of SSCs at high flow, the total sediment load at the outlet was also significantly underestimated. To improve the model's predictive capability, in the Chapter 4 I introduced sediment mobilization from localized sources of sediment.

6.1.2 What is the effect of localized sediment sources on the sediment provenance? (RQ 2)

In Chapter 4, I addressed this question by mapping the location and extent of potential localized sediment sources in the study basin, i.e. landslides and deeply incised areas, and by introducing sediment mobilization from them in the TOPKAPI-ETH model (see Sect. 2.2.2). The contribution

of the localized sources to the sediment flux is modelled as a non-linear threshold process (Eq. 2.11), and the overland flow erosivity on landslides is regulated by a parameter of gully competence (Eq. 2.13). This parameter defines the degree of development of gullies on landslide surfaces, and therefore the concentration of overland flow in rills (Eq. 2.14). Two calibrations of the model including this new feature were performed by assuming a very high and a very low gully competence, i.e. respectively strongly gullied and non-gullied landslides. Both calibrations reproduced the full range of observed SSCs, thus significantly improving the predictions by the previous version of the model (compare Fig. 3.3 and Fig. 4.3). This confirmed the hypothesis made in Chapter 3 on the contribution of localized sources, and suggests that many distributed models based on diffused hillslopes erosion only are probably not suitable for applications in mountain areas (Van Rompaey *et al.*, 2005; Borrelli *et al.*, 2014, 2018).

The two end-member simulations led to different sediment provenance: dominated by channel processes when the gully competence was minimum, and by landslides when it was maximum (Fig. 4.3). I evaluated the more representative calibration for the case study by analysing the roughness of landslide surfaces (Fig. 4.5), and by validating the simulated sediment provenance with tracing of ^{10}Be concentrations (Fig. 4.6). Both validations suggest that in the study basin gullies on landslides are predominantly poorly developed, and that sediment sources in and adjacent to the channel dominate the load at the outlet. This result is further supported by independent geomorphological observations that the connectivity between the landslides and the river network is switched off most of the time, and by the presence of cut terraces and migrating knickpoints in the inner gorges (Schwab *et al.*, 2008; Clapuyt *et al.*, 2019; Van Den Berg *et al.*, 2012).

To summarize, localized sediment sources have a key role in the sediment budget of pre-Alpine basins, in particular at high flow rates. Their morphological properties, such as the gully development on landslides, control their connectivity to the channel and therefore the provenance of sediment at the basin outlet. The simulated temporal dynamics of sediment provenance also indicates that in pre-Alpine basins this is highly variable in time and characterized by pulses of sediment from the localized sources, which dominate the load during flood events.

To further investigate the role of localized sediment sources, in the Chapter 5 I explored their dependence on the sediment availability given by the season and the hillslope activity.

6.1.3 How does suspended sediment dynamics depend on basin sediment availability? (RQ 3)

This research question has been addresses in Chapter 5, by simulating time-dependent sediment availability in the basin. I did so by including in the model a variable sediment supply by landslides as a function of their physical properties, soil moisture and intensity of hillslope activity, and by keeping track of the basin sediment availability, recharged by landslide supply and emptied by flood events (see Sect. 2.2.3).

I simulated five scenarios of sediment availability by varying the intensity of hillslope activity to generate transport- and supply-limited conditions. I bootstrapped the simulated time series to produce stochastic variability in the sediment availability, and compared the results with data from the case study and basins of similar size in Switzerland.

The results showed that an overall low sediment availability reduces the variability of SSCs and load at the outlet, by dampening the natural variability of the sediment production and transport processes (Fig. 5.6a and 5.7). Alternating conditions of low and high sediment availability overall increase the variability of suspended sediment load at the outlet (Fig. 5.7). I interpreted these conditions as representative of the strong stochasticity of mass wasting in high elevation basins, which is documented by e.g. Fuller *et al.* (2003) and Delunel *et al.* (2020), or shifts in the sediment

transport regime following a major flood or catastrophic events, as observed by e.g. Horowitz (2003).

The modelled seasonality of the basin sediment reservoir showed that, when the sediment supply by landslides is comparable to the sediment export by floods, the storage recharges in winter and empties from spring until the end of summer (Fig. 5.5). In this case, sediment starvation happens in summer, and substantially dampens the peak of suspended sediment load generated by the flood events. Observations in the case study indicate that this could be the case in the Kleine Emme basin. The model also combines the spatial distribution of sediment availability and hydrological forcing to predict the contribution of sediment sources, and highlights the key role of thick landslides located in glacial deposits when the system runs into supply limitation (Fig. 5.8).

To summarize, basin sediment availability affects the suspended sediment dynamics by influencing the magnitude, variability and seasonality of concentrations and loads at the outlet. Comparison of model results and observations suggests that basins may naturally shift from transport- to supply-limited conditions due to intermittent sediment supply. The spatial distribution of geomorphic properties that control sediment supply with respect to the hydrological forcing is key to determine the dominant sources of sediment.

6.2 Discussion and implications

Importance of resolving spatial variability

From the presented results emerges the importance of understanding and characterizing the spatial variability in the drivers of sediment mobilization and the processes of transfer to the outlet of river basins. In Chapter 3, I showed the effect of spatial distribution of precipitation and surface erodibility on erosion and transport by overland flow, and demonstrated that it affects the sediment production and connectivity of the sources to the river network. Therefore, predictive models need to resolve explicitly such variability in order to capture the correct driving mechanisms of the mobilization and transport of sediment across river basins.

Such effects are expected to be even more significant when localized sediment sources are present in a basin, because these enhance the heterogeneity of potential sediment production across the basin. In this case, the spatial distribution of erosion drivers is key to determine the combination of a strong hydrological driver with highly productive sediment sources, such as intense precipitation on major landslides. When this happens, very small areas of the basin may dominate the sediment yield of the entire basin, as it has been observed in several Alpine basins (e.g. Korup *et al.*, 2004; Schuerch *et al.*, 2006; Delunel *et al.*, 2014; Cruz Nunes *et al.*, 2015). This is the case also in the simulations presented in Chapter 5, which include sediment production from landslides. Here, the spatial distribution of hydrological forcing, morphological properties and sediment availability determines the contribution of each landslide, and 70% of the total sediment load both in supply- and transport-limited simulations is produced by landslides covering only about 1% of the basin area (Fig. 5.8).

Previous modelling work also suggested the importance of clusters of high soil moisture in the hydrological and hydromorphological response of river basins (Paschalis *et al.*, 2014; Peleg *et al.*, 2020). The modelling framework and the analysis presented in this thesis allow a spatially explicit physical explanation of the role of hydrological and morphological drivers in the source contribution of pre-Alpine basins.

Dynamic simulation of functional connectivity

The newly developed sediment component for the TOPKAPI-ETH hydrological model provides a dynamic evaluation of the functional connectivity based on the information of structural connectivity

(Wainwright *et al.*, 2011; Fryirs, 2013; Bracken *et al.*, 2015). The spatial resolution of 100 m used in the applications of this thesis is likely too coarse to fully capture the strong spatial gradients of the pre-Alpine and Alpine landscapes, as well as the very small landslides that may have a significant effect on the sediment budget. However, the model structure is such that the concepts of structural and functional connectivity are both included. Below I discuss how they are captured by the model, and the connectivity elements that emerge from the applications presented in this thesis.

In the TOPKAPI-ETH model, the information about the structural connectivity is represented thanks to its grid-based nature, which allows for a spatially distributed description of the physical properties of the study basin. In this way, the physical connection between landscape elements given by the topography is represented. This is key in the modelling of the sediment dynamics to include the information about the location of areas of sediment production with respect to the channel network. Such information is present in the model applications of this thesis, in the position of the landslides with respect to the river. This determines the mechanism with which they can be emptied, i.e. either by the overland flow only, or by both overland and river flow. Analogously, the very strong hillslope-channel connectivity in the incised areas is represented by their location along the river network.

Based on the physical properties of the basin, the hydrological processes determine the surface and subsurface water fluxes, e.g. the slope of each basin cell determines the flow direction, the land cover the evapotranspiration, and the soil properties the infiltration rate and subsurface lateral flow. By associating the surface water fluxes to sediment mobilization and transport, the sediment component of the model builds a link between the physical properties of the basin and the sediment transport processes. In this way, it represents the functional connectivity, i.e. the connection between landscape units provided by the processes of sediment transport.

Because of its spatial and temporal dimension, the representation of the functional connectivity in model is dynamic in space and time. Such representation is given in the first place by the routing of sediment on hillslopes, which depends on the magnitude of overland flow, and the topographic and land cover properties (slope and surface erodibility, Eq. 2.10). These determine the transport capacity of overland flow, which may produce transfer of the mobilized sediment until the river network, or its deposition, thus interrupting the sediment flux and disconnecting the sources from the outlet. A quantification of this component of the connectivity is given by the sediment delivery ratios in Fig. 3.9. Here, the lower structural connectivity of the south-eastern part of the basin, where the steep highly erosive slopes are separated from the river network by lower gradient floodplains, is the reason for lower sediment delivery ratios and therefore lower functional connectivity compared to the north-western part of the basin. In the second place, the periodic activation of localized sources by high bed shear stress also contributes to a dynamic representation of functional connectivity. Their degree of connectivity is given by their physical connection to the river network, the distribution in time and space of surface runoff and the interaction between the hydrological forcing and the landslide morphological properties. In our model, the latter is provided by the gully competence parameter, which determines the effectiveness of the overland flow in transferring sediment from the landslide bodies to the channel.

Evaluation of functional connectivity by means of physically based models offers an alternative approach to widely used static indicators where discharge is usually approximated as a function of the upstream area, see Heckmann *et al.* (2018) for a review. An example is provided by Mahoney *et al.* (2018), who combined a hydrological model with the spatially distributed and temporally variable probability of sediment connectivity to estimate watershed erosion. Analogously to the approach presented in this thesis, most spatially distributed and physically based model presented in Sect. 1.2.1 are also suitable for such dynamic evaluation of functional connectivity, with advantages and limitations that are connected to their structure. For example, the model by Cea *et al.* (2016) has the advantage of using a variable triangular mesh, and a flow routing that is not limited by a D4

scheme. Therefore, it is likely more accurate than the TOPKAPI-ETH model in representing the path of sediment close to the river network. A hydraulic description of the fluxes in the channel as in Cea *et al.* (2016) and Tsuruta *et al.* (2018) also improves the representation of water and sediment connectivity in the river network. On the contrary, both models do not allow deposition on the hillslopes and therefore are likely to overestimate the connectivity there. As mentioned above, the use of a higher spatial resolution also favours a more accurate description of the structural and functional connectivity.

Time-dependent sediment provenance

In the presented model, the sediment mobilized by each sediment source is routed as an independent wave on the hillslopes and in the channels. In this way, it keeps track of the sediment origin at each point of the river network and allows to estimate the contribution of each sediment source to the total load. Such information supports the construction of sediment budgets. The temporal dimension of the modelling allows the mixing of sediment sources by fluvial processes, and enables time series of the sediment provenance (Ch. 4). Such knowledge of time-dependent sediment provenance is not only useful for sediment management, but also for the use of cosmogenic radionuclides in the estimate of long-term basin-average denudation rates. In fact, this approach is based on the assumption that a river bed sediment sample is representative of long-term and catchment-averaged denudation rates of the upstream area (von Blanckenburg, 2005; Yanites *et al.*, 2009). However, these conditions are often not satisfied in river basins dominated by mass wasting events (e.g. Kober *et al.*, 2012; Savi *et al.*, 2014; Delunel *et al.*, 2014). The tool I developed in this thesis allows to identify the hydrological conditions and locations in which the sampling should be performed, to maximize the representativeness of the CRN sample. Our results show why, in a pre-Alpine basin dominated by landslides and inner gorges, sampling should be carried out preferably during low flow and as close at possible to the low flow channel.

Further information on sediment provenance can be extrapolated from the analysis of sediment availability. Our model predicts the strongest CRN fluctuations at the basin outlet in spring and summer, when the major floods take place and trigger mass wasting. However, this model application in Chapter 4 was carried out without including the possibility that landslides exhaust their sediment reservoirs. In fact, flood events also cause emptying of the basin sediment reservoir and consequent sediment starvation, which may lead to supply limitation in summer (Fig. 5.5). Therefore, it is likely that after the first major flood of the season, the fluctuations of CRN concentrations become smoother and the sampling of CRN increasingly representative as the sediment reservoir of localized sources empties. This could be proved by performing the sediment tracing with the ^{10}Be data as done in Chapter 4 for the supply-limited simulations performed in Chapter 5. This hypothesis is also supported by field observations in Alpine basins by Schuerch *et al.* (2006) and Berger *et al.* (2011), who found that sediment input from landslides and debris flows is greatest in winter and spring. Measurements by Wetzel (1994) also indicate that sediment load is dominated by mass wasting during the ablation period, while summer load by the behaviour of channel storage. A direct validation of these concepts on the sediment provenance provided by the model could be obtained with sediment tracing, consisting in the measurement of conservative properties of sediment in the sources and at the outlet, such as geochemistry and mineralogy.

Towards a comprehensive physically based representation of the suspended sediment dynamics

The model developed during this research is a step towards a comprehensive physically based representation of the suspended sediment dynamics in pre-Alpine river basins. It includes the description at high resolution of the topographic, land cover, soil and climate properties of the

basin, the characteristics of the major sediment sources, and the basin sediment availability. In this way, it allows to separate the role of each of these elements in the sediment response of a given basin setting. I demonstrated that the activation of localized sediment sources is responsible for generating the highest suspended sediment fluxes (Ch. 4), and that the model links the geomorphic properties of such sources to their contribution to the total sediment load. This happens through the gully competence parameter λ, defining the hillslope-channel connectivity (Ch. 4), and the slope and thickness of the landslides, determining their sediment supply to the river network (Ch. 5). Furthermore, by simulating the input and export from the basin sediment reservoir, the model captures its dynamics and allows to analyse the relation between sediment availability in the basin and suspended sediment load properties (Ch. 5).

Although representing several properties describing the natural complexity of the system, the number of parameters used in model remains limited and with a precise physical meaning. The most relevant model parameters are the surface erodibility α (Eq. 2.10), the river initiation threshold RT (Sect. 3.2.3.3), the gully competence parameter λ (Eq. 2.13), the localized sediment flux parameters k and μ (Eq. 2.11), and the parameter of hillslope activity c_{LS} (Eq. 2.15). α and RT describe the magnitude of the basin response to hillslope overland flow, and the mean drainage area at which the fluvial sediment transport processes become dominant over hillslope processes. They determine the magnitude of the SSCs, and the slope of the SSC-Q rating curve at low flows. λ is the key parameter to allocate the sediment load to the sources, by defining the overland flow erosivity on landslide surfaces (Eq. 2.14). In other words, it determines the degree of connectivity between the hillslopes and the channel. k and μ represent the magnitude and non-linearity of the sediment flux from localized threshold-behaviour sediment sources, and therefore determine the magnitude of SSCs, and slope of the SSC-Q rating curve at high flows. Finally, c_{LS} represents the intensity of landsliding activity on the hillslopes, and allows to modulate the response of the landslide sediment supply to the river network driven by soil moisture dynamics.

The physical meaning of the parameters facilitates the model calibration, because it allows a clear connection with field observations. Basic information that is necessary to calibrate the sediment component of the model consists in high temporal resolution measurements of discharge and suspended sediment concentrations. This characterizes the sediment rating curve, and therefore allows a first estimate of α and RT based on the low flow data, as done in Sect. 3.2.3.3, and of k and μ based on the high flows, as in Sect. 4.2.4. In Chapters 4, I also showed that a qualitative evaluation of the hillslope contribution to sediment load compared to channel contribution is possible through a simple analysis of landslide surface topography, and observations of the river morphology at the confluence of small tributaries. This provides a physical basis for the estimate of the λ and c_{LS} parameters. As mentioned in the previous section, such estimates can be improved by sediment tracing, and I showed in Chapter 4 that even relatively sparse data across the basin can be informative. Other useful measurements consist in the monitoring of landslide movements (e.g. Schwab *et al.*, 2007; Schuerch *et al.*, 2006; Handwerger *et al.*, 2019b) to distinguish whether a low sediment flux from landslides is given by low transport capacity of the streams (low k, μ or λ) or a low sediment availability in the landslides themselves (i.e. a low c_{LS} parameter).

6.3 Outlook

Further developments of the model

Several further developments of the model are possible in order to improve its representation of the physical processes. Those include a more detailed description of the erosion on hillslopes, for example by modelling the soil detachment by raindrop impact and distinguishing the erodibility of mobilized and compacted sediment, as in Hairsine and Rose (1992). Modelling of sediment supply

could also be based on a more specific description of the inputs of sediment from landslides and incised areas, for example by explicit simulation of the triggering of debris flow and bank collapses (e.g. Taccone *et al.*, 2018). Multiple grain sizes could also be included, as well as a module for bedload transport (e.g. Tsuruta *et al.*, 2018; Coulthard *et al.*, 2002).

In general, the current knowledge on sediment processes potentially allows for a highly detailed description of each component. However, an increased model complexity comes at the cost of additional parameters, applicability for practical purposes, and interpretation of the results. This is an especially critical point in the field of sediment transport, where observations are still challenging and relatively limited in time and space, and very often suffer from a high uncertainty. This represents a limitation for the calibration and validation of numerical models. In fact, at the moment it represents the main limitation of several sediment budget models available in the literature, such as DHSVM (Doten *et al.*, 2006), tRIBS (Francipane *et al.*, 2012) and CAESAR-Lisflood (Coulthard *et al.*, 2013). For this reason, I think that further developments of the numerical model presented in this thesis should be pursued with the aim of addressing specific research questions and be limited to the new elements strictly needed for such aim, rather than with the potentially overambitious scope of producing a more complete model.

With respect to the research questions addressed in this thesis, the developments that in my opinion would allow deeper insights into scientifically relevant issues without significantly increasing model complexity are the following:

1) Implementation of a temporally variable surface erodibility α to capture the seasonality of land cover properties, i.e. of the C factor in the RUSLE equation. This would add a temporal component to the spatially variable surface erodibility, in the same way as this is already included for the precipitation input, and complement the representation of the spatial and temporal variability of the suspended sediment dynamics. Such feature could be added to the model by automatically modifying the α parameter at each time step based on the day of the year, or based on the precipitation and soil moisture.

2) Introduction of the possibility to vary the parameters of gully competence λ and hillslope activity c_{LS} in space and time, in order to represent the different degrees of hillslope-channel connectivity across a river basin, and the periodic activation or deactivation of such connectivity. For example, previous works in the Kleine Emme basin suggest that the northwestern subbasins have a stronger hillslope-channel coupling than the rest of the basin, which could be represented with a higher λ than the southeastern subbasins (Schlunegger and Schneider, 2005; Norton *et al.*, 2008; Van den Berg and Schlunegger, 2012). Furthermore, Clapuyt *et al.* (2019) observed an episodic connectivity of landslides to the channel in the basin, which corresponds to periodic pulses of higher c_{LS} values. This improvement would overall allow a better representation of the spatial variability, of the activation of localized sediment sources and the prediction of the basin sediment availability.

3) Allowing fine sediment to deposit on the river bed and on the floodplain and be resuspended, and account for the mixing of sediment properties in the river bed storage, such as ^{10}Be concentrations. While this process was estimated to be of secondary importance in the Kleine Emme river basin, it is important to correctly represent the suspended sediment dynamics and fluvial mixing in other river basins. Examples of approaches that could be followed in this step are provided by many models that feature a detailed description of fluvial processes. BASEMENT (Vetsch *et al.*, 2017) and SHESED (Wicks and Bathurst, 1996) provide a 1D approach that could be suitable for implementation in TOPKAPI-ETH.

4) Explicitly introduce uncertainty in some key parameters and processes. So far the model is fully deterministic in the representation both of sediment mobilization and sediment

transport. In Chapter 5 I applied a bootstrapping technique to reproduce the randomness of hillslope landsliding activity, however this is was done as a post-processing procedure. Further developments in this respect could be pursued by random sampling of the parameter values from prescribed probability distribution within the model runs, and/or by repeated realizations of a stochastic climate (Monte Carlo analysis), as in Fuller *et al.* (2003), Belmont *et al.* (2007) and Navratil *et al.* (2011).

Potential applications

The hydrolology-sediment model TOPKAPI-ETH is a useful tool to study scenarios of possible climatic, morphological or stuctural changes in a given river basin. Among the most relevant applications is the analysis of the basin response under scenarios of climate change, as done for example for one event on the Kleine Emme by Peleg *et al.* (2020) with the CAESAR-Lisflood model. The model presented in this thesis allows the simulation of such scenarios on long time scales (≈100 years), by accounting for the effects of future temperature increase, modifications in the temporal and spatial properties of the precipitation, as well as indirect consequences of climate change such as land cover changes. We are currently working on the application of the modelling setting for the Kleine Emme under the CH2018 climate scenarios for Switzerland (NCCS, 2018).

Another very relevant application of the model is to evaluate the sediment input into reservoirs and water impoundments and the fraction potentially trapped, in order to estimate their life span (Vörösmarty *et al.*, 2003). While the implementation of sediment trapping in reservoirs is still under development in TOPKAPI-ETH, the estimate of sediment input from the upstream catchments can already be performed with the current model structure.

In future applications of the model, I also recommend to test the advantages of an automatic model calibration over a manual calibration. In this thesis, I manually calibrated the parameters by varying one of them at a time because of computational reasons. An automatic calibration would allow to identify multiple groups of parameters that equally fit the observed suspended sediment concentrations, such as the two end-members calibrations that I identified in Chapter 4. By using an automatic approach also parameter sets with intermediate values of the gully competence λ would be identified, which are probably more realistic than its extreme values, as anticipated also in Chapter 4.

Combination with remote and field measurements

Finally, I believe that future modelling efforts should be combined with further measurement data, to improve the validation of the hydrological module, as well as to help quantify and interpret the parameters of the sediment component.

Validation of the modelled overland flow. The hydrological module would benefit from a more accurate validation of the simulated overland flow in time and space, because this is the main driver of the modelled soil erosion on hillslopes. In the study basin of this thesis, discharge measurements were available at three river gauges, thus partially allowing validation of the spatial distribution of overland flow. However, this validation remains limited in space and should be complemented with spatially distributed information. A promising way in this regard is provided by comparison of the modelled soil moisture with remote sensing measurements of the soil water content. This approach would allow to validate the key variable for overland flow production, with the advantage of providing a spatially distributed information on each hillslope cell of the river basin, instead of a punctual aggregated information such as the river gauges.

Calibration and validation of the sediment parameters. In the sediment module each parameter has a concrete physical meaning (see Sect. 6.2). This implies that knowledge of the basin geomorphology and some focussed measurements of sediment properties may significantly improve the informativeness of the model. In particular, such field information could allow to select between multiple parameter sets identified by an automatic calibration.

As mentioned above, high resolution SSC-Q data is the basic information needed to calibrate the model. In this thesis, I used SSC data taken twice a week, which has to some extent limited the possibility to calibration. I believe that hourly resolution data would provide substantial benefit to the calibration, and may allow to select between equivalent calibrations, such as the end-members simulations with low and high gully competence parameter λ in Chapter 4, even without recurring to additional datasets.

The other key dataset for validation and interpretation of the modelled sediment provenance can be obtained by sediment fingerprinting. In this respect, resources should be invested in measuring time series of sediment tracers at the outlets of river basins. Although this is an expensive exercise and so far usually not performed in denudation rate studies, there is a growing interest in the CRN community to investigate landslide dominated basins (e.g. Belmont *et al.*, 2007; Kober *et al.*, 2012; Savi *et al.*, 2014), and in the fingerprinting community to link sediment provenance to climatic inputs (e.g. Navratil *et al.*, 2012). Besides cosmogenic ^{10}Be, other suitable components to trace the sediment production process include meteoric ^{10}Be, as proposed by Reusser and Bierman (2010). Additional information on the soil depth of sediment provenance can be provided by e.g. ^{137}Cs and ^{210}Pb$_{xs}$ (Olley *et al.*, 2013) and on the travel time of sediment by ^{7}Be/^{210}Pb$_{xs}$ (Matisoff *et al.*, 2005; Evrard *et al.*, 2016). Because the model accounts for three sediment sources, at least two independent tracers should be measured, which combined with the mass balance hypothesis allow to derive the three unknown source contributions. Moreover, by combining multiple tracers it is possible to compensate for the uncertainty in the measurements.

Conversely, studies that aim at reconstructing basin sediment provenance by sediment fingerprinting will benefit from the application of the presented model on the same catchment. In fact, the model results allow to generalize the observations performed on short time scales and at a limited number of locations to longer time periods and the entire basin. Moreover, the model provides a physically based concept to support the choice of statistical mixing models that are currently used (Evrard *et al.*, 2011; Blake *et al.*, 2018).

APPENDIX A

Supporting information for chapter 3

A.1 Model inputs and calibration

A.1.1 Soil erodibility and land cover-management factors

Figure A.1 shows the spatial distribution of the soil erodibility factor K and land cover-management factor C of the Universal Soil Loss Equation for the Kleine Emme river basin. The two factors were used to derive the spatial distribution of the surface erodibility parameter α of the model. The soil erodibility factor K was taken from the work of Schmidt *et al.* (2018) and the land cover-management factor was derived from Yang *et al.* (2003).

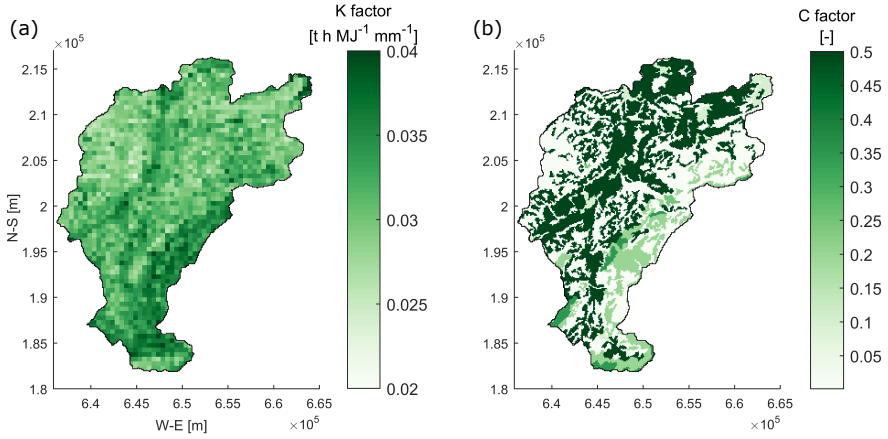

FIGURE A.1: Maps of the (a) soil erodibility USLE factor K (source: Schmidt *et al.* (2018)) and (b) cover-management factor C for the Kleine Emme basin (derived from Yang *et al.* (2003)).

A.1.2 Evaluation of sediment module performance

In this section some additional metrics that evaluate the performance of the sediment model component are presented.

In Figure A.2 the histogram of the simulated SSCs sampled at the hours of collection of suspended sediment bottle samples is compared with the histogram of measured SSCs smaller than the 85th percentile. The comparison of the two histograms provides an evaluation of the model performance in terms of SSC distributions.

To allow the comparison between the continuous time series of simulated hourly SSC and the intermittent observed SSC (twice a week), a continuous hourly time series has been extrapolated from the observations, based on the fitting of a Q-SSC rating curve. The comparison of observed and simulated SSCs is shown in Figure A.3. In Table A.1 the time series of hourly simulated and

extrapolated observed SSCs are compared by means of the correlation coefficient r, percent bias PBIAS, normalized root mean square error nRMSE and mean absolute error MAE. Coherently with the approach applied in the calibration procedure (see Sect. 3.2.3.3), we have limited this comparison to the observed SSC values lower than the 85th percentile of their distribution. As expected, the comparison shows a tendency to underestimate the observations and a lower performance at the hourly scale, which, however, improves with increasing temporal aggregation.

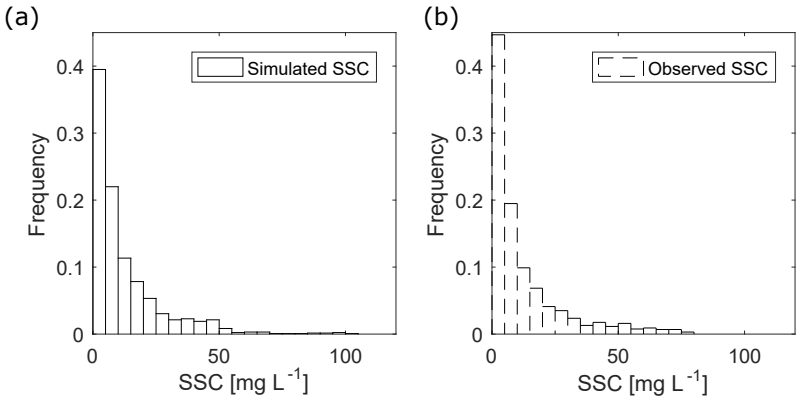

FIGURE A.2: Simulated and observed SSC frequency distributions: (a) frequency distribution of simulated SSCs at the hours of suspended sediment sample collection, (b) frequency distribution of observed SSCs smaller than the 85th percentile.

TABLE A.1: Performance of the suspended sediment simulations for the period 2004-2016 at the outlet of the river basin, in terms of correlation coefficient (r), Percent Bias (PBIAS), normalized root mean square error (nRMSE) and mean absolute error (MAE) for data simulated at the hourly resolution and aggregated to daily, monthly and annual values. The analyses has been limited to the values lower than the 85th percentile of the observations.

	r [-]	PBIAS [%]	nRMSE [-]	MAE [mg L^{-1}]
Hour	0.51	-12.14	1.02	8.86
Day	0.52	-12.14	0.91	9.18
Month	0.64	-12.14	0.52	5.64
Year	0.52	-12.14	0.19	2.28

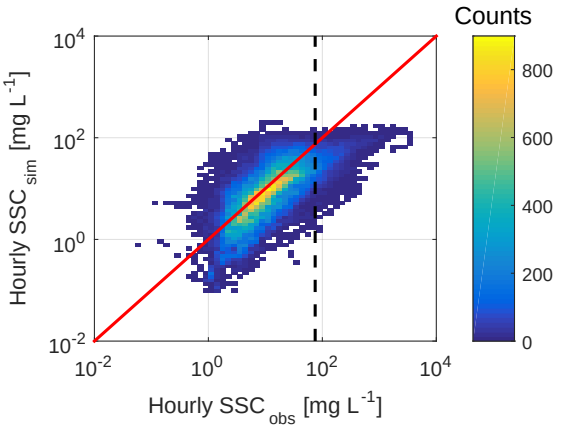

FIGURE A.3: Density plot of simulated vs observed hourly suspended sediment concentrations at the outlet of the river basin for the period 2004-2016. The black dashed line indicates the 85th percentile of the observations, to which the performance assessment has been limited. The red line gives the 1:1 fit.

A.1.3 River initiation threshold effect on the hydrological model

Table A.2 shows the influence of the river initiation threshold on the hydrological performance of the model. The performance is evaluated through the correlation coefficient (r), Nash-Sutcliffe efficiency (NSE) and root mean square error (RMSE). The conclusion we draw from this is that RT is not significantly influencing discharge predictions at the outlet.

TABLE A.2: River initiation threshold (RT) effect on hydrological model performance. Observed hourly discharge data at the outlet for the period 2004-2016 are compared with two simulations with different RT values. The model performance is evaluated by means of the correlation coefficient (r), Nash-Sutcliffe efficiency (NSE) and root mean square error (RMSE) at the hourly resolution and at the daily and monthly temporal aggregation.

	r [-]		NSE [-]		RMSE [m^3 s^{-1}]	
RT km^2	1.25	0.4	1.25	0.4	1.25	0.4
Hour	0.84	0.84	0.69	0.69	0.75	0.75
Day	0.91	0.90	0.80	0.79	0.53	0.55
Month	0.93	0.93	0.76	0.77	0.26	0.27

A.1.4 Hydrological model performance under dry and wet conditions

In Table A.3 and Figure A.4 the performance of the hydrological component of the model in reproducing events with low and high initial soil moisture (SM_0) is evaluated. These conditions have been defined as SM_0 smaller than the 20th percentile of the SM_0 distribution, and SM_0 greater than the 80th percentile. SM_0 is computed as the basin averaged soil moisture distribution at the last hour before the start of each event. The model performance for the selected events is good and comparable to the entire simulation, however Figure A.4 indicates a tendency to overestimation especially for low SM_0 events.

TABLE A.3: Performance of the hydrological model in reproducing low and high initial soil moisture (SM_0) events. Simulated and observed hourly discharge data at the outlet are compared for the selected events in terms of the correlation coefficient (r), Nash-Sutcliffe efficiency (NSE) and root mean square error (RMSE).

	low SM_0	high SM_0
r [-]	0.86	0.82
NSE [-]	0.74	0.63
RMSE [$m^3\ s^{-1}$]	0.71	0.66

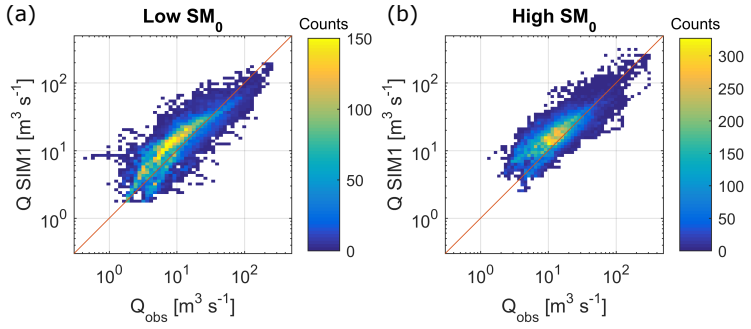

FIGURE A.4: Density plot of simulated vs observed hourly discharges at the outlet for (a) low and (b) high initial soil moisture events within the 2004-2016 period.

A.2 Suspended sediment concentration variability at the outlet

The variability of suspended sediment concentration at the outlet in the four simulations is compared by means of the SSC-Q cloud of points and a coefficient of variation that quantifies their scatter. Figure A.5 compares the modelled SSC (density plots) in SIMs 1 to 4 with the observations (lines). The comparison of SIM 1 and 3 with SIM 2 and 4 shows the effect of the spatial distribution of precipitation in stretching the bulk of the modelled concentrations towards higher values, which reflects the increase in the annual sediment load. Analogously, the effect of the spatial distribution of surface erodibility is opposite (compare SIM 1 and 2 with SIM 3 and 4). The plots are in log-log scale, so we point out that the differences between the simulations are more relevant at high concentrations.

To quantify the scatter of the SSC-Q relations independently of the mean simulated SSC, we binned the simulated discharges, computed the coefficients of variation (CVs) of the sediment concentrations in each discharge bin and reported them as a boxplot for all discharges in Figure A.6. We observe that the distribution of the CVs shifts to lower values every time a source of variability (rainfall or α distribution) is removed, therefore, we observe a general correspondence between information content of the inputs and scatter of the predictions of SSC. However, we also observe that the changes between simulations are very small, especially in the mean value, thus suggesting that the spatially distributed nature of the model itself plays a more relevant role than the variability of the analysed input variables (rainfall and surface erodibility). The comparison of observed and simulated CVs shows the amount of variability of the lower 85th percentile of observed SSCs that is captured by the model. As expected, the observed variability is much larger than the simulated one, because of the sources of variability which are not accounted for in our model.

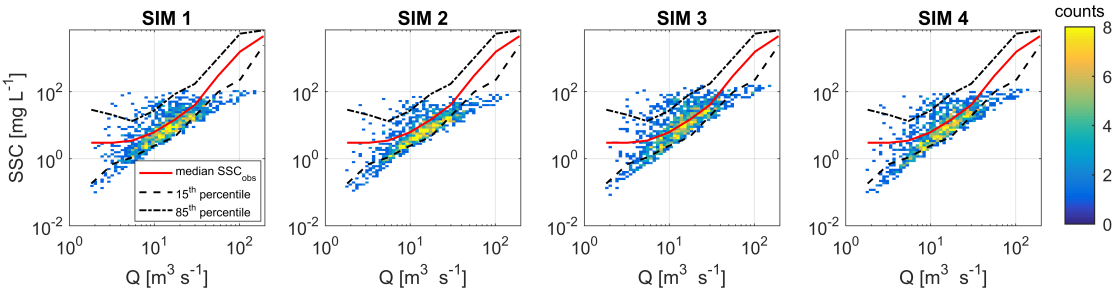

FIGURE A.5: Density plot of simulated SSC-Q values for SIM 1 to SIM 4 sampled at the time of observations, compared with observations (lines give median and 15th-85th percentiles).

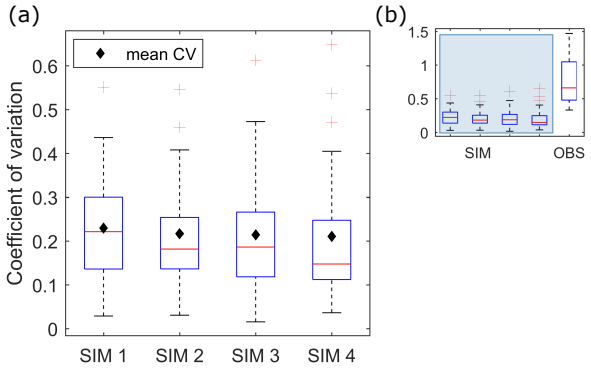

FIGURE A.6: Quantification of the SSC-Q relation scatter: (a) boxplots of the coefficients of variation of the SSC-Q relation for SIM 1 to SIM 4, (b) comparison of simulated (blue box) and observed coefficients of variations, where the observed SSCs have been truncated to the 85th percentile.

APPENDIX B

Supporting information for chapter 4

In the following I explain how the representative ^{10}Be concentrations reported in Table 4.1 for the different sediment production processes were derived, based on measurements available in the literature. Since LS_R and LS_{HS} mobilize sediment from the same source, I attributed them the same concentration, equal to the average of 5 measurements on the Rossloch landslide in the Entle subbasin by Clapuyt *et al.* (2019) (indicated as green dots in Fig. 4.1, values are reported in Table B.1).

A concentration representative of the background steady state denudation rate has been derived from samples taken above knickzones and in small basins, indicated as red dots in Fig. 4.1 and reported in Table B.1. Such samples are available in three different regions of the basin, thus allowing to partially integrate the variability across the basin and the elevation dependence. Since sediment mobilization by the *OF* process can also take place on landslide surfaces and incised areas, the representative concentration of the *OF* process has been derived as the weighted average of the background, *LS* and *I* concentrations, where the weights are the net erosion values produced by the *OF* process on the areas corresponding to the background, *LS* and *I* concentrations.

No samples were available that only integrated areas of incision, therefore I derived a representative concentration for the *I* process by means of a mass balance in the Entle subcatchment (see Fig. B.1). This basin was classified by Van Den Berg *et al.* (2012) in three areas dominated by hillslope (HS), weathering (WT) and channelized (CH) processes, where the last class largely coincides with the incised areas *I* that I mapped. In their work, Van Den Berg *et al.* (2012) provide a mean erosion rate ε for each area and for the entire Entle subbasin. A ^{10}Be concentration C for the WT and HS areas and the entire subbasin is also available from the samples indicated in Fig. B.1 (see Table B.2 for the values). With these data, I computed the ^{10}Be concentration that the CH area, i.e. the *I* area in our model, needs to have to satisfy the mass balance:

$$A_{Entle}\varepsilon_{Entle}C_{Entle} = A_{WT}\varepsilon_{WT}C_{WT} + A_{HS}\varepsilon_{HS}C_{HS} + A_I\varepsilon_I C_I \tag{B.1}$$

where A is the area of each region. The resulting representative ^{10}Be concentrations are reported in Table 4.1.

In the derivation of the representative ^{10}Be concentrations I did not explicitly account for the dependence of the cosmogenic production rates on elevation. However, the background erosion samples have been taken in the streams and therefore provide an elevation-integrated measure of the upstream areas. Moreover, I have selected samples that are distributed across the catchment and therefore partially account for the spatial variability of the cosmogenic production rate. The use of samples from the Rossloch landslides to represent the *LS* process concentration, is instead likely to provide an overestimation of the ^{10}Be concentration for this process. In fact, with respect to the distribution of all landslides in the basins, the Rossloch landslide is located at relatively higher elevations, where the cosmogenic production rate is higher. This implies that the signal produced by the LS_R and LS_{HS} processes at the outlet would be even more clearly distinguishable from that of the *OF* process. With regard to the incised area concentration, the Entle subbasin inner gorge covers a range of elevations that is representative of the location of the incised areas across the basin, and is therefore expected to be representative of the process.

Process	Elevation [m a.s.l.]	Lat [° N]	Lon [° E]	^{10}Be concentration [10^4 at/g_{Quartz}]
LS_{HS}, LS_R	1287	46.946	8.092	3.53 ± 0.28[1]
LS_{HS}, LS_R	1325	46.947	8.092	1.34 ± 0.27[1]
LS_{HS}, LS_R	1373	46.946	8.097	2.32 ± 0.58[1]
LS_{HS}, LS_R	1451	46.945	8.098	0.62 ± 0.45[1]
LS_{HS}, LS_R	1500	46.943	8.104	0.15 ± 0.53[1]
Background erosion	1132	46.9514	8.0566	6.35 ± 0.34[2]
Background erosion	1525	46.8447	8.0638	9.38 ± 0.46[3]
Background erosion	1563	46.8444	8.0563	9.66 ± 0.65[3]
Background erosion	1442	46.8506	8.0574	11.05 ± 0.50[3]
Background erosion	913	46.9712	7.966	2.59 ± 0.85[4]
Background erosion	896	46.9883	7.9708	2.85 ± 0.31[4]

TABLE B.1: Location and ^{10}Be concentrations of the samples used to compute representative concentrations of sediments mobilized by the different processes. References: [1]Clapuyt *et al.* (2019), [2]Van den Berg and Schlunegger (2012), [3] Casagrande (2014), [4] Norton *et al.* (2008).

Region	^{10}Be conc [10^4 at/g_{Quartz}]	ε [mm/yr^{-1}]	Area [km^2]
Subbasin	2.46 ± 0.13	0.42 ± 0.04	63.56
WT	6.35 ± 0.34	0.14 ± 0.01	16.19
HS	4.91 ± 0.17	0.23 ± 0.03	35.65
CH	-	1.37 ± 0.22	11.72

TABLE B.2: From Van Den Berg *et al.* (2012): ^{10}Be concentrations, mean erosion rates ε and areal extent of the Entle subbasin and its weathering (WT), hillslope (HS) and channelized (CH) process dominated regions. The ^{10}Be concentration for CH areas was not measured by Van Den Berg *et al.* (2012) and was derived in this work via a mass balance.

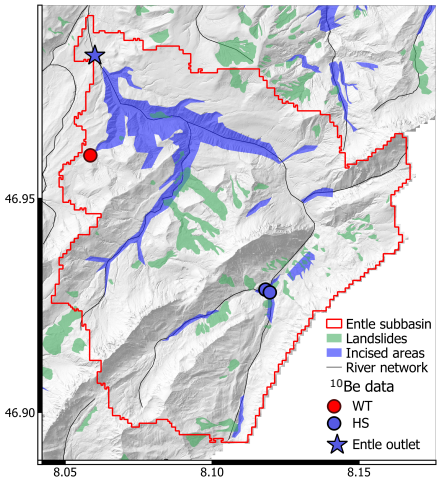

FIGURE B.1: Map of the Entle subbasin and the location of ^{10}Be samples by Van Den Berg *et al.* (2012) that were used to derive a representative concentration for the *I* process. The WT sample (red dot) was assumed to be representative of the weathering dominated area, the HS samples (blue dots) of the hillslope-processes dominated area and the outlet sample (blue star) was used to close the mass balance.

APPENDIX C

List of symbols for the sediment module

α [kg $s^{0.4}$ $m^{-4.8}$] surface erodibility of hillslopes (Eq. 2.10)

β [-] overland flow transport exponent on hillslopes (Eq. 2.10)

γ [-] slope transport exponent on hillslopes (Eq. 2.10)

k [kg m^{-1} s^{-1}] transport coefficient for sediment flux from localized sources (Eq. 2.11)

μ [-] transport exponent for sediment flux from localized sources (Eq. 2.11)

θ_c [-] dimensionless critical bed shear stress (Eq. 2.11)

λ [-] competence of gullies on landslides (Eq. 2.13)

G [-] specific gravity of sediment (Eq. 2.14)

d_s [m] grain size (Eq. 2.14)

c_{LS} [-] intensity of landsliding activity on the hillslopes (Eq. 2.15)

H [m] landslide thickness (Eq. 2.15)

$\hat{\alpha}$ [°] landslide slope (Eq. 2.15)

E [g m^{-1} s^{-1}] sum of water column - river bed sediment exchange and input from local sediment sources (Eq. 2.17)

Bibliography

Asselman N. E. (1999). Suspended sediment dynamics in a large drainage basin: The River Rhine. *Hydrological Processes*, 13(10):1437–1450. doi:10.1002/(SICI)1099-1085(199907)13:10<1437::AID-HYP821>3.0.CO;2-J.

Asselman N. E. (2000). Fitting and interpretation of sediment rating curves. *Journal of Hydrology*, 234(3-4):228–248. doi:10.1016/S0022-1694(00)00253-5.

Bakker M. M., Govers G., Doorn A., van, Quetier F., Chouvardas D. and Rounsevell M. (2008). The response of soil erosion and sediment export to land-use change in four areas of Europe: The importance of landscape pattern. *Geomorphology*, 98(3-4):213–226. doi:10.1016/j.geomorph.2006.12.027.

Ballantyne C. K. (2002). A general model of paraglacial landscape response. *Holocene*, 12(3): 371–376. doi:10.1191/0959683602hl553fa.

Bathurst A. and Burton J. C. (1998). Physically based modelling of shallow landslide sediment yield at a catchment scale. *Environmental geology*, 35(August):89–99.

Battista G., Molnar P. and Burlando P. (2020a). Modelling impacts of spatially variable erosion drivers on suspended sediment dynamics. *Earth Surface Dynamics*, 8(3):619–635. doi:10.5194/esurf-8-619-2020.

Battista G., Schlunegger F., Burlando P. and Molnar P. (2020b). Modelling localized sources of sediment in mountain catchments for provenance studies. *Earth Surface Processes and Landforms*, 45(14):3475–3487. doi:10.1002/esp.4979.

Beasley D. B., Huggins L. F. and Monke E. J. (1980). ANSWERS: A Model for Watershed Planning. *Transactions of the ASAE*, 23(4):0938–0944. doi:10.13031/2013.34692.

Belmont P., Pazzaglia F. J. and Gosse J. C. (2007). Cosmogenic 10Be as a tracer for hillslope and channel sediment dynamics in the Clearwater River, western Washington State. *Earth and Planetary Science Letters*, 264(1-2):123–135. doi:10.1016/j.epsl.2007.09.013.

Belmont P., Gran K. B., Schottler S. P., Wilcock P. R., Day S. S., Jennings C., Lauer J. W., Viparelli E., Willenbring J. K., Engstrom D. R. and Parker G. (2011). Large shift in source of fine sediment in the upper Mississippi River. *Environmental Science and Technology*, 45(20):8804–8810. doi:10.1021/es2019109.

Benda L. (1997). Stochastic forcing of sediment routing and storage From Landsliding and Debris Flow. 33(12):2849–2863.

Benda L. and Dunne T. (1997). Stochastic forcing of sediment routing and storage in channel network in channel networks. *Water Resources Research*, 33(12):2865–2880.

Bennett G. L., Molnar P., McArdell B. W. and Burlando P. (2014). A probabilistic sediment cascade model of sediment transfer in the Illgraben. *Water Resources Research*, 50(2):1225–1244. doi:10.1002/2013WR013806.

Berger C., McArdell B. W. and Schlunegger F. (2011). Sediment transfer patterns at the Illgraben catchment, Switzerland: Implications for the time scales of debris flow activities. *Geomorphology*, 125(3):421–432. doi:10.1016/j.geomorph.2010.10.019.

Beschta R. L. (1978). Long-term patterns of sediment production following road construction and logging in the Oregon Coast Range. *Water Resources Research*, 14(6):1011–1016. doi:10.1029/WR014i006p01011.

Betrie G. D., Mohamed Y. A., Van Griensven A. and Srinivasan R. (2011). Sediment management modelling in the Blue Nile Basin using SWAT model. *Hydrology and Earth System Sciences*, 15 (3):807–818. doi:10.5194/hess-15-807-2011.

Bierman P. R. and Steig E. J. (1996). Estimating rates of denudation using cosmogenic isotope abundances in sediment. *Earth Surface Processes and Landforms*, 21(2):125–139. doi:10.1002/(SICI)1096-9837(199602)21:2<125::AID-ESP511>3.0.CO;2-8.

Bilotta G. S. and Brazier R. E. (2008). Understanding the influence of suspended solids on water quality and aquatic biota. *Water Research*, 42(12):2849–2861. doi:10.1016/j.watres.2008.03.018.

Blake W. H., Boeckx P., Stock B. C., Smith H. G., Bodé S., Upadhayay H. R., Gaspar L., Goddard R., Lennard A. T., Lizaga I., Lobb D. A., Owens P. N., Petticrew E. L., Kuzyk Z. Z. A., Gari B. D., Munishi L., Mtei K., Nebiyu A., Mabit L., Navas A. and Semmens B. X. (2018). A deconvolutional Bayesian mixing model approach for river basin sediment source apportionment. *Scientific Reports*, 8(1):1–12. doi:10.1038/s41598-018-30905-9.

Bodeneignungskarte (2012). 77.2 Digitale Bodeneignungskarte der Schweiz. URL `https://www.blw.admin.ch/blw/de/home/politik/datenmanagement/geografisches-informationssystem-gis/download-geodaten.html`.

Boix-Fayos C., Vente J., de, Martínez-Mena M., Barberá G. G. and Castillo V. (2008). The impact of land use change and check-dams on catchment sediment yield. *Hydrological Processes*, 22 (25):4922–4935. doi:10.1002/hyp.7115.

Borrelli P., Märker M., Panagos P. and Schütt B. (2014). Modeling soil erosion and river sediment yield for an intermountain drainage basin of the Central Apennines, Italy. *Catena*, 114:45–58. doi:10.1016/j.catena.2013.10.007.

Borrelli P., Robinson D. A., Fleischer L. R., Lugato E., Ballabio C., Alewell C., Meusburger K., Modugno S., Schütt B., Ferro V., Bagarello V., Oost K. V., Montanarella L. and Panagos P. (2017). An assessment of the global impact of 21st century land use change on soil erosion. *Nature Communications*, 8(1). doi:10.1038/s41467-017-02142-7.

Borrelli P., Van Oost K., Meusburger K., Alewell C., Lugato E. and Panagos P. (2018). A step towards a holistic assessment of soil degradation in Europe: Coupling on-site erosion with sediment transfer and carbon fluxes. *Environmental Research*, 161(May 2017):291–298. doi:10.1016/j.envres.2017.11.009.

Borrelli P., Robinson D. A., Panagos P., Lugato E., Yang J. E., Alewell C., Wuepper D., Montanarella L. and Ballabio C. (2020). Land use and climate change impacts on global soil erosion by water (2015-2070). *Proceedings of the National Academy of Sciences of the United States of America*, 117(36):21994–22001. doi:10.1073/pnas.2001403117.

Botter M., Burlando P. and Fatichi S. (2019). Anthropogenic and catchment characteristic signatures in the water quality of Swiss rivers: a quantitative assessment. *Hydrology and Earth System Sciences*, 23(4):1885–1904. doi:10.5194/hess-23-1885-2019.

Bracken L. J., Turnbull L., Wainwright J. and Bogaart P. (2015). Sediment connectivity: A framework for understanding sediment transfer at multiple scales. *Earth Surface Processes and Landforms*, 40(2):177–188. doi:10.1002/esp.3635.

Brasington J. and Richards K. (2000). Turbidity and suspended sediment dynamics in small catchments in the Nepal Middle Hills. *Hydrological Processes*, 14(14):2559–2574. doi:10.1002/1099-1085(20001015)14:14<2559::AID-HYP114>3.0.CO;2-E.

Brooks R. H. and Corey A. T. (1964). Hydraulik properties of porous media. *Hydrology paper 3*, 3.

Brutsaert W. (2005). *Hydrology – An Introduction*. Cambridge Univ. Press.

Caine N. (1979). Rock weathering rates at the soil surface in an alpine environment. *CATENA*, 6 (2):131–144. doi:10.1016/0341-8162(79)90003-1.

Carenzo M., Pellicciotti F., Rimkus S. and Burlando P. (2009). Assessing the transferability and robustness of an enhanced temperature-index glacier-melt model. *Journal of Glaciology*, 55 (190):258–274. doi:10.3189/002214309788608804.

Casagrande J. (2014). Master Thesis "What controls erosion? Quantitative estimation of erosion using 10Be in Flühli/LU (Switzerland)". Technical report, University of Bern.

Cea L., Legout C., Grangeon T. and Nord G. (2016). Impact of model simplifications on soil erosion predictions: Application of the GLUE methodology to a distributed event-based model at the hillslope scale. *Hydrological Processes*, 30(7):1096–1113. doi:10.1002/hyp.10697.

Chen X. and Zong Y. (1998). Coastal Erosion Along the Changjiang Deltaic Shoreline, China: History and Prospective. *Estuarine, Coastal and Shelf Science*, 46(5):733–742. doi:10.1006/ecss.1997.0327.

Chiarle M., Iannotti S., Mortara G. and Deline P. (2007). Recent debris flow occurrences associated with glaciers in the Alps. *Global and Planetary Change*, 56(1-2):123–136. doi:10.1016/j.gloplacha.2006.07.003.

Church M. and Ryder J. M. (1972). Paraglacial Sedimentation: A Consideration of Fluvial Processes Conditioned by Gkciation. *GSA Bulletin*, 83:3059–3072. doi:https://doi.org/10.1130/0016-7606(1972)83[3059:PSACOF]2.0.CO;2.

Clapuyt F., Vanacker V., Schlunegger F., Christl M. and Van Oost K. (2019). Spatio-temporal dynamics of sediment transfer systems in landslide-prone alpine catchments. *Solid Earth*, pages 1–22. doi:10.5194/se-2018-139.

CLC (2014). Corine Land Cover (CLC) map 2012. URL `https://land.copernicus.eu/pan-european/corine-land-cover/clc-2012`.

Clinnick P. F. (1985). Buffer strip management in forest operations: A review. *Australian Forestry*, 48(1):34–45. doi:10.1080/00049158.1985.10674421.

Coe J. A. (2012). Regional moisture balance control of landslide motion: Implications for landslide forecasting in a changing climate. *Geology*, 40(4):323–326. doi:10.1130/G32897.1.

Coe J. A., Ellis W. L., Godt J. W., Savage W. Z., Savage J. E., Michael J. A., Kibler J. D., Powers P. S., Lidke D. J. and Debray S. (2003). Seasonal movement of the Slumgullion landslide determined from global positioning system surveys and field instrumentation, July 1998-March 2002. *Engineering Geology*, 68(1-2):67–101. doi:10.1016/S0013-7952(02)00199-0.

Cohen S., Kettner A. J., Syvitski J. P. and Fekete B. M. (2013). WBMsed, a distributed global-scale riverine sediment flux model: Model description and validation. *Computers and Geosciences*, 53:80–93. doi:10.1016/j.cageo.2011.08.011.

Collins A. L. and Walling D. E. (2004). Progress in Physical Geography Documenting catchment suspended sediment sources : problems , approaches and prospects. *Progress in Physical Geography*, 2:159–196. doi:10.1191/0309133304pp409ra.

Collins A. L., Walling D. E., Webb L. and King P. (2010). Apportioning catchment scale sediment sources using a modified composite fingerprinting technique incorporating property weightings and prior information. *Geoderma*, 155(3-4):249–261. doi:10.1016/j.geoderma.2009.12.008.

Collins D. N. (1989). Seasonal development of subglacial drainage and suspended sediment delivery to melt waters beneath an alpine glacier. *Annals of Glaciology*, 13:45–50. doi:10.1017/s026030550000762x.

Cooper R. J., Krueger T., Hiscock K. M. and Rawlins B. G. (2015). High-temporal resolution fluvial sediment source fingerprinting with uncertainty: A Bayesian approach. *Earth Surface Processes and Landforms*, 40(1):78–92. doi:10.1002/esp.3621.

Costa A., Anghileri D. and Molnar P. (2018a). Hydroclimatic control on suspended sediment dynamics of a regulated Alpine catchment: A conceptual approach. *Hydrology and Earth System Sciences*, 22(6):3421–3434. doi:10.5194/hess-22-3421-2018.

Costa A., Molnar P., Stutenbecker L., Bakker M., Silva T. A., Schlunegger F., Lane S. N., Loizeau J. L. and Girardclos S. (2018b). Temperature signal in suspended sediment export from an Alpine catchment. *Hydrology and Earth System Sciences*, 22(1):509–528. doi:10.5194/hess-22-509-2018.

Coulthard T. J., Macklin M. G. and Kirkby M. J. (2002). A cellular model of Holocene upland river basin and alluvial fan evolution. *Earth Surface Processes and Landforms*, 27(3):269–288. doi:10.1002/esp.318.

Coulthard T. J., Neal J. C., Bates P. D., Ramirez J., Almeida G. A., de and Hancock G. R. (2013). Integrating the LISFLOOD-FP 2D hydrodynamic model with the CAESAR model: Implications for modelling landscape evolution. *Earth Surface Processes and Landforms*, 38(15):1897–1906. doi:10.1002/esp.3478.

Cruz Nunes F., Delunel R., Schlunegger F., Akçar N. and Kubik P. W. (2015). Bedrock bedding, landsliding and erosional budgets in the Central European Alps. *Terra Nova*, 27(5):370–378. doi:10.1111/ter.12169.

Davies-Colley R. J. and Smith D. G. (2001). Turbidity, suspended sediment, and water clarity: A review. *Journal of the American Water Resources Association*, 37(5):1085–1101. doi:10.1111/j.1752-1688.2001.tb03624.x.

Nijs M. A., de, Winterwerp J. C. and Pietrzak J. D. (2009). On harbour siltation in the fresh-salt water mixing region. *Continental Shelf Research*, 29(1):175–193. doi:10.1016/j.csr.2008.01.019.

Vente J., de, Poesen J., Bazzoffi P., Van Rompaey A. and Verstraeten G. (2006). Predicting catchment sediment yield in mediterranean environments: The importance of sediment sources and connectivity in Italian drainage basins. *Earth Surface Processes and Landforms*, 31(8): 1017–1034. doi:10.1002/esp.1305.

Delunel R., Beek P. A., van der, Bourlès D. L., Carcaillet J. and Schlunegger F. (2014). Transient sediment supply in a high-altitude Alpine environment evidenced through a 10Be budget of the Etages catchment (French Western Alps). *Earth Surface Processes and Landforms*, 39(7): 890–899. doi:10.1002/esp.3494.

Delunel R., Schlunegger F., Valla P. G., Dixon J., Glotzbach C., Hippe K., Kober F., Molliex S., Norton K. P., Salcher B., Wittmann H., Akçar N. and Christl M. (2020). Late-Pleistocene catchment-wide denudation patterns across the European Alps. *Earth-Science Reviews*, 211. doi:10.1016/j.earscirev.2020.103407.

D'Haen K., Dusar B., Verstraeten G., Degryse P. and De Brue H. (2013). A sediment fingerprinting approach to understand the geomorphic coupling in an eastern Mediterranean mountainous river catchment. *Geomorphology*, 197:64–75. doi:10.1016/j.geomorph.2013.04.038.

Dixon J. C. and Thorn C. E. (2005). Chemical weathering and landscape development in mid-latitude alpine environments. *Geomorphology*, 67(1-2 SPEC. ISS.):127–145. doi:10.1016/j.geomorph.2004.07.009.

Dominic J. A., Aris A. Z. and Sulaiman W. N. A. (2015). Factors Controlling the Suspended Sediment Yield During Rainfall Events of Dry and Wet Weather Conditions in A Tropical Urban Catchment. *Water Resources Management*, 29(12):4519–4538. doi:10.1007/s11269-015-1073-0.

Doomen A. M. C., Wijma E., Zwolsman J. J. G. and Middelkoop H. (2008). Predicting suspended sediment concentrations in the Meuse river using a supply-based rating curve. *Hydrological Processes*, 22(12):1846–1856. doi:10.1002/hyp.6767.

Doten C. O., Bowling L. C., Lanini J. S., Maurer E. P. and Lettenmaier D. P. (2006). A spatially distributed model for the dynamic prediction of sediment erosion and transport in mountainous forested watersheds. *Water Resources Research*, 42(4):1–15. doi:10.1029/2004WR003829.

Dürst Stucki M., Schlunegger F., Christener F., Otto J. C. and Götz J. (2012). Deepening of inner gorges through subglacial meltwater - An example from the UNESCO Entlebuch area, Switzerland. *Geomorphology*, 139-140:506–517. doi:10.1016/j.geomorph.2011.11.016.

Duvert C., Gratiot N., Evrard O., Navratil O., Némery J., Prat C. and Esteves M. (2010). Drivers of erosion and suspended sediment transport in three headwater catchments of the Mexican Central Highlands. *Geomorphology*, 123(3-4):243–256. doi:10.1016/j.geomorph.2010.07.016.

Evrard O., Navratil O., Ayrault S., Ahmadi M., Némery J., Legout C., Lefèvre I., Poirel A., Bonté P. and Esteves M. (2011). Combining suspended sediment monitoring and fingerprinting to determine the spatial origin of fine sediment in a mountainous river catchment. *Earth Surface Processes and Landforms*, 36(8):1072–1089. doi:10.1002/esp.2133.

Evrard O., Laceby J. P., Huon S., Lefèvre I., Sengtaheuanghoung O. and Ribolzi O. (2016). Combining multiple fallout radionuclides (137Cs, 7Be, 210Pbxs) to investigate temporal sediment source dynamics in tropical, ephemeral riverine systems. *Journal of Soils and Sediments*, 16(3): 1130–1144. doi:10.1007/s11368-015-1316-y.

Fatichi S., Rimkus S., Burlando P., Bordoy R. and Molnar P. (2015). High-resolution distributed analysis of climate and anthropogenic changes on the hydrology of an Alpine catchment. *Journal of Hydrology*, 525:362–382. doi:10.1016/j.jhydrol.2015.03.036.

Ferguson R. I. (1986). River Loads Underestimated by Rating Curves. *Water Resources Research*, 22(1):74–76. doi:10.1029/WR022i001p00074.

FOEN (2010). Hydrologisches Jahrbuch der Schweiz 2010. Technical report, Swiss Federal Office for the Environment.

Francipane A., Ivanov V. Y., Noto L. V., Istanbulluoglu E., Arnone E. and Bras R. L. (2012). TRIBS-Erosion: A parsimonious physically-based model for studying catchment hydro-geomorphic response. *Catena*, 92:216–231. doi:10.1016/j.catena.2011.10.005.

Frank F., Huggel C., McArdell B. W. and Vieli A. (2019). Landslides and increased debris-flow activity: A systematic comparison of six catchments in Switzerland. *Earth Surface Processes and Landforms*, 44(3):699–712. doi:10.1002/esp.4524.

Frei C. and Schär C. (1998). A precipitation climatology of the Alps from high-resolution rain-gauge observations. *International Journal of Climatology*, 18(8):873–900. doi:10.1002/(SICI)1097-0088(19980630)18:8<873::AID-JOC255>3.0.CO;2-9.

Fryirs K. (2013). (Dis)Connectivity in catchment sediment cascades: A fresh look at the sediment delivery problem. *Earth Surface Processes and Landforms*, 38(1):30–46. doi:10.1002/esp.3242.

Fryirs K. and Brierley G. J. (1999). Slope – channel decoupling in Wolumla catchment , New South Wales, Australia : the changing nature of sediment sources following European settlement. *Catena*, 35:41–63. doi:https://doi.org/10.1016/S0341-8162(98)00119-2.

Fryirs K., Brierley G. J., Preston N. J. and Spencer J. (2007). Catchment-scale (dis)connectivity in sediment flux in the upper Hunter catchment, New South Wales, Australia. *Geomorphology*, 84 (3-4):297–316. doi:10.1016/j.geomorph.2006.01.044.

Fuller C. W., Willett S. D., Hovius N. and Slingerland R. (2003). Erosion Rates for Taiwan Mountain Basins: New Determinations from Suspended Sediment Records and a Stochastic Model of Their Temporal Variation. *The Journal of Geology*, 111(1):71–87. doi:10.1086/344665.

Fuller I. C. and Marden M. (2010). Rapid channel response to variability in sediment supply: Cutting and filling of the Tarndale Fan, Waipaoa catchment, New Zealand. *Marine Geology*, 270 (1-4):45–54. doi:10.1016/j.margeo.2009.10.004.

Gao P. (2008). Understanding watershed suspended sediment transport. *Progress in Physical Geography*, 32(3):243–263. doi:10.1177/0309133308094849.

Garcia-Torres L., Benites J., Martinez-Vilela A. and Holgado-Cabrera A. (2003). *Conservation agriculture*. doi:10.1007/978-94-017-1143-2_35.

Govaerts B., Verhulst N., Castellanos-Navarrete A., Sayre K. D., Dixon J. and Dendooven L. (2009). Conservation agriculture and soil carbon sequestration: Between myth and farmer reality. *Critical Reviews in Plant Sciences*, 28(3):97–122. doi:10.1080/07352680902776358.

Grill G., Lehner B., Thieme M., Geenen B., Tickner D., Antonelli F., Babu S., Borrelli P., Cheng L., Crochetiere H., Ehalt Macedo H., Filgueiras R., Goichot M., Higgins J., Hogan Z., Lip B., McClain M. E., Meng J., Mulligan M., Nilsson C., Olden J. D., Opperman J. J., Petry P.,

Reidy Liermann C., Sáenz L., Salinas-Rodríguez S., Schelle P., Schmitt R. J. P., Snider J., Tan F., Tockner K., Valdujo P. H., Soesbergen A., van and Zarfl C. (2019). Mapping the world's free-flowing rivers. *Nature*, 569(7755):215–221. doi:10.1038/s41586-019-1111-9.

Haddadchi A., Ryder D. S., Evrard O. and Olley J. (2013). Sediment fingerprinting in fluvial systems: Review of tracers, sediment sources and mixing models. *International Journal of Sediment Research*, 28(4):560–578. doi:10.1016/S1001-6279(14)60013-5.

Hairsine P. B. and Rose C. W. (1992). Modeling water erosion due to overland flow using physical principles: 2. Rill flow. *Water Resources Research*, 28(1):245–250. doi:10.1029/91WR02381.

Hancock G., Evans K., Willgoose G., Moliere D., Saynor M. and Loch R. (2000). Medium-term erosion simulation of an abandoned mine site using the SIBERIA landscape evolution model. *Australian Journal of Soil Research*, 38(2):249–263.

Hancock G. R., Webb A. A. and Turner L. (2017). Sediment transport in forested head water catchments – Calibration and validation of a soil erosion and landscape evolution model. *Journal of Hydrology*, 554:12–23. doi:10.1016/j.jhydrol.2017.08.049.

Handwerger A. L., Fielding E. J., Huang M. H., Bennett G. L., Liang C. and Schulz W. H. (2019a). Widespread Initiation, Reactivation, and Acceleration of Landslides in the Northern California Coast Ranges due to Extreme Rainfall. *Journal of Geophysical Research: Earth Surface*, 124(7): 1782–1797. doi:10.1029/2019JF005035.

Handwerger A. L., Huang M.-h., Fielding E. J., Booth A. M. and Bürgmann R. (2019b). A shift from drought to extreme rainfall drives a stable landslide to catastrophic failure. *Scientific Reports*, 9(1):1569. doi:10.1038/s41598-018-38300-0.

Hansen M. C., Potapov P. V., Moore R., Hancher M., Turubanova S. A., Tyukavina A., Thau D., Stehman S. V., Goetz S. J., Loveland T. R., Kommareddy A., Egorov A., Chini L., Justice C. O. and Townshend J. R. G. (2013). High-Resolution Global Maps of 21st-Century Forest Cover Change. *Science*, 342(6160):850–853. doi:10.1126/science.1244693.

Heckmann T., Cavalli M., Cerdan O., Foerster S., Javaux M., Lode E., Smetanová A., Vericat D. and Brardinoni F. (2018). Indices of sediment connectivity: opportunities, challenges and limitations. *Earth-Science Reviews*, (December 2017):1–32. doi:10.1016/j.earscirev.2018.08.004.

Hinderer M., Kastowski M., Kamelger A., Bartolini C. and Schlunegger F. (2013). River loads and modern denudation of the Alps - A review. *Earth-Science Reviews*, 118:11–44. doi:10.1016/j.earscirev.2013.01.001.

Hobbs P. R., Sayre K. and Gupta R. (2008). The role of conservation agriculture in sustainable agriculture. *Philosophical Transactions of the Royal Society B: Biological Sciences*, 363(1491): 543–555. doi:10.1098/rstb.2007.2169.

Horowitz A. J. (2003). An evaluation of sediment rating curves for estimating suspended sediment concentrations for subsequent flux calculations. *Hydrological Processes*, 17(17):3387–3409. doi:10.1002/hyp.1299.

Horowitz A. J., Elrick K. A. and Smith J. J. (2001). Estimating suspended sediment and trace element fluxes in large river basins: Methodological considerations as applied to the NASQAN programme. *Hydrological Processes*, 15(7):1107–1132. doi:10.1002/hyp.206.

Hovius N., Stark C. P., Hao-Tsu C. and Jiun-Chuan L. (2002). Supply and Removal of Sediment in a Landslide-Dominated Mountain Belt: Central Range, Taiwan. *The Journal of Geology*, 108(1): 73–89. doi:10.1086/314387.

Iverson R. M. and Major J. J. (1987). Rainfall, ground-water flow, and seasonal movement at Minor Creek landslide, northwestern California: physical interpretation of empirical relations. *Geological Society of America Bulletin*, 99(4):579–594. doi:10.1130/0016-7606(1987)99<579:RGFASM>2.0.CO;2.

Jakob M., Bovis M. and Oden M. (2005). The significance of channel recharge rates for estimating debris-flow magnitude and frequency. *Earth Surface Processes and Landforms*, 30(6):755–766. doi:10.1002/esp.1188.

Jerolmack D. J. and Paola C. (2010). Shredding of environmental signals by sediment transport. *Geophysical Research Letters*, 37(19):1–5. doi:10.1029/2010GL044638.

Kampf S. K., Brogan D. J., Schmeer S., MacDonald L. H. and Nelson P. A. (2016). How do geomorphic effects of rainfall vary with storm type and spatial scale in a post-fire landscape? *Geomorphology*, 273:39–51. doi:10.1016/j.geomorph.2016.08.001.

Kao S. J., Lee T. Y. and Milliman J. D. (2005). Calculating highly fluctuated suspended sediment fluxes from mountainous rivers in Taiwan. *Terrestrial, Atmospheric and Oceanic Sciences*, 16(3): 653–675. doi:10.3319/TAO.2005.16.3.653(T).

Kasten F. and Czeplak G. (1980). Solar and terrestrial radiation dependent on the amount and type of cloud. *Solar Energy*, 24(2):177–189. doi:10.1016/0038-092X(80)90391-6.

Kim J. and Ivanov V. Y. (2014). On the nonuniqueness of sediment yield at the catchment scale. *Water Resources Research*, (1):1025–1045. doi:10.1002/2013WR014580.Received.

Knight J. and Harrison S. (2009). Sediments and future climate. *Nature Geoscience*, 2(4):230. doi:10.1038/ngeo491.

Kober F., Hippe K., Salcher B., Ivy-Ochs S., Kubik P. W., Wacker L. and Hählen N. (2012). Debris-flow-dependent variation of cosmogenically derived catchment-wide denudation rates. *Geology*, 40(10):935–938. doi:10.1130/G33406.1.

Kondolf G. M. (1997). Hungry water: Effects of dams and gravel mining on river channels. *Environmental Management*, 21(4):533–551. doi:10.1007/s002679900048.

Korup O., McSaveney M. J. and Davies T. R. (2004). Sediment generation and delivery from large historic landslides in the Southern Alps, New Zealand. *Geomorphology*, 61(1-2):189–207. doi:10.1016/j.geomorph.2004.01.001.

Kron W., Löw P. and Kundzewicz Z. W. (2019). Changes in risk of extreme weather events in Europe. *Environmental Science and Policy*, 100(June):74–83. doi:10.1016/j.envsci.2019.06.007.

Lang A., Bork H.-R. and Preston N. (2003). Changes in sediment flux and storage within a fluvial system : some examples from the Rhine catchment. *Hydrological Processes*, 3334:3321–3334. doi:10.1002/hyp.1389.

Lehner B., Liermann C. R., Revenga C., Vörömsmarty C., Fekete B., Crouzet P., Döll P., Endejan M., Frenken K., Magome J., Nilsson C., Robertson J. C., Rödel R., Sindorf N. and Wisser D. (2011). High-resolution mapping of the world's reservoirs and dams for sustainable river-flow management. *Frontiers in Ecology and the Environment*, 9(9):494–502. doi:10.1890/100125.

Liébault F., Gomez B., Page M., Marden M., Peacock D., Richard D. and Trotter C. M. (2005). Land-use change, sediment production and channel response in upland regions. *River Research and Applications*, 21(7):739–756. doi:10.1002/rra.880.

Liu Z. and Todini E. (2002). Towards a comprehensive physically-based rainfall-runoff model. *Hydrology and Earth System Sciences*, 6(5):859–881. doi:10.5194/hess-6-859-2002.

Liu Z. and Todini E. (2005). Assessing the TOPKAPI non-linear reservoir cascade approximation by means of a characteristic lines solution. *Hydrological Processes*, 19(10):1983–2006. doi:10.1002/hyp.5662.

Liu Z., Martina M. L. and Todini E. (2005). Flood forecasting using a fully distributed model: Application of the TOPKAPI model to the Upper Xixian Catchment. *Hydrology and Earth System Sciences*, 9(4):347–364. doi:10.5194/hess-9-347-2005.

López-Tarazón J. A., Batalla R. J., Vericat D. and Balasch J. C. (2010). Rainfall, runoff and sediment transport relations in a mesoscale mountainous catchment: The River Isábena (Ebro basin). *Catena*, 82(1):23–34. doi:10.1016/j.catena.2010.04.005.

Lukens C. E., Riebe C. S., Sklar L. S. and Shuster D. L. (2016). Grain size bias in cosmogenic nuclide studies of stream sediment in steep terrain. *Journal of Geophysical Research: Earth Surface*, 121(5):978–999. doi:10.1002/2016JF003859.

Mahoney D. T., Fox J. F. and Al Aamery N. (2018). Watershed erosion modeling using the probability of sediment connectivity in a gently rolling system. *Journal of Hydrology*, 561(April): 862–883. doi:10.1016/j.jhydrol.2018.04.034.

Malmon D. V., Dunne T. and Reneau S. L. (2003). Stochastic Theory of Particle Trajectories through Alluvial Valley Floors. *The Journal of Geology*, 111(5):525–542. doi:10.1086/376764.

Marks S. D. and Rutt G. P. (1997). Fluvial sediment inputs to upland gravel bed rivers draining forested catchments: Potential ecological impacts. *Hydrology and Earth System Sciences*, 1(3): 499–508. doi:10.5194/hess-1-499-1997.

Matisoff G., Wilson C. G. and Whiting P. J. (2005). The 7Be/210PbXS ratio as an indicator of suspended sediment age or fraction new sediment in suspension. *Earth Surface Processes and Landforms*, 30(9):1191–1201. doi:10.1002/esp.1270.

Mekonnen M., Keesstra S. D., Stroosnijder L., Baartman J. E. and Maroulis J. (2015). Soil Conservation Through Sediment Trapping: A Review. *Land Degradation and Development*, 26 (6):544–556. doi:10.1002/ldr.2308.

Milliman J. D. and Syvitski J. P. (1992). Geomorphic/Tectonic Control of Sediment Discharge to the Ocean: The Importance of Small Mountainous Rivers. *Journal of Geology*, 41(3-4):211–212. doi:10.1016/S0012-8252(96)00025-6.

Misset C., Recking A., Legout C., Poirel A., Cazilhac M., Esteves M. and Bertrand M. (2019). An attempt to link suspended load hysteresis patterns and sediment sources configuration in alpine catchments. *Journal of Hydrology*, 576(April):72–84. doi:10.1016/j.jhydrol.2019.06.039.

Montgomery D. R. (2007). Soil erosion and agricultural sustainability. *Proceedings of the National Academy of Sciences*, 104(33):13268–13272. doi:10.1073/pnas.0611508104.

Montgomery D. R. (2012). *Dirt: the erosion of civilizations*. Univ of California Press.

Moriasi D. N., Arnold J. G., Liew M. W. V., Bingner R. L., Harmel R. D. and Veith T. L. (2007). Model evaluation guidelines for systematic quantification of accuracy in watershed simulations. *Transactions of the ASABE*, 50(3):227–234. doi:10.1234/590.

Nanson G. C. (1974). Bedload and suspended-load transport in a small, steep, mountain stream. *American Journal of Science*, 274(5):471–486. doi:10.2475/ajs.274.5.471.

Navratil O., Esteves M., Legout C., Gratiot N., Nemery J., Willmore S. and Grangeon T. (2011). Global uncertainty analysis of suspended sediment monitoring using turbidimeter in a small mountainous river catchment. *Journal of Hydrology*, 398(3-4):246–259. doi:10.1016/j.jhydrol.2010.12.025.

Navratil O., Evrard O., Esteves M., Legout C., Ayrault S., Némery J., Mate-Marin A., Ahmadi M., Lefèvre I., Poirel A. and Bonté P. (2012). Temporal variability of suspended sediment sources in an alpine catchment combining river/rainfall monitoring and sediment fingerprinting. *Earth Surface Processes and Landforms*, 37(8):828–846. doi:10.1002/esp.3201.

NCCS (2018). CH2018 climate scenarios. URL `https://www.nccs.admin.ch/nccs/en/home/the-nccs/priority-themes/ch2018-climate-scenarios.html`.

Nearing M. A., Foster G. R., Lane L. J. and Finkner S. C. (1989). A Process-Based Soil Erosion Model for USDA-Water Erosion Prediction Project Technology. *Transactions of the ASAE*, 32 (5):1587–1593.

Nearing M. A., Pruski F. F. and O'Neal M. R. (2004). Expected climate change impacts on soil erosion rates: A review. *Journal of Soil and Water Conservation*, 59(1):43–50.

Niemi N. A., Oskin M., Burbank D. W., Heimsath A. M. and Gabet E. J. (2005). Effects of bedrock landslides on cosmogenically determined erosion rates. *Earth and Planetary Science Letters*, 237(3-4):480–498. doi:10.1016/j.epsl.2005.07.009.

Norton K. P., Blanckenburg F., von, Schlunegger F., Schwab M. and Kubik P. W. (2008). Cosmogenic nuclide-based investigation of spatial erosion and hillslope channel coupling in the transient foreland of the Swiss Alps. *Geomorphology*, 95(3-4):474–486. doi:10.1016/j.geomorph.2007.07.013.

Olarieta J. R., Besga G., Rodríguez R., Usón A., Pinto M. and Virgel S. (1999). Sediment enrichment ratios after mechanical site preparation for Pinus radiata plantation in the Basque Country. *Geoderma*, 93:255–267.

Olley J., Brooks A., Spencer J., Pietsch T. and Borombovits D. (2013). Subsoil erosion dominates the supply of fine sediment to rivers draining into Princess Charlotte Bay, Australia. *Journal of Environmental Radioactivity*, 124:121–129. doi:10.1016/j.jenvrad.2013.04.010.

Owens P. N., Batalla R. J., Collins A. J., Gomez B., Hicks D. M., Horowitz A. J., Kondolf G. M., Marden M., Page M. J., Peacock D. H., Petticrew E. L., Salomons W. and Trustrum N. A. (2005). Fine-grained sediment in river systems: Environmental significance and management issues. *River Research and Applications*, 21(7):693–717. doi:10.1002/rra.878.

Pappas C., Fatichi S., Rimkus S., Burlando P. and Huber M. O. (2015). The role of local-scale heterogeneities in terrestrial ecosystem modeling. *Journal of Geophysical Research: Biogeosciences*, 120(2):341–360. doi:10.1002/2014JG002735.

Parker G. and Andres D. (1976). Detrimental effects of river channelization. *Rivers '76, Proc. Symp. on inland waterways for navigation, flood control and water diversrions.*, 2:1248–1266.

Parkyn S. M., Davies-Colley R. J., Cooper A. B. and Stroud M. J. (2005). Predictions of stream nutrient and sediment yield changes following restoration of forested riparian buffers. *Ecological Engineering*, 24(5 SPEC. ISS.):551–558. doi:10.1016/j.ecoleng.2005.01.004.

Paschalis A., Fatichi S., Molnar P., Rimkus S. and Burlando P. (2014). On the effects of small scale space-time variability of rainfall on basin flood response. *Journal of Hydrology*, 514:313–327. doi:10.1016/j.jhydrol.2014.04.014.

Peleg N., Skinner C., Fatichi S. and Molnar P. (2020). Temperature effects on the spatial structure of heavy rainfall modify catchment hydro-morphological response. *Earth Surface Dynamics*, 8 (1):17–36. doi:10.5194/esurf-8-17-2020.

Pelletier J. D. (2012). A spatially distributed model for the long-term suspended sediment discharge and delivery ratio of drainage basins. *Journal of Geophysical Research: Earth Surface*, 117(2): 1–15. doi:10.1029/2011JF002129.

Pellicciotti F., Brock B., Strasser U., Burlando P., Funk M. and Corripio J. (2005). An enhanced temperature-index glacier melt model including the shortwave radiation balance: Development and testing for Haut Glacier d'Arolla, Switzerland. *Journal of Glaciology*, 51(175):573–587. doi:10.3189/172756505781829124.

Peucker-Ehrenbrink B. (2009). Land2Sea database of river drainage basin sizes, annual water discharges, and suspended sediment fluxes. *Geochemistry, Geophysics, Geosystems*, 10(6):1–10. doi:10.1029/2008GC002356.

Phillips J. D. (2011). Evolutionary geomorphology: Thresholds and nonlinearity in landform response to environmental change. *Hydrol. Earth Syst. Sci.*, pages 196–214. doi:10.5194/hessd-3-365-2006.

Pimentel D., Allen J., Beers A., Guinand L., Linder R., McLaughlin P., Meer B., Musonda D., Perdue D., Poisson S., Siebert S., Stoner K., Salazar R. and Hawkins A. (1987). World Agriculture and Soil Erosion. *BioScience*, 37(4):277–283. doi:10.2307/1310591.

Priestley C. H. B. and Taylor R. J. (1972). On the Assessment of Surface Heat Flux and Evaporation Using Large-Scale Parameters. *Monthly Weather Review*, 100(2):81–92. doi:10.1175/1520-0493(1972)100<0081:OTAOSH>2.3.CO;2.

Prosser I. P. and Rustomji P. (2000). Sediment transport capacity relations for overland flow. *Progress in Physical Geography*, 24(2):179–193. doi:10.1177/030913330002400202.

Pulley S. and Collins A. L. (2018). Tracing catchment fine sediment sources using the new SIFT (SedIment Fingerprinting Tool) open source software. *Science of the Total Environment*, 635: 838–858. doi:10.1016/j.scitotenv.2018.04.126.

Pulley S., Foster I. and Collins A. L. (2017). The impact of catchment source group classification on the accuracy of sediment fingerprinting outputs. *Journal of Environmental Management*, 194: 16–26. doi:10.1016/j.jenvman.2016.04.048.

Quinton J. N., Govers G., Van Oost K. and Bardgett R. D. (2010). The impact of agricultural soil erosion on biogeochemical cycling. *Nature Geoscience*, 3(5):311–314. doi:10.1038/ngeo838.

Renard K., Foster G., Weesies G., McCool D. and Yoder D. (1997). *Predicting Soil Erosion by Water: A Guide to Conservation Planning with the Revised Universal Soil Loss Equation (RUSLE)*. U.S. Department of Agriculture Research Service, Washington.

Reusser L. J. and Bierman P. R. (2010). Using meteoric 10Be to track fl uvial sand through the Waipaoa River basin, New Zealand. *Geology*, 38(1):47–50. doi:10.1130/G30395.1.

Rickenmann D., Badoux A. and Hunzinger L. (2016). Significance of sediment transport processes during piedmont floods: The 2005 flood events in Switzerland. *Earth Surface Processes and Landforms*, 41(2):224–230. doi:10.1002/esp.3835.

Robinson D. A., Panagos P., Borrelli P., Jones A., Montanarella L., Tye A. and Obst C. G. (2017). Soil natural capital in Europe; A framework for state and change assessment. *Scientific Reports*, 7(1):1–14. doi:10.1038/s41598-017-06819-3.

Roering J. J., Kirchner J. W. and Dietrich W. E. (1999). Evidence for nonlinear, diffusive sediment transport on hillslopes and implications for landscape morphology. *Water Resources Research*, 35(3):853–870. doi:10.1029/1998WR900090.

Salcher B. C., Kober F., Kissling E. and Willett S. D. (2014). Glacial impact on short-wavelength topography and long-lasting effects on the denudation of a deglaciated mountain range. *Global and Planetary Change*, 115(April):59–70. doi:10.1016/j.gloplacha.2014.01.002.

Salvucci G. D. and Entekhabi D. (1994). Explicit expressions for Green-Ampt (delta function diffusivity) infiltration rate and cumulative storage. *Water Resources Research*, 30(9):2661–2663. doi:10.1029/94WR01494.

Savi S., Norton K., Picotti V., Brardinoni F., Akçar N., Kubik P. W., Delunel R. and Schlunegger F. (2014). Effects of sediment mixing on 10Be concentrations in the Zielbach catchment, central-eastern Italian Alps. *Quaternary Geochronology*, 19:148–162. doi:10.1016/j.quageo.2013.01.006.

Schlunegger F. and Hinderer M. (2003). Pleistocene/Holocene climate change, re-establishment of fluvial drainage network and increase in relief in the Swiss Alps. *Terra Nova*, 15(2):88–95. doi:10.1046/j.1365-3121.2003.00469.x.

Schlunegger F. and Norton K. P. (2013). Water versus ice: The competing roles of modern climate and Pleistocene glacial erosion in the Central Alps of Switzerland. *Tectonophysics*, 602:370–381. doi:10.1016/j.tecto.2013.03.027.

Schlunegger F. and Schneider H. (2005). Relief-rejuvenation and topographic length scales in a fluvial drainage basin, Napf area, Central Switzerland. *Geomorphology*, 69(1-4):102–117. doi:10.1016/j.geomorph.2004.12.008.

Schmidt J. C. and Wilcock P. R. (2008). Metrics for assessing the downstream effects of dams. *Water Resources Research*, 44(4). doi:10.1029/2006WR005092.

Schmidt S., Ballabio C., Alewell C., Panagos P. and Meusburger K. (2018). Filling the European blank spot—Swiss soil erodibility assessment with topsoil samples. *Journal of Plant Nutrition and Soil Science*, 181(5):737–748. doi:10.1002/jpln.201800128.

Schoonover J. E., Williard K. W. J., Zaczek J. J., Mangun J. C. and Carver A. D. (2006). Agricultural sediment reduction by giant cane and forest riparian buffers. *Water, Air, and Soil Pollution*, 169 (1-4):303–315. doi:10.1007/s11270-006-3111-2.

Schuerch P., Densmore A. L., McArdell B. W. and Molnar P. (2006). The influence of landsliding on sediment supply and channel change in a steep mountain catchment. *Geomorphology*, 78 (3-4):222–235. doi:10.1016/j.geomorph.2006.01.025.

Schumm S. A. (1979). Geomorphic thresholds: the concept and its applications. *Transactions Institute of British Geographers*, 4(4):485–515. doi:10.2307/622211.

Schwab M., Läderach C., Rieke-Zapp D. and Schlunegger F. (2007). Slip rates variability and sediment mobilization on a shallow landslide in the northern Swiss Alps. *Swiss Journal of Geosciences*, 100(2):281–292. doi:10.1007/s00015-007-1218-0.

Schwab M., Rieke-Zapp D., Schneider H., Liniger M. and Schlunegger F. (2008). Landsliding and sediment flux in the Central Swiss Alps: A photogrammetric study of the Schimbrig landslide, Entlebuch. *Geomorphology*, 97(3-4):392–406. doi:10.1016/j.geomorph.2007.08.019.

Schwarb M. (2000). The alpine precipitation climate evaluation of a high-resolution analysis scheme using comprehensive rain-gauge data. *ETH Zurich Research Collection*. doi:10.3929/ethz-a-010782581.

Seeger M., Errea M. P., Beguería S., Arnáez J., Martí C. and García-Ruiz J. M. (2004). Catchment soil moisture and rainfall characteristics as determinant factors for discharge/suspended sediment hysteretic loops in a small headwater catchment in the Spanish pyrenees. *Journal of Hydrology*, 288(3-4):299–311. doi:10.1016/j.jhydrol.2003.10.012.

Sellier V., Navratil O., Laceby J. P., Allenbach M., Lefèvre I. and Evrard O. (2020). Reconstructing the impact of nickel mining activities on sediment supply to the rivers and the lagoon of South Pacific Islands: lessons learnt from the Thio early mining site (New Caledonia). *Geomorphology*, page 107459. doi:10.1016/j.geomorph.2020.107459.

Shah S. M., O'Connell P. E. and Hosking J. R. (1996). Modelling the effects of spatial variability in rainfall on catchment response. 2. Experiments with distributed and lumped models. *Journal of Hydrology*, 175(1-4):89–111. doi:10.1016/S0022-1694(96)80007-2.

Siakeu J., Oguchi T., Aoki T., Esaki Y. and Jarvie H. P. (2004). Change in riverine suspended sediment concentration in central Japan in response to late 20th century human activities. *Catena*, 55(2):231–254. doi:10.1016/S0341-8162(03)00120-6.

Slaymaker O. (1993). The sediment budget of the lillooet river basin, british columbia. *Physical Geography*, 14(3):304–320. doi:10.1080/02723646.1993.10642482.

Smith B. P., Naden P. S., Leeks G. J. and Wass P. D. (2003). The influence of storm events on fine sediment transport, erosion and deposition within a reach of the River Swale, Yorkshire, UK. *Science of the Total Environment*, 314-316(03):451–474. doi:10.1016/S0048-9697(03)00068-8.

Stutenbecker L., Delunel R., Schlunegger F., Silva T. A., Šegvić B., Girardclos S., Bakker M., Costa A., Lane S. N., Loizeau J. L., Molnar P., Akçar N. and Christl M. (2018). Reduced sediment supply in a fast eroding landscape? A multi-proxy sediment budget of the upper Rhône basin, Central Alps. *Sedimentary Geology*, 375:105–119. doi:10.1016/j.sedgeo.2017.12.013.

Stutenbecker L., Costa A., Bakker M., Anghileri D., Molnar P., Lane S. N. and Schlunegger F. (2019). Disentangling human impact from natural controls of sediment dynamics in an Alpine catchment. *Earth Surface Processes and Landforms*, 44(14):2885–2902. doi:10.1002/esp.4716.

SwissAlti3D (2017). SwissAlti3D - The high precision digital elevation model of Switzerland. URL https://shop.swisstopo.admin.ch/en/products/height_models/alti3D.

Syvitski J. and Kettner A. (2011). Sediment flux and the anthropocene. *Philosophical Transactions of the Royal Society A: Mathematical, Physical and Engineering Sciences*, 369(1938):957–975. doi:10.1098/rsta.2010.0329.

Syvitski J., Vörösmarty C. J., Kettner A. J. and Green P. (2005). Impact of Humans on the Flux of Terrestrial Sediment to the Global Coastal Ocean. *Science*, 308(5720):376–380. doi:10.1126/science.1109454.

Syvitski J. P. and Milliman J. D. (2007). Geology, geography, and humans battle for dominance over the delivery of fluvial sediment to the coastal ocean. *Journal of Geology*, 115(1):1–19. doi:10.1086/509246.

Taccone F., Antoine G., Delestre O. and Goutal N. (2018). A gravity-driven runoff and erosion model for sediment transfers at the catchment scale. *E3S Web of Conferences*, 40:1–8. doi:10.1051/e3sconf/20184004019.

Todini E. (1995). New Trends in Modelling Soil Processes from Hillslope to GeM Scales. In Oliver H. and Oliver S., editors, *The role of water and the hydrological cycle in global change*, page 472. Nato ASI Series.

Tsuruta K., Hassan M. A., Donner S. D. and Alila Y. (2018). Development and Application of a Large-Scale, Physically Based, Distributed Suspended Sediment Transport Model on the Fraser River Basin, British Columbia, Canada. *Journal of Geophysical Research: Earth Surface*, 123 (10):2481–2508. doi:10.1029/2017JF004578.

Turowski J. M., Rickenmann D. and Dadson S. J. (2010). The partitioning of the total sediment load of a river into suspended load and bedload: A review of empirical data. *Sedimentology*, 57 (4):1126–1146. doi:10.1111/j.1365-3091.2009.01140.x.

Uber M., Legout C., Nord G., Crouzet C., Demory F. and Poulenard J. (2019). Comparing alternative tracing measurements and mixing models to fingerprint suspended sediment sources in a mesoscale Mediterranean catchment. *Journal of Soils and Sediments*, 19(9):3255–3273. doi:10.1007/s11368-019-02270-1.

Uber M., Nord G., Legout C. and Cea L. (2020). How do modeling choices impact the representation of structural connectivity and the dynamics of suspended sediment fluxes in distributed soil erosion models? *Earth Surface Dynamics Discussions*, (August):1–34. doi:10.5194/esurf-2020-64.

Valbuena D., Erenstein O., Homann-Kee Tui S., Abdoulaye T., Claessens L., Duncan A. J., Gérard B., Rufino M. C., Teufel N., Rooyen A., van and Wijk M. T., van (2012). Conservation Agriculture in mixed crop-livestock systems: Scoping crop residue trade-offs in Sub-Saharan Africa and South Asia. *Field Crops Research*, 132:175–184. doi:10.1016/j.fcr.2012.02.022.

Van den Berg F. and Schlunegger F. (2012). Alluvial cover dynamics in response to floods of various magnitudes: The effect of the release of glaciogenic material in a Swiss Alpine catchment. *Geomorphology*, 141-142:121–133. doi:10.1016/j.geomorph.2011.12.030.

Van Den Berg F., Schlunegger F., Akçar N. and Kubik P. (2012). 10Be-derived assessment of accelerated erosion in a glacially conditioned inner gorge, Entlebuch, Central Alps of Switzerland. *Earth Surface Processes and Landforms*, 37(11):1176–1188. doi:10.1002/esp.3237.

Van Dongen R., Scherler D., Wittmann H. and Von Blanckenburg F. (2019). Cosmogenic 10 Be in river sediment: Where grain size matters and why. *Earth Surface Dynamics*, 7(2):393–410. doi:10.5194/esurf-7-393-2019.

Maren D. S., van, Winterwerp J. C., Wu B. S. and Zhou J. J. (2009). Modelling hyperconcentrated flow in the Yellow River. *Earth Surface Processes and Landforms*, 34(4):596–612. doi:10.1002/esp.1760.

Van Rompaey A., Bazzoffi P., Jones R. J. and Montanarella L. (2005). Modeling sediment yields in Italian catchments. *Geomorphology*, 65(1-2):157–169. doi:10.1016/j.geomorph.2004.08.006.

Van Rompaey A. J., Verstraeten G., Van Oost K., Govers G. and Poesen J. (2001). Modelling mean annual sediment yield using a distributed approach. *Earth Surface Processes and Landforms*, 26 (11):1221–1236. doi:10.1002/esp.275.

VanSickle J. and Beschta R. L. (1983). Supply-based models of suspended sediment transport in streams. *Water Resources Research*, 19(3):768–778. doi:10.1029/WR019i003p00768.

Vaughan A. A., Belmont P., Hawkins C. P. and Wilcock P. (2017). Near-Channel Versus Watershed Controls on Sediment Rating Curves. *Journal of Geophysical Research: Earth Surface*, 122(10): 1901–1923. doi:10.1002/2016JF004180.

Vercruysse K., Grabowski R. C. and Rickson R. J. (2017). Suspended sediment transport dynamics in rivers: Multi-scale drivers of temporal variation. *Earth-Science Reviews*, 166:38–52. doi:10.1016/j.earscirev.2016.12.016.

Vetsch D., Siviglia A., Ehrbar D., Facchini M., Kammamer S., Koch A., Peter S., Vonwiller L., Gerber M., Farshi D., Mueller R., Rousselot P., Veprek R. and Faeh R. (2017). System Manuals of BASEMENT, Version 2.7. Technical report, VAW ETH Zurich. URL `www.basement.ethz.ch`.

Blanckenburg F., von (2005). The control mechanisms of erosion and weathering at basin scale from cosmogenic nuclides in river sediment. *Earth and Planetary Science Letters*, 237(3-4): 462–479. doi:10.1016/j.epsl.2005.06.030.

Vörösmarty C. J., Meybeck M., Fekete B., Sharma K., Green P. and Syvitski J. P. (2003). Anthropogenic sediment retention: Major global impact from registered river impoundments. *Global and Planetary Change*, 39(1-2):169–190. doi:10.1016/S0921-8181(03)00023-7.

Wainwright J., Turnbull L., Ibrahim T. G., Lexartza-Artza I., Thornton S. F. and Brazier R. E. (2011). Linking environmental régimes, space and time: Interpretations of structural and functional connectivity. *Geomorphology*, 126(3-4):387–404. doi:10.1016/j.geomorph.2010.07.027.

Walling D. E. (1977). Assessing the accuracy of suspended sediment rating curves for a small basin. *Water Resources Research*, 13(3):531–538. doi:10.1029/WR013i003p00531.

Walling D. E. (1983). The sediment delivery problem. *Journal of Hydrology*, 65:209–237. doi:10.1016/0022-1694(83)90217-2.

Walling D. E. (2005). Tracing suspended sediment sources in catchments and river systems. *Science of the Total Environment*, 344(1-3 SPEC. ISS.):159–184. doi:10.1016/j.scitotenv.2005.02.011.

Walling D. E. (2006). Human impact on land-ocean sediment transfer by the world's rivers. *Geomorphology*, 79(3-4):192–216. doi:10.1016/j.geomorph.2006.06.019.

Walling D. E. (2008). The changing sediment loads of the world's rivers. *IAHS-AISH Publication*, 20(325):323–338. doi:10.2478/v10060-008-0001-x.

Walling D. E. and Webb B. W. (1982). The reliability of suspended sediment load data. *Journal of the American Medical Association*, 248(17):2180. doi:10.1001/jama.248.17.2180.

Wass P. D. and Leeks G. J. L. (1999). Suspended sediment Fluxes in the Humber catchment , UK. *Hydrological Processes*, 953(April 1998).

Wenger A. S., Johansen J. L. and Jones G. P. (2011). Suspended sediment impairs habitat choice and chemosensory discrimination in two coral reef fishes. *Coral Reefs*, 30(4):879–887. doi:10.1007/s00338-011-0773-z.

Wetzel K.-F. (1994). The significance of fluvial erosion, channel storage and gravitational processes in sediment production in a small mountainous catchment area. In *Dynamics and Geomorphology of Mountain Rivers*, pages 141–160. Springer Berlin Heidelberg, Berlin, Heidelberg. doi:10.1007/BFb0117837. URL `http://link.springer.com/10.1007/BFb0117837`.

Wichmann V., Heckmann T., Haas F. and Becht M. (2009). A new modelling approach to delineate the spatial extent of alpine sediment cascades. *Geomorphology*, 111(1-2):70–78. doi:10.1016/j.geomorph.2008.04.028.

Wicks J. M. and Bathurst J. C. (1996). SHESED: A physically based, distributed erosion and sediment yield component for the SHE hydrological modelling system. *Journal of Hydrology*, 175(1-4):213–238. doi:10.1016/S0022-1694(96)80012-6.

Winterwerp J. C., Borst W. G. and De Vries M. B. (2005). Pilot study on the erosion and rehabilitation of a mangrove mud coast. *Journal of Coastal Research*, 21(2):223–230. doi:10.2112/03-832A.1.

Wittmann H., Blanckenburg F., von, Kruesmann T., Norton K. P. and Kubik P. W. (2007). Relation between rock uplift and denudation from cosmogenic nuclides in river sediment in the Central Alps of Switzerland. *Journal of Geophysical Research: Earth Surface*, 112(4):1–20. doi:10.1029/2006JF000729.

Woolhiser D., Smith R. E. and Goodrich D. (1990). A Kinematic Runoff and Erosion Model. (March).

Yang D., Kanae S., Oki T., Koike T. and Musiake K. (2003). Global potential soil erosion with reference to land use and climate changes. *Hydrological Processes*, 17(14):2913–2928. doi:10.1002/hyp.1441.

Yanites B. J., Tucker G. E. and Anderson R. S. (2009). Numerical and analytical models of cosmogenic radionuclide dynamics in landslide-dominated drainage basins. *Journal of Geophysical Research: Earth Surface*, 114(1). doi:10.1029/2008JF001088.

Yu L. (2002). The Huanghe (Yellow) River: A review of its development, characteristics, and future management issues. *Continental Shelf Research*, 22(3):389–403. doi:10.1016/S0278-4343(01)00088-7.

Zabaleta A., Martínez M., Uriarte J. A. and Antigüedad I. (2007). Factors controlling suspended sediment yield during runoff events in small headwater catchments of the Basque Country. *Catena*, 71(1):179–190. doi:10.1016/j.catena.2006.06.007.